IDENTIFICATION, CHARACTERIZATION AND RESUSCITATION OF VIABLE BUT NON-CULTURABLE CAMPYLOBACTER JEJUNI

by

Kaidi Wang

Department of Food Science and Agricultural Chemistry

McGill University, Montreal

April 2024

A thesis submitted to McGill University in partial fulfillment of the requirements of the degree of Doctor in Philosophy

First published on April 12, 2025

© Kaidi Wang, 2024

Table of Contents

Abstract

The presence and resuscitation of viable but non-culturable (VBNC) pathogens in food processing environments and food products pose a significant risk to public health. VBNC pathogens can evade detection by the conventional culturing methods but maintain the potential to cause foodborne illnesses when resuscitated. *Campylobacter jejuni* is a leading bacterial cause of human gastrointestinal disease worldwide. *C. jejuni* can enter the VBNC state to survive under stresses, such as starvation, low temperature, and presence of food preservatives. However, the characteristics of pure VBNC *C. jejuni* and its formation and resuscitation in the agri-food system have not been well studied. This thesis aimed to identify and characterize VBNC *C. jejuni* cells at single-cell resolution, as well as investigate its resuscitation capability and identify the potential resuscitation stimuli.

First, we developed an automated optofluidic platform combining Raman optical tweezers, a microfluidic "lab-on-a-chip" device, and machine learning techniques for single-cell identification and sorting. A reliable spectral recovery technique based on conditional generative adversarial network was also proposed and the spectral acquisition was accelerated by over 10 times. Using convolutional neural network (CNN), this platform achieved an overall accuracy of 94.9% for the classification of 5 major foodborne bacteria at single-cell level, including *C. jejuni*.

Using the proposed Raman tweezers system and CNN, VBNC *C. jejuni* was identified from its culturable counterpart at the single-cell resolution with high accuracies ranging from 91.7% to 93.4%. We further utilized a gradient-weighted class activation mapping to highlight the spectral regions that contribute most to the CNN-based identification of VBNC cells. Molecular

compositional alterations in proteins, nucleic acids, lipids, and peptidoglycans were deciphered during the VBNC formation. This culture-independent approach represents an unprecedented platform for accurate identification and comprehensive characterization of VBNC bacteria at single-cell level.

Presence of resuscitation stimuli is a critical factor to resuscitate VBNC pathogens. Resuscitation of VBNC *C. jejuni* was successfully achieved in embryonated chicken eggs. Since the eggs at different embryonic stages exhibited varied capabilities of promoting the resuscitation of VBNC *C. jejuni*, we further conducted mass spectrometry-based metabolomics and lipidomics to examine the compositional changes in different eggs. The potential compounds that might contribute to the resuscitation were identified, providing insights on the mechanism underlying the resuscitation of VBNC *C. jejuni*.

Overall, this thesis project aids in a better understanding of the characteristics and resuscitation of VBNC *C. jejuni* in the food supply chain. It provides insights on mitigating *Campylobacter* contamination in the environment and agri-foods**,** demonstrating significant relevance in improving food safety and public health.

Résumé

La présence et la réanimation de pathogènes viables mais non cultivables (VBNC) dans l'environnement de traitement des aliments et dans les produits alimentaires représentent un risque significatif pour la santé publique. Les pathogènes VBNC peuvent échapper à la détection par les méthodes de culture conventionnelles, mais conservent le potentiel de causer des maladies d'origine alimentaire lorsqu'ils sont ressuscités. *Campylobacter jejuni* est l'une des principales causes de maladies gastro-intestinales chez l'homme dans le monde entier. *C. jejuni* peut entrer dans l'état VBNC pour survivre à des conditions défavorables telles que la famine, les températures basses et la présence d'agents de conservation. Cependant, les caractéristiques de *C. jejuni* VBNC pur, ainsi que sa formation et sa réanimation dans les systèmes agroalimentaires, n'ont pas été suffisamment étudiées. Cette thèse vise à identifier et caractériser les cellules de *C. jejuni* VBNC à une résolution monocellulaire, ainsi qu'à étudier sa capacité de réanimation et à identifier les stimuli potentiels de réanimation.

Tout d'abord, nous avons développé une plateforme optofluidique automatisée combinant des pincettes optiques Raman, un dispositif microfluidique "lab-on-a-chip" et des techniques d'apprentissage automatique pour l'identification et le tri à une résolution monocellulaire. Une technique de récupération spectrale fiable basée sur un réseau génératif antagoniste conditionnel a également été proposée, et la vitesse d'acquisition spectrale a été augmentée de plus de 10 fois. Cette plateforme a atteint une précision globale de 94,9 % pour la classification de 5 bactéries d'origine alimentaire majeures à un niveau monocellulaire, y compris *C. jejuni*.

En utilisant le système de pincettes Raman proposé, *C. jejuni* VBNC a été identifié par rapport à son homologue cultivable à une résolution monocellulaire avec des précisions élevées allant de 91,7 % à 93,4 %. Nous avons ensuite utilisé une cartographie d'activation de classe pondérée par gradient pour surligner les régions spectrales qui contribuent le plus à l'identification des cellules VBNC basée sur CNN. Des altérations compositionnelles moléculaires dans les protéines, les acides nucléiques, les lipides et les peptidoglycanes ont été identifiées pendant la formation de VBNC. Cette approche indépendante de la culture représente une plateforme sans précédent pour l'identification précise et la caractérisation complète des bactéries VBNC à un niveau monocellulaire.

La présence de stimuli de réanimation est un facteur critique pour ressusciter les pathogènes VBNC. La réanimation de *C. jejuni* VBNC a été réussie dans des œufs de poulet embryonnés. Comme les œufs à différents stades embryonnaires présentaient des capacités variées à favoriser la réanimation de *C. jejuni* VBNC, nous avons ensuite réalisé des études métabolomique et lipidomique basées sur la spectrométrie de masse pour examiner les changements de composition dans différents œufs. Les composés qui pourraient potentiellement contribuer à la réanimation ont été identifiés, fournissant un aperçu sur le mécanisme responsable de la réanimation de *C. jejuni* VBNC.

Dans l'ensemble, ce projet de thèse contribue à une meilleure compréhension des caractéristiques et de la réanimation de *C. jejuni* VBNC dans la chaîne d'approvisionnement alimentaire. Il offre des perspectives sur la réduction de la contamination par *Campylobacter* dans l'environnement et

les produits agroalimentaires, démontrant une pertinence significative pour l'amélioration de la sécurité alimentaire et de la santé publique.

Organization of Thesis

This thesis is organized in the manuscript format and consists of six chapters. Chapter 1 includes a general introduction, research hypotheses and objectives of this thesis. Chapter 2 is a comprehensive literature review of the major topics involved in this research. Chapters 3 to 5 are presented in the form of peer-reviewed manuscripts, comprising abstract, introduction, materials and methods, results and discussion, and conclusion in each chapter. Specifically, Chapter 3 is modified from a manuscript published in *Analytical Chemistry*, and studies in Chapter 4 and Chapter 5 have both been submitted for publication with the candidate as the first author. Bridging texts between the manuscripts provide the logical transition from one chapter to the next. Finally, Chapter 6 is an overall conclusion of the thesis, covering the contributions to original knowledge and future perspectives.

Contribution of Authors

The works presented in this thesis were all conducted by Kaidi Wang under the supervision of Dr. Xiaonan Lu. Kaidi Wang designed and performed the experiments, collected and analyzed the data, and prepared the manuscripts and thesis. Dr. Xiaonan Lu provided the research funding and facilities, guided Kaidi Wang in designing and conducting the experiments, as well as edited and reviewed the manuscripts and thesis. The contributions of other coauthors are listed below.

Chapter 3: Dr. Keng C. Chou and Dr. Xiangyun Ma assisted in the construction of the Raman tweezers system. Dr. Xiangyun Ma provided inputs to the data analysis.

Chapter 4: Dr. Xiangyun Ma contributed to the data analysis. Dr. Keng C. Chou edited and reviewed the manuscript.

Chapter 5: Dr. Yaxi Hu provided guidance on refining the methodology for the metabolomics study. Arusha Fleming contributed to collecting and testing the eggs.

Publications *([#] Co-first author; * Corresponding author)*

Research articles included in this thesis

1. **Wang, K**.[#], Ma, X.[#], Chou, K. C., Li, Q., & Lu, X.* (2022). Conditional generative adversarial network for spectral recovery to accelerate single-cell Raman spectroscopic analysis. *Analytical Chemistry, 94(2),* 577-582.
2. **Wang, K.**, Ma, X., Chou, K. C., & Lu, X.* An automated Raman tweezers system combined with microfluidics and machine learning for accurate identification and sorting of single bacterial cell. *Submitted.*
3. **Wang, K.**, Ma, X., Chou, K. C., & Lu, X.* Single-cell identification and characterization of

viable but non-culturable *Campylobacter jejuni* using Raman tweezers system coupled with machine learning. *Submitted.*

4. **Wang, K.**, Hu, Y., Fleming, A., & Lu, X.* Resuscitation of viable but non-culturable *Campylobacter jejuni* in embryonated chicken eggs and metabolomic profiling to identify the potential resuscitation stimuli. *Submitted.*

Research articles not included in this thesis

5. **Wang, K.**, Chen, J., Martiniuk, J., Ma, X., Li, Q., Measday, V., & Lu, X.* (2023). Species identification and strain discrimination of fermentation yeasts *Saccharomyces cerevisiae* and *Saccharomyces uvarum* using Raman spectroscopy and convolutional neural networks. *Applied and Environmental Microbiology*, *89*, e01673-23.
6. Longchamps, PL., He, Y., **Wang, K.**, & Lu, X.* (2022) Detection of pathogens in foods using microfluidic "lab-on-a-chip": A mini review. *Journal of Agriculture and Food Research, 10,* 100430.
7. Yu, Z., **Wang, K.,** & **Lu X.*** (2021). Flexible cellulose nanocrystal-based bionanocomposite film as a smart photonic material responsive to humidity. *International Journal of Biological Macromolecules*, 188, 385-390.
8. **Wang, K.**[#], Han, L.[#], Ma, L., Delaquis, P., Bach, S., Feng, J., & Lu, X.* (2020). Rapid determination of viable but non-culturable *Escherichia coli* O157:H7 and *Salmonella enterica* in fresh produce by loop-mediated isothermal amplification coupled with a propidium monoazide treatment. *Applied and Environmental Microbiology*, *86*, e02566-19.
9. Lv, R., **Wang, K.,** Feng, J., Heeney, D. D., Liu, D., & Lu, X.* (2019). Detection and quantification of viable but non-culturable *Campylobacter jejuni*. *Frontiers in Microbiology*, *10*, 2920.

10. **Wang, K.**[#], Chen, L.[#], Luo, Y.*, & Lu, X.* A new strategy for baseline correction based on spectral variations. *Submitted.*
11. Tong, S., **Wang, K**., Trimble, M., Chen, Y., Liu, L., Duan, J., Lu, X. * & Hsiao, W.* Longitudinal and cross-sectional sampling and whole genome sequencing of *Campylobacter* in a chicken abattoir reveals highly dynamic population structure. *Submitted*.
12. Huang, S., **Wang, K.,** Lu, X., & Wang, Y.* Cellulose nanocrystals constructed chevaux-de-frise: effect of surface topography on mechano-bactericidal activity. *Submitted*.

Presentations

1. **Oral presentation: Wang, K.,** Fleming, A., Lu, X.* Resuscitation of viable-but-nonculturable *Campylobacter jejuni* in embryonated chicken eggs. 2023 International Association for Food Protection Annual Meeting. Toronto, ON, Canada. July 16-19, 2023.
2. **Poster competition (2nd Place): Wang, K.,** Han, L., Fleming, A., Lu, X.* Fate of viable but non-culturable *Escherichia coli* O157:H7 and *Salmonella enterica* serovar Typhimurium on field-grown lettuce. 2023 International Association for Food Protection Annual Meeting. Toronto, ON, Canada. July 16-19, 2023.
3. **Oral presentation:** Liu, J., **Wang, K.,** Ma, L., Lu, X.* Qualitative risk assessment of viable-but-nonculturable *Escherichia coli* O157:H7 and *Salmonella enterica* serovar Typhimurium on field-grown Romaine lettuce. 2023 International Association for Food Protection Annual Meeting. Toronto, ON, Canada. July 16-19, 2023.
4. **Oral presentation: Wang, K.,** Lu, X.* Rapid identification of foodborne bacteria using single-cell Raman spectroscopic analysis. 2023 McGill University Lister Family Engaged Science Initiative and Let's Talk Science. Montreal, QC, Canada. May 25, 2023.

5. **Oral presentation: Wang, K.,** Ma, X., Lu, X.* Rapid identification of foodborne bacteria using single-cell Raman spectroscopic analysis combined with a conditional generative adversarial network. 2023 Spring American Chemical Society Annual Meeting. Indianapolis, IN, USA. March 26-30, 2023.
6. **Poster competition:** Longchamps, PL., **Wang, K.**, Fleming, A., Lu, X.* Formation of viable but nonculturable *Campylobacter jejuni* in simulated food processing environment. 2023 Spring American Chemical Society Annual Meeting. Indianapolis, IN, USA. March 26-30, 2023.
7. **Oral presentation: Wang, K.,** Ma, X., Lu, X.* Rapid identification of *Campylobacter jejuni* using single-cell Raman spectroscopic analysis combined with a conditional generative adversarial network. 2022 *Campylobacter*, *Helicobacter* and Related Organisms Conference. Yangzhou, China. November 14-19, 2022.
8. **Oral competition (2nd Place): Wang, K.,** Ma, X., Lu, X.* Rapid identification of foodborne bacteria using single-cell Raman spectroscopic analysis combined with a conditional generative adversarial network. 2022 International Association for Food Protection Annual Meeting. Pittsburgh, Pennsylvania, USA. July 31-August 3, 2022.
9. **Poster competition (2nd place):** Longchamps, PL., **Wang, K.**, Lu, X.* Formation of viable but nonculturable *Campylobacter jejuni* in simulated food processing environment. 2021 Undergraduate Student Research Award Poster Presentation of McGill University. Montreal, QC, Canada. September 16, 2021.

Awards and Accomplishments

1. Margaret A. Gilliam Fellowship, McGill University, 2020-2021

2. Grad Excellence Award, McGill University, 2020-2024
3. Clifford Wong Fellowship, McGill University, 2020-2023
4. Differential Fee Waivers for International Students, McGill University, 2021-2022
5. Fonds de recherche du Québec- Nature et technologies (FRQNT), 2022-2024
6. Travel Award for 2022 International Association for Food Protection (IAFP) Annual Meeting
7. 2nd Place in Student Presentation Award Competition, IAFP, 2022
8. Travel Award for 2023 American Chemical Society (ACS) Annual Meeting
9. Teranishi Graduate Fellowship in Food Chemistry, ACS, 2023
10. Developing Scientist Competition Awards, IAFP, 2023

Acknowledgement

First, I would like to express my deepest appreciation to my supervisor, Dr. Xiaonan Lu, for his support, encouragement, and unwavering trust throughout my doctoral journey. His passion towards research and scientific accomplishments have always inspired me to strive for excellence and pursue my own academic aspirations. Thanks for his invaluable mentorship in all perspectives that has not only shaped the development of this thesis but also significantly fostered my personal and professional growth.

I extend my sincere gratitude to my thesis committee members, Dr. Jennifer Ronholm, Dr. Stephane Bayen and Dr. Sara Mahshid, for their insightful comments, guidance, and dedication.

This thesis project would not have been completed without the support from my collaborators. My special thanks go to Dr. Keng C. Chou and Dr. Xiangyun Ma, for their participation in the construction of the Raman instrument. I would also express my heartfelt gratitude to Dr. Yaxi Hu for hosting me to work in her lab and training on essential knowledge and skills in metabolomics. I am also grateful to Dr. Yang Lin for the constructive advice that he provided on fluidic dynamics. Their expertise and supportive collaboration made the interdisciplinary projects manageable and enjoyable.

I would like to thank all my current lab mates at McGill and former lab mates at UBC, who have made the working environment intellectually stimulating and enjoyable. I will always treasure the friendship and happy memories that we have created together. Particularly, a heartfelt thank

goes to my “egg buddy”, MSc-to-be Arusha Fleming. Thank you for taking care of our tedious lab chores, being my special English coach, and making all the BSC time full of laughter.

I also appreciate all the company and support from my lovely friends in Sainte-Anne and elsewhere in the world. Each conversation, grocery shopping, meal gathering, and video-call with all of you have greatly enriched my life. I would thank my best friend, Mei Geng, for always having my back throughout the past 14 years. Although we are eight-thousand kilometers apart most of the time, she is the one I can share any joy and suffering. A special thank is owed to “the secret boy”, thank you for your patience, encouragement and always being there for me.

Last but certainly not least, I express my most sincere thanks to my parents and my sister. Their endless love, encouragement, and understanding have been the pillars of my courage and strength all the time.

Dedication

Dedicated to myself, for becoming stronger through the journey.

List of Figures

List of Tables

List of Abbreviations

AI-2	Autoinducer-2
ANOVA	Analyses of variance
AUC	Area under the curve
BS	Beam splitter
CCD	Charge-coupled device
CGAN	Conditional generative adversarial networks
CMOS	Complementary metal oxide semiconductor
CNN	Convolutional neural network
CTC	5-cyano-2,3-ditolyl tetrazolium chloride
D	Discriminator
DIC	Differential interference contrast
DM	Dichroic mirror
DVC	Direct viable count
EMA	Ethidium monoazide
F	Filter
FC	Fold change
FCM	Flow cytometry
G	Generator
GBS	Guillain-Barré syndrome
Grad-CAM	Gradient-weighted class activation mapping
GUI	Graphical user interface

HCA	Hierarchical cluster analysis
L	Lens
LAMP	Loop-mediated isothermal amplification
LC-MS	Liquid chromatography mass spectrometry
LOD	Limit of detection
LOS	Lipooligosaccharides
LReLU	Leaky rectified linear unit
M	Mirror
MALDI-TOF/MS	Matrix-assisted laser desorption ionization time-of-flight mass spectrometry
MHB	Mueller-Hinton broth
MHBA	Mueller-Hinton blood agar
MTBE	Methyl tert-butyl ether
NA	Numerical aperture
OC	Overnight culture
PBS	Phosphate buffered saline
PCA	Principal component analysis
PCM	Phase-contrast microscopy
PDMS	Polydimethylsiloxane
PEP	Phosphoenolpyruvate
PLS-DA	Partial least squares-discriminant analysis
PMA	Propidium monoazide

ppGpp	Guanosine tetraphosphate
QC	Quality control
QS	Quorum sensing
ROC	Receiver operating characteristic
Rpf	Resuscitation promotion factor
RSD	Relative standard deviation
RT	Reverse transcription
SM	Smoothing
SNR	Signal-to-noise ratio
SRGAN	Spectral recovery conditional generative adversarial network
SVM	Support vector machine
TCA	Tricarboxylic acid
TEM	Transmission electron microscopy
UHPLC	Ultra-high performance liquid chromatography
VBNC	Viable but non-culturable
VIP	Variable importance in the projection
WD	Working distance
WT	Wavelet transformation

Chapter 1: General Introduction

1.1 Introduction

Campylobacter is one of the leading causes of bacterial gastroenteritis worldwide (Kaakoush et al., 2015). It has been reported that approximately 1.5 million cases of campylobacteriosis occur annually in the United States (CDC, 2018). Among them, *C. jejuni* is responsible for over 95% of the total cases. Typical symptoms of *C. jejuni* infection include watery to bloody diarrhea, abdominal pain, and fever. Severe complications, such as Guillaine-Barré syndrome and reactive arthritis, might also be developed (Man, 2011). *C. jejuni* is a prevalent commensal bacterium in the intestinal tracts of domesticated and wild birds and mammals. The most common transmission route of *C. jejuni* is the consumption of contaminated food, particularly poultry products, raw milk or drinking water (J. Silva et al., 2011). *C. jejuni* is microaerobic and sensitive to environmental stresses because it lacks several important stress-response factors, including oxidative stress response factor SoxRS and global stationary phase stress response factor RpoS (Murphy et al., 2006). However, *C. jejuni* is highly prevalent in various food processing environments, such as poultry farms and slaughter facilities (Murphy et al., 2006). One of the hypotheses to interpret this paradox is that *C. jejuni* can survive in unfavorable conditions by entering a viable-but-non-culturable (VBNC) state (Bronowski et al., 2014).

VBNC state is a special physiological state in which bacterial cells retain membrane integrity and metabolic activity but cannot be cultivated on routine culture media (Oliver, 2005). Entering VBNC state has been recognized as a survival strategy for bacteria in response to adverse conditions, including temperature shift, starvation, oxidative stress, desiccation, presence of food preservatives and antibiotic treatment (Zhao et al., 2017). Food industries routinely apply diverse

physical and chemical stresses to inactivate foodborne pathogens and these stressors may possibly induce *C. jejuni* to enter the VBNC state (Gunasekera et al., 2002; Moreno et al., 2007). VBNC cells can evade conventional culture-based detection and demonstrate the capability to resuscitate and regain virulence under favorable conditions (Zhao et al., 2017). Therefore, the presence of VBNC *C. jejuni* in agri-foods poses a serious risk to the food industry and public health.

As conventional cultivation-based methods significantly underestimate the presence of VBNC cells, novel culture-independent and reliable approaches are demanded to identify *C. jejuni* in the VBNC state. VBNC cells are generally formed within a mixture of various bacterial populations (e.g., culturable cells and injured cells), further challenging the selective identification and characterization of VBNC population. Raman optical tweezers system, the combination of optical tweezers and Raman spectroscopy, has the potential to identify and manipulate single bacterial cells without labeling (Redding et al., 2015). Raman spectroscopy is a non-destructive technique that can rapidly characterize the biochemical compositions of a biological sample, enabling the discrimination of individual cells with unique phenotypic properties (Butler et al., 2016). The laser can also generate an optical gradient trapping to manipulate the cell at the focal spot (Huang et al., 2009). Microfluidic “lab-on-a-chip” system has been reported to be highly compatible with Raman optical tweezers system that allows automatic and continuous sorting of targeted cells (Chrimes et al., 2013; Landenberger et al., 2012). Therefore, the integration of Raman optical tweezers and microfluidic device holds promise for non-destructive identification and characterization of VBNC cells at single-cell level. Furthermore, the “fingerprinting” of single-cell Raman spectra can reveal the biochemical variations between VBNC cells and their

culturable counterparts, providing insights to the formation mechanism of the VBNC state. To the best of our knowledge, no study has utilized Raman optical tweezers for the single-cell identification and characterization of VBNC *C. jejuni*.

VBNC cells can resuscitate and restore pathogenicity under suitable conditions. Resuscitation is the process during which VBNC cells retrieve cultivability and metabolic activity to normal levels (Ramamurthy et al., 2014), posing a significant health concern. Therefore, it is necessary to understand the factors that can promote resuscitation and take effective measures to reduce the potential risk. Removal of stresses is the most common method to achieve the resuscitation of VBNC cells, such as nutrient supplementation for starvation induction and increasing temperature for low-temperature induction (Dong et al., 2020). However, resuscitation could not be achieved by simply reversing the adverse stresses in certain cases (Whitesides & Oliver, 1997). Presence of resuscitation stimulus is another critical factor to ensure successful resuscitation. VBNC *C. jejuni* has been reported to resuscitate in biological hosts, including chicken (Stern et al., 1994), mouse (Baffone et al., 2006) and Caco-2 cells (Chaisowwong et al., 2011). Embryonated chicken eggs also have the potential to provide biological stimuli for facilitating the resuscitation of VBNC cells. The eggs contain a sufficient and well-balanced supply of nutrients that might support the metabolic activity and regrowth of VBNC bacteria. Little is known about the resuscitation of VBNC *C. jejuni* in embryonated chicken eggs and the underlying mechanisms of VBNC resuscitation remain largely unexplored.

1.2 Hypotheses

1) Raman optical tweezers combined with microfluidics have the potential to achieve single-cell identification and sorting of *C. jejuni*.
2) VBNC *C. jejuni* cells can be discriminated from the culturable counterparts at the single-cell resolution using Raman optical tweezers and machine learning.
3) VBNC *C. jejuni* can resuscitate in embryonated chicken eggs and there are major compounds in eggs responsible for facilitating the resuscitation process.

1.3 Objectives

The main objective of this thesis is to better understand the formation, characteristics, and resuscitation of VBNC *C. jejuni* in agri-food systems. Three individual objectives are listed below:

1) To develop an automated Raman tweezers system coupled with a microfluidics device and machine learning for accurate identification and sorting of single *C. jejuni* cells.
2) To identify and characterize the VBNC *C. jejuni* at the single-cell level using the proposed Raman tweezers system and investigate the molecular compositional changes during the VBNC formation.
3) To investigate the resuscitation of VBNC *C. jejuni* in embryonated chicken eggs and to identify the major contributing compounds using untargeted metabolomics profiling.

Chapter 2: Literature Review

2.1 *Campylobacter*

2.1.1 Overview of *Campylobacter*

The genus *Campylobacter* was first proposed in 1963 (On, 2001) and currently comprises over 26 species (Kaakoush et al., 2015). *Campylobacter* species are Gram-negative bacteria and have small-size (0.2 to 0.8-µm in width by 0.5 to 5-µm in length), spiral and rod-shaped cells. Most *Campylobacter* species exhibit corkscrew-like motility by a single polar flagellum or bipolar flagella at both ends of the cells, with exception of no flagellum in *C. gracilis* (Debruyne et al., 2008). *Campylobacter* is non-spore-forming and requires fastidious conditions for growth. This bacterium is thermophilic with the optimal growth temperature between 37 to 42˚C and incapable of propagating at temperature below 30˚C due to the absence of cold shock protein genes (Joana Silva et al., 2011). Most *Campylobacter* species prefer to grow under microaerobic atmosphere conditions [CO_2 (3-10%), O_2 (3-5%), N_2 (80-85%)]. They are not able to survive at pH below 4.9 or above 9.0 and the optimal pH is at 6.5-7.5. *Campylobacter* is non-fermentative and the main energy sources are amino acids or intermediates of tricarboxylic acid cycle (Joana Silva et al., 2011). Most *Campylobacter* strains demonstrate antibiotic resistance to fluoroquinolones and cephalothin.

Campylobacter is well recognized as a major bacterial cause of human gastroenteritis disease worldwide. It was estimated to cause approximately 145,000 foodborne illnesses and 565 hospitalizations in Canada every year (Thomas et al., 2015), outnumbering the infections caused by other common foodborne pathogens, including *Salmonella*, *Listeria monocytogenes* and Shiga toxigenic *Escherichia coli*. *Campylobacter* illnesses also affect 14.3 per 100,000 population in

the United States (US) (Crim et al., 2014) and ~ 9.2 million cases were estimated in the European Union (EU) annually (Havelaar et al., 2013). The annual healthcare costs for campylobacteriosis can reach $80 million in Canada, $1.56 billion in the US, and €2.4 billion in the EU (Devleesschauwer et al., 2017), leading to a significant economic burden. *C. jejuni* is responsible for most campylobacteriosis cases (80-90%), followed by *C. coli* (10%) and an emerging species *C. lari* (<1%) (Robinson, 1981). The infection dose can be as low as 500 to 800 cells (Robinson, 1981). Common clinical symptoms of campylobacteriosis include diarrhea, fever, nausea, and abdominal pain, and usually occur 2 to 5 days following the ingestion of *Campylobacter*-contaminated food or water. Campylobacteriosis is usually self-limiting, but clinical interventions are required for severe and prolonged infections. It can also lead to post-infection autoimmune complications, namely Guillain-Barré syndrome (GBS), Miller Fisher syndrome and reactive arthritis. *Campylobacter* infection can affect individuals across all age groups but is particularly prevalent in children (less than 4 years old), elderly and immunocompromised patients (Kaakoush et al., 2015).

Campylobacter species are commensal bacteria commonly found in the intestinal tract of various animals, including avian, sheep, swine and cattle. Consumption of contaminated food, such as undercooked poultry meat, raw milk and drinking water, is one of the major transmission routes of *Campylobacter* infections. Poultry product is considered as the primary source of *Campylobacter* contamination, accounting for 50%-80% of the human campylobacteriosis (Hazards, 2011). High prevalence of *Campylobacter* species has been reported in broiler chickens, poultry farms and their surrounding environment. Domesticated animals are also significant reservoirs of *Campylobacter* (Blaser et al., 1980) and thus lead to the frequent

contamination of meats and unpasteurized dairy products. Besides, direct contact with farm and companion animals is another risk factor for *Campylobacter* infections.

2.1.2 Nutrient acquisition and metabolism of *C. jejuni*

C. jejuni exhibits a remarkable capability to colonize in the gastrointestinal tract of diverse hosts and survive in different environments, including water systems, farms, processing plants and food products. Although the metabolism of nutrient acquisition in *C. jejuni* has not been completely elucidated yet, a flexible metabolic pattern is necessary to make efficient use of the nutrients available in each setting. *C. jejuni* is distinguished from other enteropathogenic pathogens, such as *Salmonella*, *Listeria monocytogenes* and enteropathogenic *E. coli,* due to its limited capability to catabolize carbohydrates (Parkhill et al., 2000). Most of the *C. jejuni* strains are unable to utilize glucose, galactose and other sugars as they lack the essential transporters and some key enzymes involved in the glycolytic pathway. For example, *C. jejuni* does not contain glucokinase that is required for the phosphorylation of extracellular glucose (Velayudhan & Kelly, 2002). Phosphofructokinase is also absent in *C. jejuni*, which phosphorylates fructose-6-phosphate to fructose-1,6-bisphosphate in glycolysis. A special L-fucose pathway has been identified in certain *C. jejuni* strains (Stahl et al., 2011), but the mechanisms underlying this metabolic pathway require further exploration.

Amino acids are recognized as the primary nutrient and energy sources for *C. jejuni.* A limited selection of growth-promoting amino acids are utilized by this pathogen, typically with a sequential order of serine, aspartate, asparagine, and glutamate, although this preference may differ among various strains (Stahl et al., 2012). Proline can also be metabolized by *C. jejuni*

when other nutrients are deficient (Weingarten et al., 2009). Notably, these amino acids are highly abundant in both chicken and human intestines (Parsons, 1984), providing sufficient nutrient profiles for the *in vivo* growth of *C. jejuni*. Specific transporters are required to acquire these amino acids (**Figure 2.1**) (Burnham & Hendrixson, 2018). For instance, the uptake of serine relies on SdaC protein (Velayudhan et al., 2004), and the Peb1 system serves as a transporter for both aspartate and glutamate (Del Rocio Leon-Kempis et al., 2006).

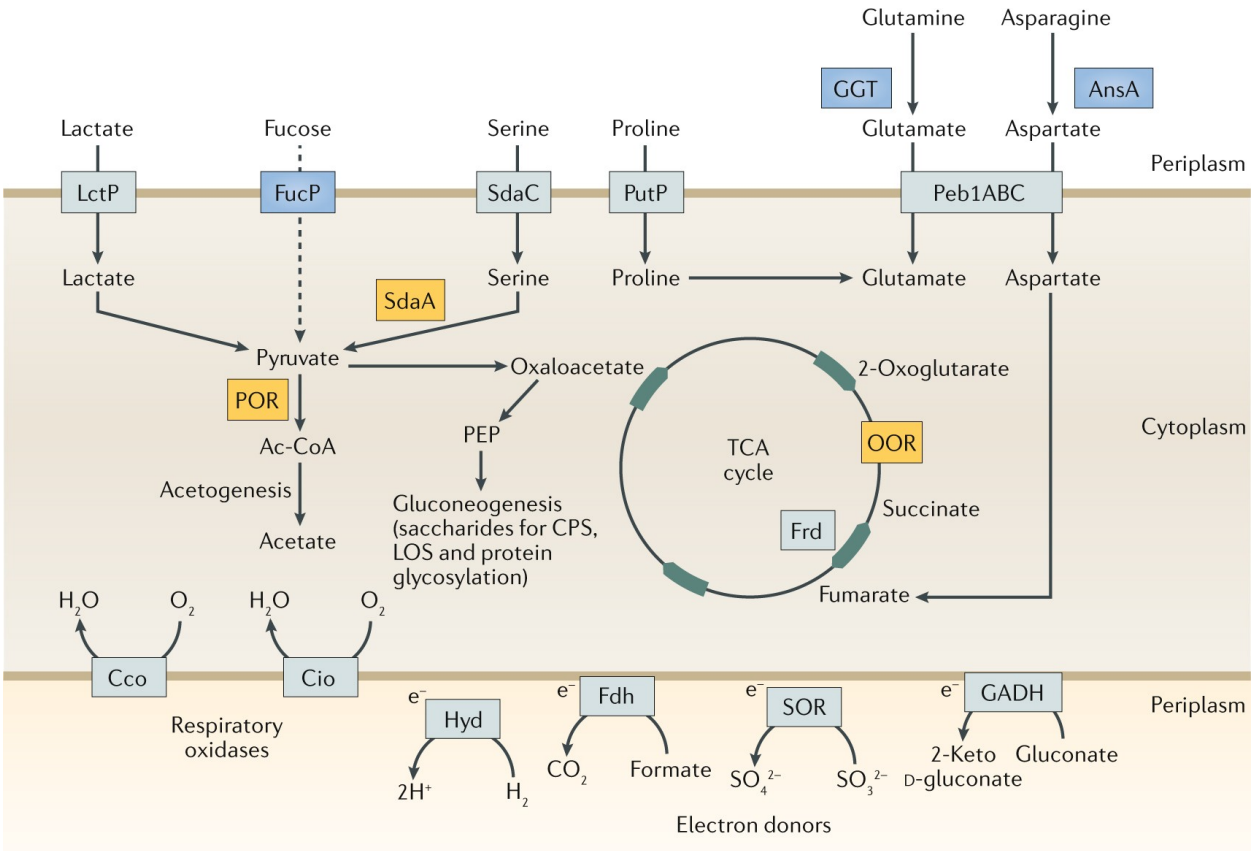

Figure 2.1 Summary of major metabolic pathways involved in *Campylobacter jejuni*. Amino acids and keto acids serve as the primary carbon sources that fuel the tricarboxylic acid (TCA) cycle and various anabolic pathways in *C. jejuni*. Lactate and fucose are also precursors of pyruvate, but only certain *C. jejuni* strains possess the ability to transport and metabolize fucose. Respiratory oxidases that utilize oxygen as the primary terminal electron acceptor are displayed

at the bottom, including the cbb3-type cytochrome c oxidase (Cco) and the cyanide-insensitive cytochrome bd-like quinol oxidase (Cio) (Burnham & Hendrixson, 2018).

Within *C. jejuni* cells, the catabolism of serine is not only associated with the synthesis of over ten other amino acids but it also acts as a precursor for pyruvate (Gao et al., 2017). Pyruvate subsequently participates in the acetogenesis by being catabolized into acetyl-CoA and fuels the tricarboxylic acid (TCA) cycle through the conversion into oxaloacetate. Transformation of oxaloacetate into phosphoenolpyruvate is an initiation step for gluconeogenesis to generate saccharides for various purposes. Besides, glutamate and aspartate can enter the TCA cycle by being converted into 2-oxoglutarate and fumarate, respectively (Guccione et al., 2008).

Organic acids and intermediates of TCA cycle also play crucial roles in the central metabolism of *C. jejuni*. Previous studies identified pyruvate, fumarate, 2-oxoglutarate, malate, succinate and lactate in *C. jejuni* as chemoattractants (Vegge et al., 2009; Wright et al., 2009). Lactate is taken up into *C. jejuni* via the transporter protein LctP and subsequently catabolized into pyruvate (Thomas et al., 2011), an essential carbon substrate. *C. jejuni* relies predominantly on the TCA cycle to fulfill its energy requirements. It demonstrates the ability to transport various TCA cycle intermediates and directly utilizes them as nutrients. For instance, the permease KgtP enables the transportation of 2-oxoglutarate, and succinate, fumarate and malate are transported via C_4-dicarboxylate transporters, namely DcuA and DcuB (Guccione et al., 2008). Another previous work indicated that *C. jejuni* could also use pyruvate as the carbon source when cultivated on growth medium (Mendz et al., 1997). However, no specific transporters for pyruvate have been identified in *C. jejuni*, leaving the mechanism of pyruvate transportation to be unknown.

C. jejuni harbors a distinct and complex respiration chain that contains various electron donors and acceptors (Hofreuter, 2014). Genome sequence analysis revealed the presence of two terminal oxidases in *C. jejuni*, including the cbb3-type cytochrome c oxidase (Cco) and the cyanide-insensitive cytochrome bd-like quinol oxidase (Cio) (Sellars et al., 2002). Cco demonstrates high oxygen affinity and is mainly responsible for respiration under oxygen-limited environment. In addition, *C. jejuni* is equipped with other oxygen-independent respiratory chains that employ specific metabolites (e.g., SO_3^{2-}, formate and gluconate) as electron donors (Sellars et al., 2002). A variety of oxidases were involved in these processes, such as hydrogenase (Hyd), formate dehydrogenase (Fdh), sulfite:cytochrome c oxidoreductase (SOR), and gluconate dehydrogenase (GADH). Taken together, acquisition of highly diverse nutrients and metabolic pathways enable *C. jejuni* to overcome the resistance and thrive in various hosts and environmental conditions.

2.2 Survival strategies of *C. jejuni*

C. jejuni is generally considered as a fastidious microorganism that is sensitive to various stresses, such as low pH, oxidative stress, temperature fluctuation, osmotic pressure and insufficient nutrients (Kaakoush et al., 2015). However, this bacterium is widely spread in the environment and agri-food systems as one of the major foodborne pathogens. This implies that *C. jejuni* can adopt different strategies to survive under unfavorable conditions. Understanding the stress response mechanisms in *C. jejuni* can aid in reducing the prevalence of this pathogen and mitigating the incidence of campylobacteriosis. Major bacterial stress response strategies identified in *C. jeuni* include the activation of stress response systems, biofilm formation, and entry into a dormancy state (Kim et al., 2021).

C. jejuni lacks several stress adaptive responses that are commonly present in other foodborne bacterial pathogens, such as the global stationary-phase sigma factor RpoS, cold shock protein and oxidative stress regulator SoxRS (Park, 2002). Alternatively, other regulatory systems have been identified and characterized in *C. jejuni* depending on the stresses encountered. For example, heat shock proteins, such as HtrB, HrcA and DnaK, were synthesized in *C. jejuni* when subjected to elevated temperature during pasteurization or cooking (Parkhill et al., 2000). Under starvation conditions, *C. jejuni* can activate a stringent response encoded by *spoT* gene and produce more guanosine tetraphosphate (ppGpp) to downregulate transcription and upregulate amino acid synthesis (Park, 2002). Osmotic pressure represents another prevalent stressor encountered during food processing and *in vivo* colonization. ATP binding cassette transporter regulator *htrB* gene and poly P synthesis gene *ppk1* have been reported to be responsible for the hyperosmotic resistance in *C. jeuni* (Kim et al., 2021). A variety of stress response genes that contribute to the survival of *C. jejuni* under different adverse conditions are comprehensively summarized in **Table 2.1 (**reviewed in (Bolton, 2015; Kim et al., 2021; Park, 2002)).

The formation of biofilm also plays a critical role in the persistence of *C. jejuni* in the environment. Biofilms are generally referred to matrix-enclosed bacterial communities that are adherent to interfaces or surfaces (Costerton et al., 1995). *C. jejuni* has the ability to form mono- or multi-species biofilms under both laboratory conditions and natural environment, such as the water supplies and plumbing systems in poultry-related facilities and food processing plants (Reuter et al., 2010). Bacterial cells within the biofilms are well protected and display a remarkably higher resistance to the external stress compared to their planktonic counterparts

(Fux et al., 2005). For instance, previous studies highlighted that *C. jejuni* could survive in water systems and atmospheric environment for up to twice of the duration by harnessing the protective mechanism of biofilm formation (Asakura et al., 2007; Joshua et al., 2006). Furthermore, biofilm enhances the resistance of *C. jejuni* to disinfectants and antimicrobial agents, making the eradication of this pathogen to be more challenging.

Entering a dormancy state is another key strategy employed by *C. jejuni* in response to stressors. Two dormancy phenomena have been described in non-spore-forming bacteria, namely persisters and viable but non-culturable (VBNC) state. Antibiotic persisters are defined as a subpopulation of bacteria exhibiting superior tolerance to antibiotic treatment despite that the majority of the population are susceptible to the same treatment (Fisher et al., 2017). In contrast to antibiotic-resistant cells that harbor heritable genetic determinants, the formation of persisters is believed to arise stochastically due to the fluctuations of gene expression or be induced by environmental factors, such as antibiotics treatment, low pH, oxidative stress and starvation (Wood et al., 2013). Recent studies revealed that persister cells of *C. jejuni* formed upon exposure to penicillin G (Morcrette et al., 2020) and ciprofloxacin (Ovsepian et al., 2020), potentially leading to recurrent infections and prolonged treatment. The emergence of bacterial persisters has drawn substantial attention in biomedicine and healthcare due to their significant potential to undermine antibiotic efficacy.

In addition, *C. jejuni* is able to enter VBNC state to combat stressful conditions. VBNC state describes a special physiological condition in which bacterial cells maintain the membrane integrity and minimal metabolic activity but are incapable of forming colonies on the laboratory

media (Ramamurthy et al., 2014). VBNC cells can evade the routine culture-based detection and survive for extended periods under hostile environment due to enhanced tolerance to a wide range of stresses. Furthermore, VBNC cells possess the ability to revert to the culturable state and regain the virulence when the environmental conditions turn to favorable, posing a significant health concern. The formation of VBNC *Campylobacter* was first reported by Rollins and Colwell in 1986 (Rollins & Colwell, 1986) and more studies have emerged regarding the induction conditions, molecular mechanism and resuscitation of VBNC *C. jejuni*. Further elaboration of the VBNC state will be provided in the next sections.

Table 2.1 Stress response factors that are responsible for the survival of *Campylobacter jejuni* under different adverse conditions.

Stressor	Gene	Function	Reference
Nitrosative stress	*nrfA*	Nitrite reductase, formate-dependent	(Einsle, 2011)
	cgb	Single-domain hemoglobin in mediating resistance to nitric oxide	(Elvers et al., 2004)
	nssR	Single-domain hemoglobin	(Avila-Ramirez et al., 2013)
Heat shock	*htrB*	Promotes abiotic and biotic stress tolerance	(Poli et al., 2012)
	htrA	High-temperature requirement A-like protease and chaperones	(Svensson et al., 2008)

	groES/groEL	Chaperonin	(Laranjo & Oliveira, 2011)
	dnaK	Chaperonin	
	hslU	Proteomics analysis of drought stress-responsive proteins	(Xu et al., 2009)
	hrcA	Conserved ATP-dependent proteases to stress tolerance and virulence	(Cohn et al., 2007)
Starvation	*ppk1*	Quorum sensing genes/inhibiting polyphosphate kinase	(Sarabhai et al., 2015)
	spoT	Cytosolic ascorbate peroxidase/peroxiredoxins	(Gangaiah et al., 2010)
	ppk2	Adenylate cyclase gene/membrane location of the protein	
Osmotic pressure	*htrB*	ATP binding cassette transporter components	(Lin et al., 2009)
	ppk1	Inhibiting polyphosphate kinase	(Sarabhai et al., 2015)
	cj1226c	Influences biofilm formation	(Svensson et al., 2008)
Low pH	*htrB*	ATP binding cassette transporter components PaqP and PaqQ	(Lin, 2008)

Oxidative stress	*spoT*	Quorum sensing genes /inhibiting polyphosphate kinase	(Sarabhai et al., 2015)
	perR	Negative regulator of the response to peroxide stress	(Park, 2002)
	sodB/sodF	Iron cofactored superoxide dismutase	
	ahpC	Alkyl hydroperoxide reductase	
	cj1556	Influence biofilm formation	(Svensson et al., 2008)
Global regulation	*crp/fnr*	Member of the catabolite gene activator protein/anaerobic regulatory protein family	
	rpoD	The primary sigma factor	

2.3 Viable but non-culturable (VBNC) state

VBNC state has been recognized as a survival strategy adopted by many bacteria to cope with adverse environmental conditions. VBNC state was firstly proposed in 1982 and it is a unique physiological state where bacteria cannot grow on the conventional culture media but can still maintain basic metabolic activity. Up until now, over 100 species of microorganisms comprising 68 foodborne pathogenic bacteria have been described to enter the VBNC state, such as *Campylobacter*, *Salmonella*, *Listeria*, *Vibrio*, *Yersinia*, and *E. coli* O157:H7 (Zhao et al., 2017).

Food products are easily exposed to stressful environmental conditions during processing, transportation and storage, such as oxidative stress (atmospheric environment), extreme

temperature (cooking or refrigeration), low pH (acidic additives or fermentation), antimicrobials (disinfection treatment) and osmotic pressure (addition of salt or other food preservatives) (Begley & Hill, 2015). The pathogenic bacteria existing in the food products therefore have a high chance to enter the VBNC state when exposed to these harsh conditions. For example, *C. jejuni* strains were induced into the VBNC state under aerobic (Oh et al., 2015), low temperature (Chaisowwong et al., 2012) and acidic conditions (Chaveerach et al., 2003), respectively. Formation of *E. coli* O157:H7 VBNC cells were observed on spinach and lettuce during exposure to low temperature (Dinu & Bach, 2013) and UV treatment (Zhang et al., 2015). The presence of VBNC pathogens has been widely documented in different types of food products, including poultry (Chen et al., 2019), grapefruit juice (Nicolo et al., 2011), vegetables (Dinu & Bach, 2011), seafoods (Cao et al., 2019) and dairy products (Barron & Forsythe, 2007).

VBNC bacterial cells demonstrate a series of distinct features compared to the culturable cells, involving morphological changes, reduced level of gene expression and metabolism, as well as enhanced tolerance to physical and chemical stresses. VBNC cells are generally considered to be non-pathogenic, but the virulence of VBNC pathogens can be maintained at a low level or regained after resuscitation under favorable conditions and subsequently cause infections (Zhao et al., 2017). For example, virulence-associated genes (*flaA, flaB, cadF,ciaB,cdtA,cdtB*, and *cdtC*) were still expressed minimally in the VBNC cells of *C. jejuni* and the VBNC cells retained the capability to invade human Caco-2 cells *in vitro* (Chaisowwong et al., 2012). The VBNC cells of *Listeria monocytogenes* resuscitated in the embryonated eggs demonstrated similar level of virulence compared to that of culturable cells (Cappelier et al., 2007). Substantial evidence has also indicated the potential involvement of VBNC pathogens in foodborne outbreaks. For

instance, a foodborne incident in Japan was attributed to salted salmon roe that was possibly contaminated by VBNC *E. coli* O157 (Makino et al., 2000). In another outbreak caused by dried squids, the presence of VBNC *Salmonella* Oranienburg was observed and confirmed by the following resuscitation (Asakura et al., 2002). Therefore, the presence of VBNC pathogens in agri-food systems poses a serious risk to human health and a comprehensive understanding of the VBNC state is needed to effectively address this challenge.

2.4 Detection of VBNC bacteria

Considering the significant risk posed by foodborne pathogens in the VBNC state, accurate and reliable methods to detect VBNC cells are crucial to ensuring food safety and public health. As VBNC cells are unable to be cultivated on the conventional media, alternative culture-independent techniques have been developed for rapid diagnosis of VBNC cells based on their viability. Previous reviews summarized the common detection methods currently used for VBNC pathogens (**Figure 2.2**), including cell staining and microscopic enumeration, nucleic acid amplifications, biosensors, and spectroscopy-based methods (Dong et al., 2020; Gao et al., 2021; Zhao et al., 2017).

Direct viable count (DVC) has been firstly used to detect VBNC cells based on the absorption ability of substate (Kogure et al., 1979). VBNC cells can elongate upon exposure to antibiotics (e.g., nalidixic acid, aztreonam, ciprofloxacin), thus enabling the direct cell enumeration under microscope (Xu et al., 1982). Double staining with 5-cyano-2,3-ditolyl tetrazolium chloride (CTC) and 4,6-diamino-2 phenylindole (DAPI) is a more effective detection method (Rodriguez et al., 1992). With the enzymes of the respiratory chain in the VBNC cells, CTC is catalyzed into

red fluorescent salt while DAPI can counterstain all the cells with blue fluorescence, allowing the quantification of both VBNC and total cells simultaneously (Cappelier et al., 2005). However, both methods are hindered by relatively low sensitivity.

Recently, LIVE/DEAD BacLight fluorescence staining assay has been established for detection of VBNC bacteria based on the assessment of cell membrane integrity (Cunningham et al., 2009; Liu et al., 2017). It contains two fluorescent nucleic acid stains, green-fluorescent dye SYTO 9 and red fluorescent propidium iodide (PI). SYTO 9 can enter both viable and dead cells, while PI can only penetrate dead cells with compromised cell membranes and stain them in red. The presence of VBNC cells (in green) can be examined by fluorescence microscopy or quantified using fluorescence microplate reader and flow cytometry (FCM). The combination with FCM significantly improves the detection sensitivity and achieves superior results compared to DVC or CTC staining methods (Postnikova et al., 2015; Santander et al., 2018).

Molecular-based diagnostic approaches have also emerged for determination of VBNC bacteria. These methods target on evaluation of gene expression or nucleic acid amplifications, such as reverse transcription quantitative polymerase chain reaction (RT-qPCR), real-time PCR (qPCR) and loop-mediated isothermal amplification (LAMP). Bacterial mRNAs have extremely short half-life of 3-5 min and thus can be regarded as a biomarker for cell viability (Sheridan et al., 1998). Housekeeping genes, including *16S*/*23S rRNA* and *rpoS* genes, are usually constantly expressed in the VBNC cells and selected as the target genes of RT-qPCR to detect bacteria in the VBNC state. RT-qPCR has been utilized in the identification of various VBNC pathogens, such as *Salmonella* (Fey et al., 2004), *Vibrio parahaemolyticus* (Coutard et al., 2007) and *E. coli*

(Lothigius et al., 2010). However, lack of stably expressed genes and low purification of mRNA restrict the application of RT-qPCR in certain cases.

Conventional qPCR has been widely used for bacterial detection and quantification, but it is not possible to directly distinguish the DNA from dead and viable cells. To circumvent this issue, ethidium monoazide (EMA) and propidium monoazide (PMA) have been coupled with qPCR to selectively quantify DNA from viable cells (i.e., VBNC cells) (Chang & Lin, 2018; Kibbee & Örmeci, 2017; Lothigius et al., 2010). EMA and PMA are membrane-impermeable dyes that can only penetrate the dead cells with damaged cell membrane to bind to the intracellular DNA. In the subsequent qPCR, the amplification of DNA from dead cells are therefore suppressed and only viable cells are quantified. PMA-qPCR has been applied to detect VBNC *E. coli* O157:H7 on lettuce and spinach leaf and a limit of detection (LOD) of 10^3 CFU/g leaf was achieved (Dinu & Bach, 2011). Another DNA amplification technique, LAMP, has also been combined with PMA to quantify VBNC cells. Lu and coauthors successfully established species-specific PMA-LAMP assays for determination of *S. enterica* and *E. coli* VBNC cells in both pure culture and fresh produce, respectively (Han et al., 2020). In another study, PMA-LAMP was used to detect the viable *V. parahaemolyticus* with a 10-fold higher LOD compared to that of PMA-qPCR, while shorter analysis time was required in PMA-LAMP assay (i.e., 45 min vs 1 h) (Zhong et al., 2016).

VBNC microbial populations exhibit distinct characteristics of the cellular compositions compared to the culturable counterparts, which might be considered as markers for selective detection of VBNC bacterial cells. Recently, spectroscopy-based methods have been adopted for

the diagnosis of VBNC cells based upon their unique biochemical compositions, such as mass spectrometry (MS) and Raman spectroscopy (Gao et al., 2021). MS is a powerful analytical tool that can precisely separate and identify various molecules by measuring their mass to charge ratio. The compositional investigation of the whole bacterial cells can be easily achieved especially with the development of matrix-assisted laser desorption ionization time-of-flight mass spectrometry (MALDI-TOF MS) (Ashfaq et al., 2022). MALDI-TOF/MS was applied to evaluate *E. faecalis* in different states, including the culturable, VBNC and resuscitated cells (Kuehl et al., 2011). VBNC *E. faecalis* were clearly distinguished from other populations using principal component analysis based on their mass spectra.

Raman spectroscopy is a non-destructive vibrational spectroscopic technique that characterizes the molecular structure and biochemical compositions of samples based upon light scattering. A Raman spectrum can provide comprehensive compositional information of the entire bacterial cell (Stöckel et al., 2016), including nucleic acids, protein, carbohydrates and lipids (Huang et al., 2004). This "molecular fingerprinting" enables the discrimination of different bacterial species or even the same species under different physiological states. Raman spectroscopy stands as a versatile and valuable tool for bacterial detection due to its rapid, non-destructive nature and high specificity. In a recent study, Raman spectroscopy combined with heavy water (D_2O) labeling was conducted to distinguish VBNC cells of *Aeromonas*, *Pseudomonas*, *E. coli*, and *S. aureus* based on the intensity ratio of C-D band to C-H band (Guo et al., 2019). The metabolic activities of these VBNC bacteria could be quantified at single cell level in a rapid and reliable manner. Isotope labeled Raman spectroscopy has also been applied to recognize the metabolic biomarker of chlorine-induced VBNC *Pseudomonas aeruginosa* (Qi et al., 2022). However, due

to the inherent weakness and intricate nature of Raman scattering signals, subtle spectral differences among closely related samples (i.e., VBNC and culturable cells) might not be easily discerned by traditional chemometrics and pose challenges to accurate detection. With the state-of-art machine learning algorithms, the minor spectral variation among different samples could be better interpreted and thus the classification accuracy can be enhanced (Lussier et al., 2020). Therefore, it is promising to achieve the identification of VBNC cells directly based on the spectral features without isotope labeling. Furthermore, the laser employed in the Raman spectroscopic system can also create a gradient optical trap, termed as optical tweezer, allowing the manipulation of the focused cell(s) without physical contact (Huang et al., 2009). Therefore, Raman optical tweezers can achieve simultaneous characterization and manipulation of single bacterial cells without labeling and destruction (Fang et al., 2019), making the identification process more efficient and potentially applicable in real-time scenarios. The applications of using Raman optical tweezer to identify and sort VBNC cells are currently limited and warrant further exploration.

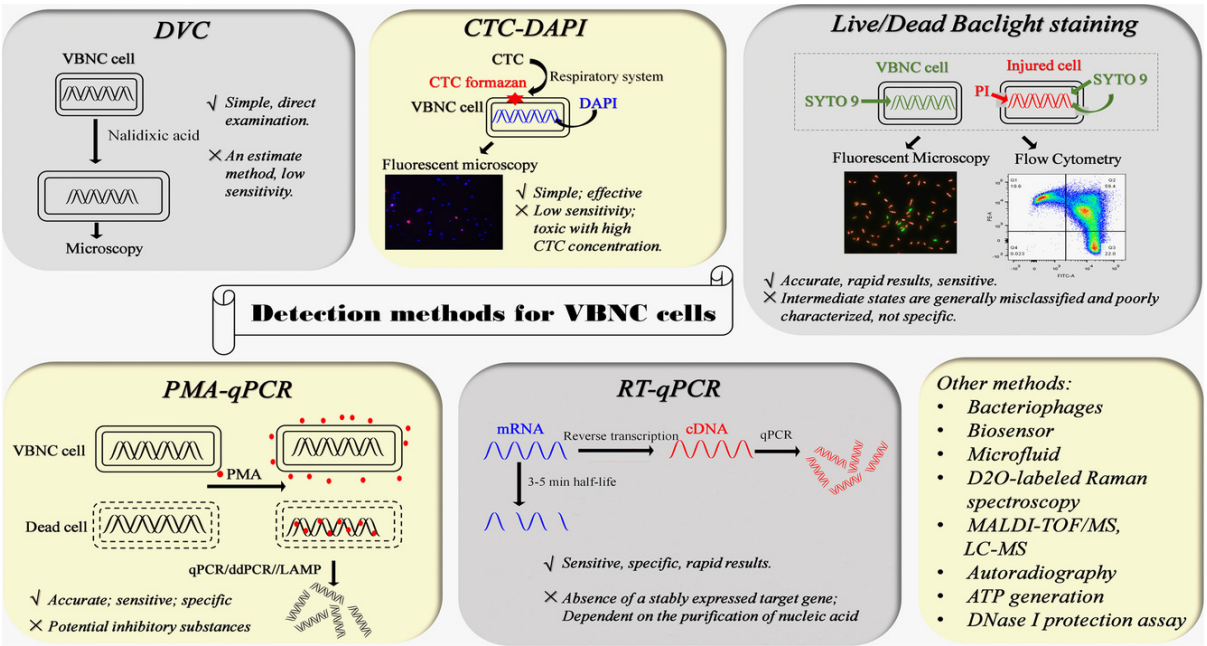

Figure 2.2 Summary of major detection methods used for VBNC cells. DVC: direct viable count; CTC: 5-cyano-2,3-ditolyl-tetrazolium chloride; PMA-qPCR: propidium monoazide combined with real-time PCR; RT: reverse transcription; MALDI-TOF/MS: matrix-assisted laser desorption ionization time-of-flight mass spectrometry; LC-MS: liquid chromatography mass spectrometry.

2.5 Resuscitation of VBNC bacteria

Resuscitation refers to the process in which VBNC cells restore the culturability and normal metabolic activities under favorable conditions (Dong et al., 2020). The resuscitated VBNC cells could resume the virulence and potentially lead to infections. To date, more than 20 species of foodborne pathogens have been verified to possess the capability of resuscitating from the VBNC state (Zhang et al., 2021), posing a significant threat to food safety and human health. Therefore, it is imperative to investigate the factors that can facilitate the resuscitation and implement effective measures to mitigate the potential risks.

2.5.1 Resuscitation conditions

As VBNC state is usually induced by adverse stresses, removal of the external stresses is the most common method to achieve the resuscitation. For example, temperature upshift has been applied to resuscitate the VBNC cells triggered by low temperature (Abdallah et al., 2008; Combarros et al., 2016; Mariam et al., 2017). VBNC cells formed under starvation induction can be recovered by supplement of rich nutrients in the culture media (Pasquaroli et al., 2013; Pinto et al., 2011). In another study, *E. coli* O104:H4 lost the culturability upon exposure to toxic concentrations of copper ions and relieving the stress using copper-ion chelation could facilitate its resuscitation (Aurass et al., 2011).

However, simply reversing the stresses are unable to promote the resuscitation of some VBNC bacterial cells. For instance, VBNC *V. vulnificus* induced at low temperature could not grow on nutrient-rich medium after cultivation at elevated temperatures (Pasquaroli et al., 2013). Up to now, over 100 bacterial species can enter VBNC state while the resuscitation has only been confirmed in approximately 20 species, indicating that it is challenging to identify appropriate conditions to support the resuscitation of most VBNC bacteria (Zhang et al., 2021). Besides the physical stimuli such as temperature upshift, various chemical stimuli have been proven to mediate the resuscitation, including sodium pyruvate (Liao et al., 2018; Morishige et al., 2013; Pasquaroli et al., 2013), vitamin B (Sun et al., 2008), amino acids (Pinto et al., 2011), and Tween 20 (Zhong et al., 2009). Sodium pyruvate is one of the primary stimuli for VBNC resuscitation by serving as a carbon source and a reactive oxygen scavenger. It can facilitate the biosynthesis of DNA and proteins in VBNC bacterial cells and thus initiate the resuscitation.

VBNC cells can also achieve resuscitation in biological hosts, such as eukaryotic cells, embryonated chicken eggs, animal models and human volunteers (Amel et al., 2008; Dong et al., 2020). VBNC cells of *V. cholerae* and *C. jejuni* reverted to a culturable state after co-cultivation with HT-29 cells (Imamura et al., 2015) and Caco-2 cells (Chaisowwong et al., 2012), respectively. Resuscitation of VBNC *C. jejuni* has also been verified after passage through embryonated chicken eggs (Cappelier et al., 1999), 1-week-old chicks (Stern et al., 1994) and mouse intestines (Baffone et al., 2006). Biological hosts generally comprise diverse compositions and provide a suitable environment for promoting VBNC resuscitation. However, the specific biological stimuli within the host that can contribute to the resuscitation of VBNC cells remain unclear and further research is demanded.

2.5.2 Resuscitation mechanisms

The mechanisms of VBNC resuscitation are still largely unknown but several putative mechanisms have been proposed to better understand this process (**Figure 2.3**). Quorum sensing (QS) signaling has been reported to be associated with the resuscitation of VBNC cells. Ayrapetyan and coauthors validated that autoinducer-2 (AI-2) could restore the culturability of VBNC *V. vulnificus* cells while its AI-2 deletion mutant did not show resuscitation capability (Ayrapetyan et al., 2014). RpoS protein also plays an important role in the AI-2 associated resuscitation process, as the mutant strains with *rpoS* deletion could not be recovered with the addition of exogenous AI-2 (Bari et al., 2013). The functional mechanism of AI-2 is probably related to the increased antioxidative capability and illustrated in **Figure 2.3AB**. Briefly, the *rpoS* expression and catalase (KatG) production are decreased in VBNC bacterial cells without the presence of AI. When the concentration of AI-2 is high, it could bind to the specific receptor

on the cell membrane and eventually upregulate the expression of catalase and lead to VBNC resuscitation (Dong et al., 2020).

Resuscitation promoting factor (Rpf) also assumes a crucial role in the regrowth of VBNC bacterial cells (Mukamolova et al., 1998). Rpf is a conserved protein that is produced by the growing cells and can be secreted to extracellular space as autocrine or paracrine signaling molecule. Rpf-mediated resuscitation has been firstly discovered in *Micrococcus luteus* that comprises five Rpf-like proteins (Kaprelyants et al., 1994). The presence of Rpf has also been identified in other bacterial species, including *L. monocytogenes*, *Mycobacterium*, *Streptomyces*, *Corynebacterium* and *S. enterica* serovar Typhimurium (Gupta & Srivastava, 2012; Panutdaporn et al., 2006; Pinto et al., 2015; Ramamurthy et al., 2014; Zhu et al., 2003). Several speculations have been proposed regarding the working mechanism of Rpf (Dong et al., 2020). As shown in **Figure 2.3C**, Rpf might directly bind to the receptors on the membrane of VBNC cells and trigger the resuscitation (Pinto et al., 2015). It is also hypothesized that Rpf exhibits lysozyme-like activity to break the peptidoglycans on the cell wall (Mukamolova et al., 2006). As the thickened peptidoglycan layer of VBNC cells impedes cell division, cleavage of extra cross-linking by Rpf can partially remove this barrier and resume cell growth (Keep et al., 2006). In another hypothesis, the fragments of peptidoglycan (i.e., free muropeptide) may function as 'second messengers' and interact with other receptors to promote the resuscitation of VBNC bacterial cells (Nikitushkin et al., 2013).

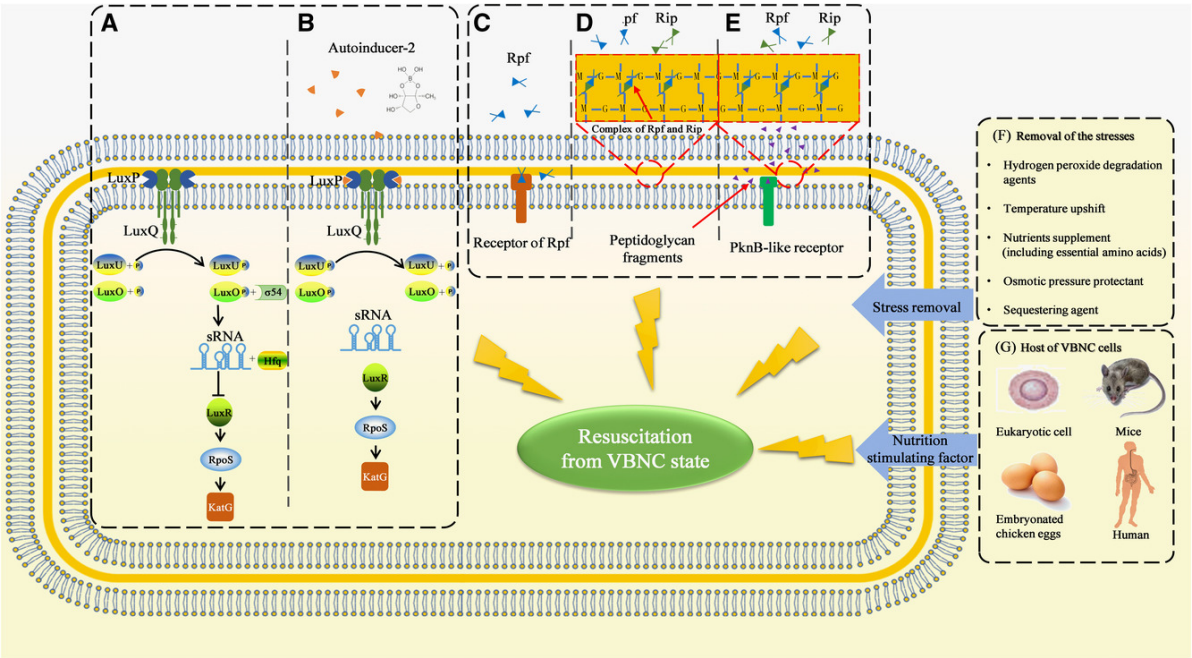

Figure 2.3 Putative mechanisms for the resuscitation of VBNC cells. (A) Quorum-sensing signal compound autoinducer-2 (AI-2) is considered as a vital promoting factor for the resuscitation of VBNC cells. Without AI-2, the production of catalase (KatG) is reduced, causing a high sensitivity to peroxide and loss of culturability. (B) When a high concentration of AI-2 (yellow triangle) is present, it can bind to LuxP/Q and eventually increase the production of KatG. This elevated antioxidant activity enables the revival of VBNC cells. (C) Resuscitation promotion factor (Rpf) can bind to the receptors on the VBNC cell membrane and initiate the resuscitation. (D) A complex containing Rpf and Rif is able to cleave the glycosidic and peptide bonds and modify the cell wall compositions. Resuscitation of VBNC cells is then triggered by the remodel of cell wall. (E) Peptidoglycan fragments (purple triangles) can be generated from the cell wall by Rpf and Rif complex, which will bind to the PknB-like receptors to stimulate the resuscitation. (F) Removal of external stress is crucial to the VBNC resuscitation. (G) Various biological hosts can provide essential nutrients or stimulating factors to promote the resuscitation of VBNC cells. (Dong et al., 2020)

Connecting Text

Chapter 2 provided a comprehensive review of *Campylobacter* and VBNC state. We firstly summarized the basic concepts of *C. jejuni*, covering the characteristics, prevalence, and transmission, as well as nutrient acquisition and metabolism. The stress response strategies adopted by *C. jejuni* to survive under adverse environments were also introduced. In addition, this review described various aspects of the VBNC state, including the risks posed to food safety, detection methods, resuscitation factors, and putative mechanisms. It was highlighted that a reliable method for single-cell identification of VBNC *C. jejuni* is demanded. In Chapter 3, we developed a novel optofluidic platform combining optical tweezing, Raman spectroscopy, microfluidics and machine learning for automated identification and sorting of single bacterial cells, including *C. jejuni*. A reliable spectral recovery technique based on conditional generative adversarial network was also proposed to accelerate the data acquisition and improve the spectral quality. Part of the Chapter 3 has been published in *Analytical Chemistry.*

Chapter 3: An automated Raman tweezers system combined with microfluidics and machine learning for accurate identification and sorting of single bacterial cells

3.1 Abstract

Raman optical tweezers system is a powerful tool for single-cell studies to investigate cellular heterogeneity. Here, we developed a novel optofluidic platform combining optical tweezing, Raman spectroscopy, microfluidics and machine learning for automated identification and sorting of single microbial cells. Raman optical tweezers system was designed and constructed in-house with a 671-nm laser, a spectrometer and a phase-contrast microscope. This setup enables simultaneous identification of individual cells based on Raman spectral features and selective manipulation via optical tweezering. A polydimethylsiloxane (PDMS)-based microfluidic device was integrated with this system to provide precise regulation of sample flow, facilitating the continuous single-cell sorting. The operational procedures were fully automated using a customized and user-friendly software program with minimal manual intervention. As Raman-based single-cell analysis is usually hindered by a low spectral signal-to-noise ratio (SNR), we also established a reliable spectral recovery conditional generative adversarial network (SRGAN) that could accelerate the spectral acquisition by one order of magnitude (i.e., 30 s vs. 3 s) via improving the SNR by ~6 times. The proposed platform was applied to the identification of 5 major foodborne bacteria at single-cell level and a high accuracy of 94.9% was achieved by using a convolutional neural network. This label-free approach enables rapid identification and nondestructive sorting of single living cells and can couple with other

molecular single-cell techniques such as RNA sequencing for downstream characterizations, offering unprecedented insights into various biological events.

3.2 Introduction

Single-cell analysis is an ideal approach to investigate the compositional and functional cell-to-cell heterogeneity in complex microbial communities [1, 2]. There is an increasing need for analytical methods to comprehensively monitor the phenotypic and physiological changes of single living cells. Raman spectroscopy provides non-invasive and label-free "molecular fingerprints" of cellular compositions, allowing the differentiation of cell types or physiological states based on the spectral variations [3]. Raman spectroscopy has been widely used in numerous biological applications, such as bacterial identification, cancer diagnostics and tissue engineering [4-6]. Recently, optical tweezers have been coupled with Raman spectroscopy to form a Raman tweezers system, also named as laser tweezers Raman spectroscopy, to achieve simultaneous manipulation and characterization of single cells in the fluidic environments [7]. Optical tweezers can trap and manipulate the microscopic particles at focal spot without physical contact, due to the gradient force and scattering force generated from the focused beam [8]. By combining the optical trapping and Raman spectroscopic profiling in one optical setup, Raman tweezers system represents a versatile platform for accurate identification and selective isolation of single cells. For example, Huang and coauthors applied Raman tweezers to isolate individual yeast cells from a microbial mixture within a capillary tube [9]. In another study, 4 different types of cells were separated at single-cell level using Raman optical tweezers and a successful isolation rate of ~90% was achieved [10].

Remarkably, microfluidics has been reported to be highly compatible with Raman tweezers system. Microfluidic "lab-on-a-chip" devices can precisely manipulate a small volume of fluids and provide efficient transport and positioning of samples for single-cell analysis [11]. Besides,

microfluidic chips can offer continuous flow with digital syringe pumps, allowing high-throughput screening of individual cells in a well-controlled manner [12]. As the integration of optics and microfluidics, optofluidic systems have been employed for continuous identification and sorting of blood cells, bacterial cells and cancer cells at single-cell level [13-15]. However, most Raman tweezers systems in the previously reported studies were manually operated and demanded substantial operational involvement at different steps, such as determination of cell capture and moving cells to the desired location *in situ*. This process is highly labor-intensive particularly for handling numerous cells in large-scale studies. In addition, manual operations may introduce human bias causing challenges to ensure both consistency and reproducibility. Developing automated procedures for this Raman spectroscopic-based optofluidic platform is thus crucial to reduce human labor and generate reliable analytical results.

A significant challenge in single-cell analysis using Raman spectroscopy is its low signal-to-noise ratio (SNR). Raman signal is inherently weak (~10^{-8} scattering probability), especially from a single cell [16]. Thus, the subtle spectral variations from different cells are easily overwhelmed by the background noise, including shot noise, autofluorescence, and detector readout noise [3]. Consequently, spectral recovery is needed to achieve more accurate qualitative or quantitative analysis. Numerous mathematical techniques have been used to remove the spectral background noise, including polynomial fitting [17], Savitzky–Golay smoothing [18], first and second derivatives [19], wavelet transform [20], and Fourier transform [21]. However, most of these methods have limitations. For example, polynomial fitting algorithms estimate a baseline using a low-order polynomial that may not be suitable for spectra with high noise. The first and second derivatives require prior knowledge of noise and signal components for peak

selection and peak shift. Recently, conditional generative adversarial networks (CGAN) have shown considerable success in various fields [22], such as image translation, speech enhancement, and video generation. In CGAN, two separate models, namely a *generator* and a *discriminator*, are trained simultaneously in an adversarial manner. It provides effective signal enhancement and works end-to-end with no explicit assumptions. However, the potential of CGAN in Raman spectral processing has not yet been explored.

In this study, we reported a Raman tweezers system integrated with microfluidics for label-free identification and sorting of single microbial cells. The Raman tweezers were designed, assembled, and optimized in-house and a software program was developed to facilitate an automatic process with minimal operator inputs. To improve the quality of single-cell Raman spectra, we proposed an effective CGAN-based framework named Spectral Recovery Generative Adversarial Network (SRGAN) for spectral processing. The performance of this optofluidic platform combined with machine learning techniques was evaluated for the identification of 5 major foodborne bacteria including *Campylobacter jejuni* at single-cell level. The proposed approach demonstrates various advantages and has the potential to become a multipurpose tool for future applications in different fields.

3.3 Results and discussion

3.3.1 Configuration of Raman tweezers system combined with a microfluidic device

We developed an automated Raman spectroscopic-based optofluidic platform that combines optical tweezers, Raman microspectroscopy and microfluidic “lab-on-a-chip” to achieve rapid and non-destructive identification and sorting of single microbial cells. **Figure 3.1** and **Figure**

3.2 display the schematic illustration (details in **Material and Methods**) and photographs of the Raman tweezers system constructed in our laboratory, respectively. This system mainly consists of a laser source, a spectrometer, a microscope with three-dimensional motorized stage, cameras, a microfluidic device, and optical pathways. Selection criteria and functions of these key components labeled in the photographs are elaborated below.

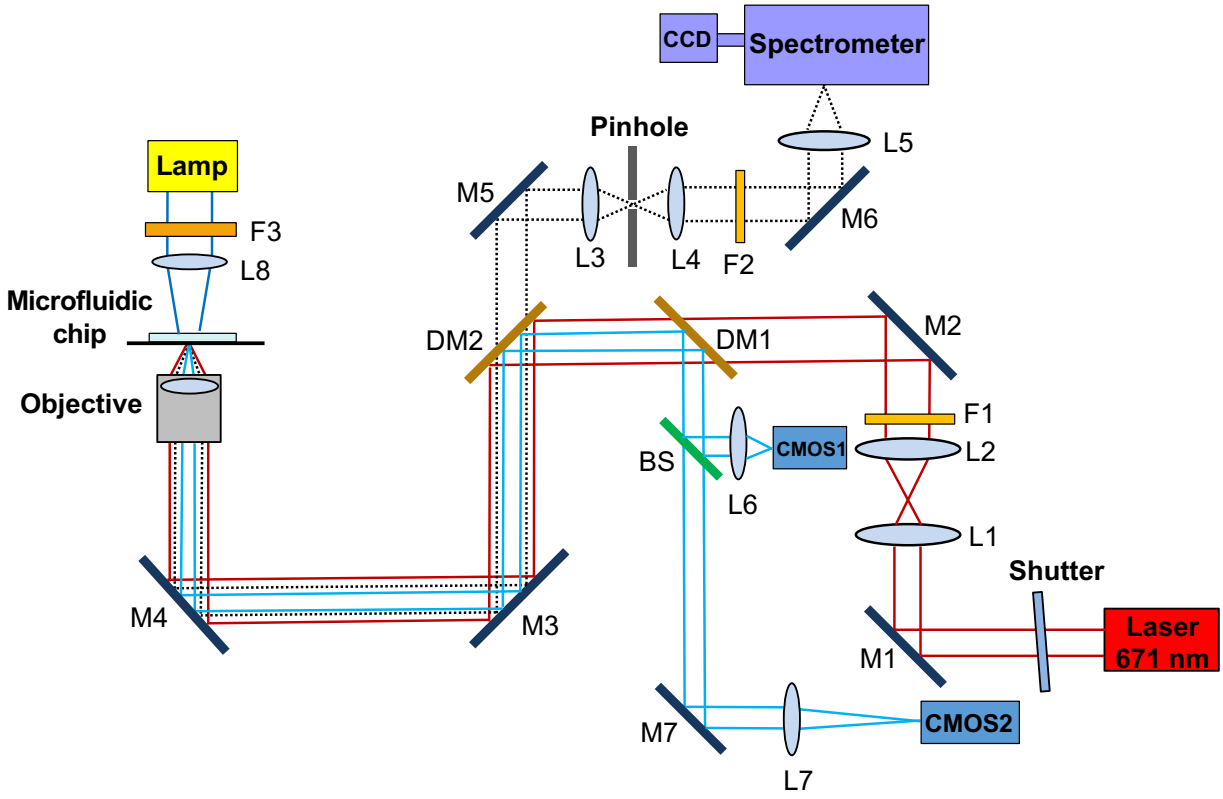

Figure 3.1 Schematic diagram of the configuration of Raman optical tweezers. A single 671-nm laser beam (solid red line) is used for both Raman excitation and optical tweezering. The dotted black line indicates the Raman scattering generated from the samples. Imaging light emitted from the phase-contrast microscope is displayed as the solid blue line. M: mirror; L: lens; F: filter; DM: dichroic mirror; BS: beam splitter.

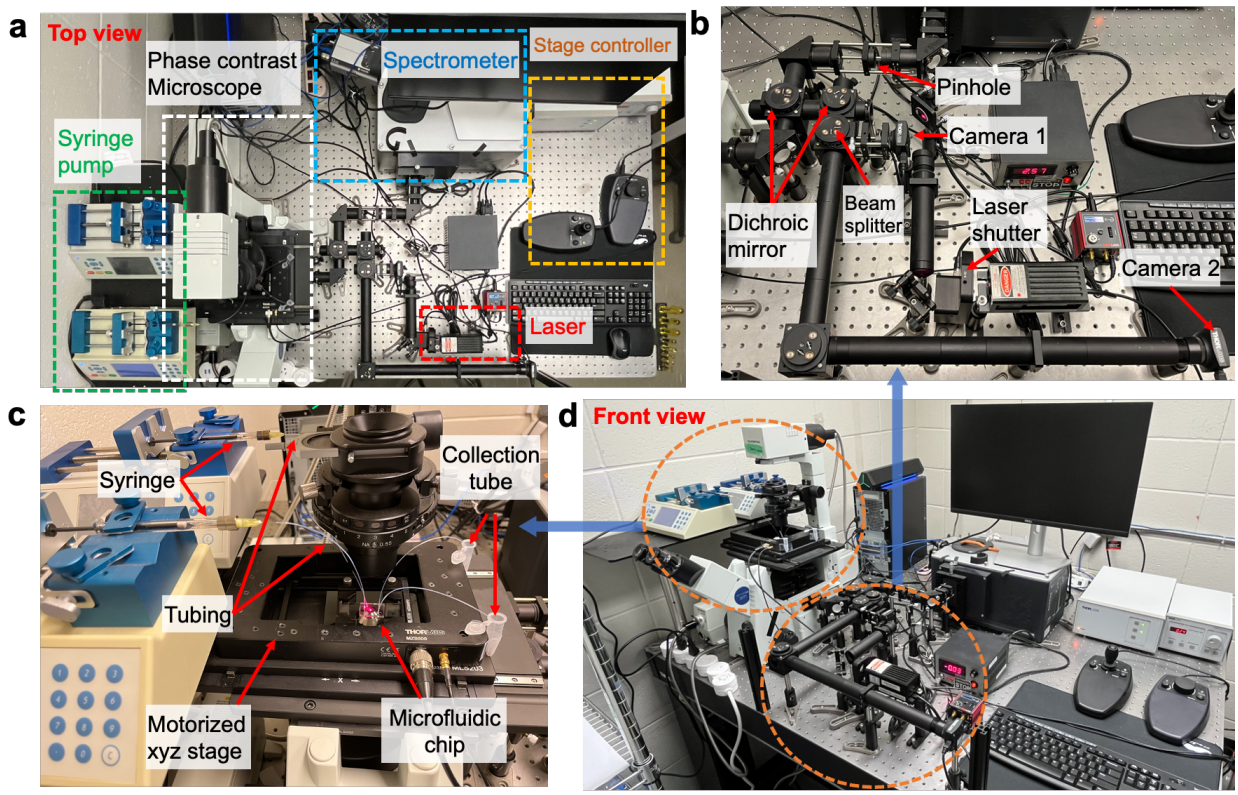

Figure 3.2 Setup of the home-built Raman optical tweezers system. (a, d) Top and front view of the Raman tweezers system, comprising a laser source and shutter, an inverted phase-contrast microscope, a spectrometer, syringe pumps for the microfluidic device (panel c), control panel for the motorized xyz microscope stage (panel c), two cameras and optical elements (panel b). (b) Configuration of the light delivery path. Key optical elements are labeled here and other details are available in Figure 3.1. (c) Assembly of the microfluidic device and syringe pumps. The microfluidic chip is fixed on the xyz motorized stage with the glass coverslip facing downward to the objective (see details in Figure 3.4).

Laser source

To select an appropriate laser source for the Raman tweezers system, we need to consider three main factors, namely the optical tweezing capability, Raman intensity derived from single cell, and potential photodamage to the trapped cell. As Raman scattering efficiency is inversely proportional to the 4^{th} power of the laser wavelength while a shorter wavelength generally demonstrates a higher possibility of photophoretic cell damage [23], the choice of the laser

wavelength is a delicate trade-off. Most previous studies of Raman optical tweezers utilized two lasers (e.g., 1064 nm and 532 nm) for optical trapping and Raman measurement, respectively [10, 24, 25]. In this study, a 671-nm Diode Pumped Solid State (DPSS) red laser with an adjustable laser power from 0 to 200 mW was selected as the single excitation source. Raman scattering efficiency at 671 nm is 1.87 times and 6.23 times higher than that at 785 nm and 1064 nm, respectively. Besides, stable trapping of bacterial cells by using 671-nm laser was validated based on visual examination. Reproducible spectra were collected from continuous measurements of the same cell, indicating limited photodegradation of the bacterial cells. Therefore, laser beam of 671 nm serves as both optical tweezers and Raman excitation source in our system, providing a desirable balance of optical trapping, Raman intensity and cell photodamage.

Optical beam shutter

An optical beam shutter was used as a switch to rapidly control the on/off of laser by either allowing or blocking the light path. Utilizing a rotary electro-mechanical actuator, the optical shutter could achieve an activation time (open or close an aperture with a blade) of less than 4.08 ms. This quick response time is essential for our Raman tweezers system where precise and fast control of light exposure is required to accelerate single-cell analysis. To prevent the reflection of laser beam from the blade back into the laser aperture, the optical shutter was positioned in front of the laser at a slight angle.

Microscope

A phase-contrast microscope was equipped in the Raman tweezers system to enable direct visualization of the transparent single bacterial cells without staining. It has a Nomarski

differential interference contrast (DIC) system to enhance the contrast of bacterial cells in the micrograph, showing their stereoscopic shapes with a better clarity. The DIC images of the trapped cell were illuminated by a lamp and recorded by 2 cameras to monitor the laser trapping and cell manipulation. Besides, the inverted setup of this microscope offers advantages of simplifying the setup of the microfluidic chip (i.e., coverslip facing downward) and allowing more working space for micromanipulation in our study.

Objective

Numerical aperture (NA) is a critical parameter of the objective that can determine the optical trapping capability. As bacterial cells can be considered as Mie particles [26], the objectives should have a high NA > 0.7. Considering the hydraulic resistance in the microfluidic chip, a higher NA is preferred to provide enhanced trapping power as well as improve the collection of Raman signals. However, the size of the laser focal spot decreases as the NA increases. For example, the laser spot is smaller than 400 nm when employing a NA = 1.4 objective in our system. There is a trade-off between the trapping power and trapping area. After attempting objectives with NA of 0.7-1.4, a 60× objective with NA = 0.9 and working distance (WD) = 0.2 mm was finally selected. By using this objective, the optical tweezers were able to capture the single bacterial cell and ensure a stable trapping during the movement in the microfluidic chip.

Stage

As the objective is immobilized, cell manipulation using optical tweezers is realized by moving the microfluidic chip fixed on the microscope stage. We used a three-dimensional (3D) scanning stage to precisely control the movement of the chip. Travel range of the motorized xy stage is

110 mm × 75 mm with a high positional accuracy of < 3.0 μm, which is suitable to transport the trapped bacterial cell to different locations in the microfluidic chip. The z-axis stage is primarily employed to vertically scan bacterial cells floating in the microfluidic channel at different depths, and thus it is featured with a movement resolution of 25 nm for high precision. The stages and controllers can provide computer-controlled positioning and active location feedback to ensure the reliability of cell manipulation.

Cameras

Two complementary metal oxide semiconductor (CMOS) cameras with different magnifications of 20× and 100× were employed in our platform to record imaging from the microscope. CMOS is a commonly used image sensor in various applications due to the advantages of faster readout speed, lower cost and energy consumption compared to other technologies such as charge coupled device (CCD) cameras [27]. The position of laser beam within the microfluidic chip was monitored by the 20× magnification camera to guide the movement of xyz microscope stage. The 100× magnification camera provides a zoomed in image to better visualize small bacterial cells, allowing us to inspect the process of single-cell capture, translocation, and release in real time. Visual observation is vital to confirm the reliability of optical tweezering.

Spectrometer

Spectrometer is an essential component in the Raman tweezers system for collecting Raman signals. A dispersive spectrometer equipped with different lines of gratings and a manual slit assembly was chosen. Grating could disperse Raman signals into discrete wavelengths for the detection by CCD camera. A higher density of the lines in grating can enhance spectral

resolution but reduce measurement efficiency. In our system, a grating with 830 lines/mm was adopted to collect the "fingerprinting region" of bacterial cells (i.e., 400 - 1,800 cm^{-1}) with a spectral resolution of 2 cm^{-1}, which is 8 times faster than an 1,800 lines/mm grating. The entrance slit was adjusted to 50 μm, allowing a sufficient optical throughput and a satisfying spectral resolution.

Pinhole

Given the inherent weakness of Raman scattering, low SNR is a common challenge for single-cell Raman spectra. Confocal pinhole represents a powerful approach to improve the spectral SNR [28], and thus it was introduced in our Raman tweezers system. A pinhole was placed before the spectrometer and served as a spatial filter. It could selectively allow Raman scattering from the focal spot to pass through while block the light from the regions outside the focal plane. This selective filtering enhances the spectral quality and improves the spatial resolution in confocal Raman microspectroscopy. Pinholes in smaller sizes offer superior noise reduction ability, but the collected Raman signals are reduced correspondingly. By testing pinholes with sizes of 30, 40 and 50 μm in our system, we chose the 40-μm pinhole as it generated the highest SNR for single-cell Raman spectra.

3.3.2 Optical tweezering and microfluidic sorting

A polydimethylsiloxane (PDMS) microfluidic chip was integrated with the Raman optical tweezers for single-cell sorting. **Figure 3.3** shows the design of the chip pattern. Microfluidic chip is immobilized on the 3D scanning microscope stage with the coverslip side facing downward (**Figure 3.4**). The laser beam is focused into the sample flow region through a high

NA 60× objective. The highly focused laser beam can generate an optical trap at the focal spot based on the light scattering force and gradient force as illustrated in **Figure 3.4c**. These forces act as "tweezers" to hold the microscopic objects (e.g., single bacterial cell) firmly in the optical trap. Individual cell in the microfluidic chamber is randomly captured by the optical tweezers, and the location of the trapped cell can be precisely manipulated in three dimensions by moving the xyz scanning stage. Besides optical tweezering, Raman spectrum of the cell can be collected simultaneously for further characterization. Laser beam is focused at the vertical middle of the microfluidic channel (i.e., ~25 μm above the glass coverslip) to mitigate the interference of Raman signals originating from either PDMS or glass.

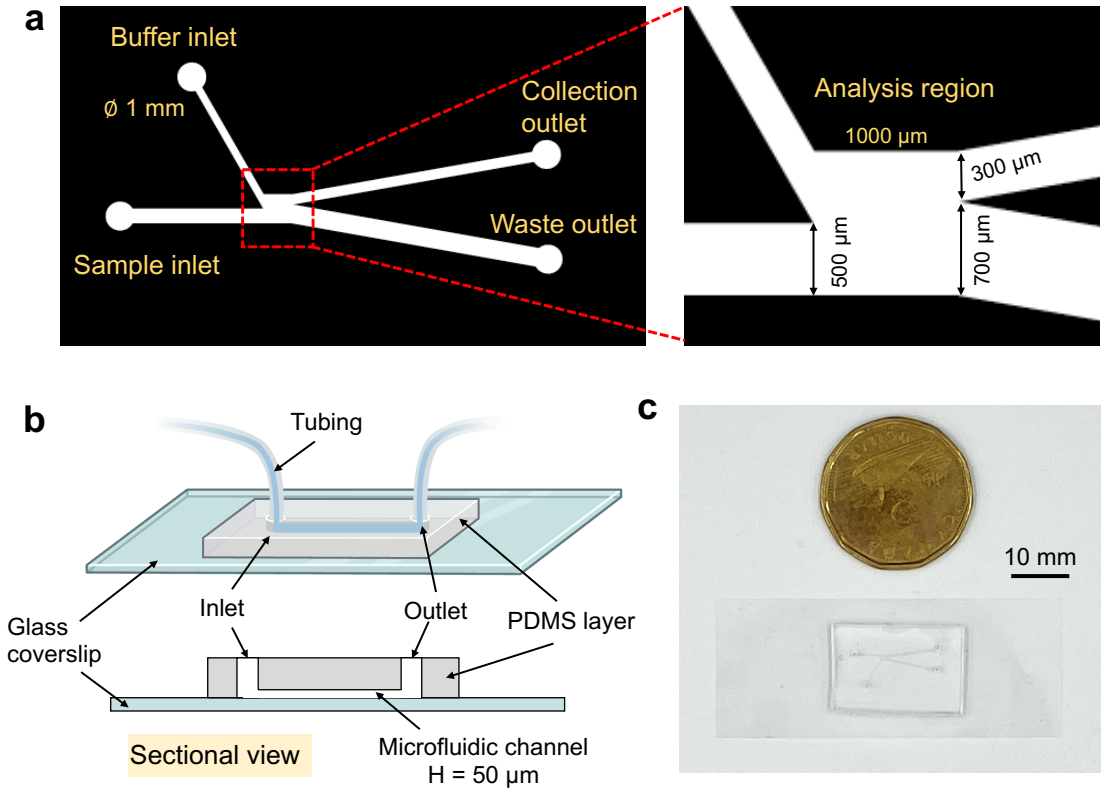

Figure 3.3 Illustration of the polydimethylsiloxane (PDMS)-based microfluidic device. (a) Mask pattern for the fabrication of PDMS layer. White regions represent the microfluidic

channels. (b) Schematic illustration of the microfluidic chip assembly. The microfluidic pattern is simplified with only one inlet and one outlet for better visualization. (c) Photograph of the fabricated microfluidic chip. The length and width of PDMS slab are 22 mm and 15 mm, respectively.

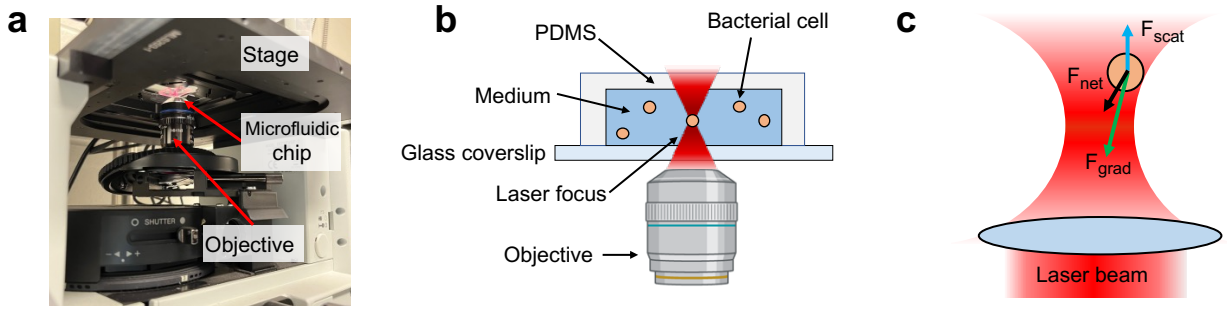

Figure 3.4 Diagram of the laser focus and optical tweezering. Photograph (a) and scheme (b) of the laser focusing on the sample within the microfluidic device. The microfluidic chip is mounted on the stage of an inverted microscope with the coverslip side facing the objective. A single bacterial cell in the solution is trapped by the laser beam at the focal spot. (c) Optical trapping of the focused bacterial cell. The forces acting on the trapped cell mainly include two forces: i) gradient force (Fgrad) pulling the cell towards the centerline of the beam and ii) scattering force (Fscat) pushing the cell along the direction of the beam. The net force (Fnet) determines the cell towards the focal spot, enabling an optical trapping within the focused beam. The red shaded area indicates the intensity gradient of the focused laser beam.

The combination of microfluidic device and Raman tweezers is the key to achieve continuous and automated single cell sorting (**Figure 3.5**). Microfluidics enable precise control over the sample with specific flow rates and directions. Sample solution and buffer solution are separately injected into the chip via different inlets. By tuning the flow rates, sample stream is focused to one side of the analysis channel by the buffer flow so that the cells directly flow into the waste outlet without entering the collection outlet in the default setting (i.e., no optical sorting). Optical tweezers can capture an individual cell and translocate it to the evaluation region to acquire Raman spectra. After analyzing the Raman spectra using the established neural networks, a

decision is made to guide the subsequent sorting step. Specifically, if the trapped cell is the target of interest, it would be manipulated to the collection region, released, and carried to the collection outlet via the buffer flow; otherwise, it is returned back via the tweezers and flow into the waste outlet after being released. Then, the process starts over to capture another bacterial cell.

The entire cell identification and sorting procedures are executed by using an in-house LabVIEW program with full automation. The details of graphical user interface **(**GUI) are presented in **Figure 3.6** and the workflow of single-cell sorting is described in **Figure 3.5** (see details in **Section 3.5.4**). Notably, the automated process of cell trap, movement and release are visually monitored via the 2 cameras in real time to confirm the reliability.

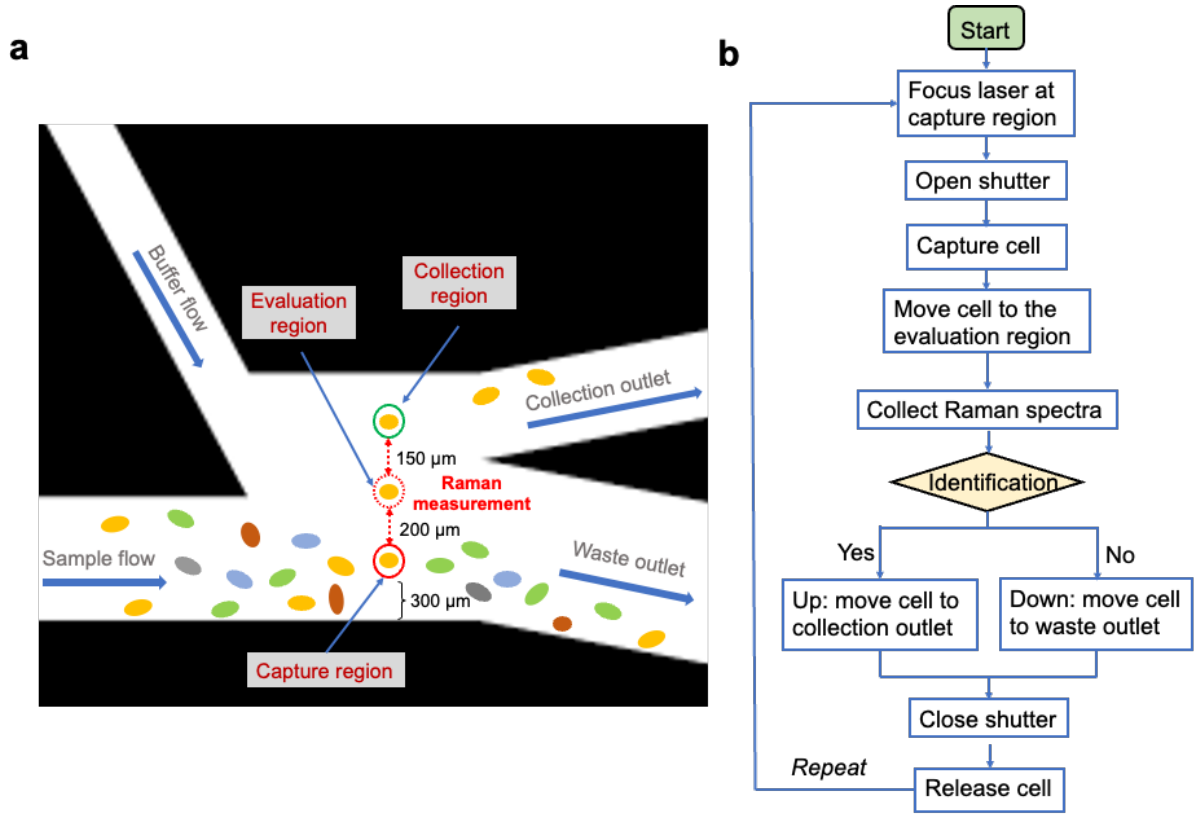

Figure 3.5 Schematic illustration of the principle (a) and workflow (b) of Raman spectroscopic-based optofluidic platform. Bacterial solution is injected into the microfluidic chip from the sample inlet and the cells flow along the main channel. A buffer flow is also introduced to push the sample stream to one side of the channel so that the cells only flow into the waste outlet by default. Optical tweezers are focused on the capture region and randomly trap the flowing single cell (solid red circle), and then immediately move it to the evaluation region without sample stream (dashed red circle) to collect Raman spectra. The obtained Raman spectra are analyzed using the established machine learning models (i.e., SRGAN and CNN) to generate an output to determine if the trapped cell is the target of interest or not. The targeted cell would be further carried to the collection region (solid green circle) and released into the collection outlet by closing the shutter; while the untargeted cell would be moved back to the capture region, released and flow into the waste outlet. The entire process is repeated for the subsequent cells.

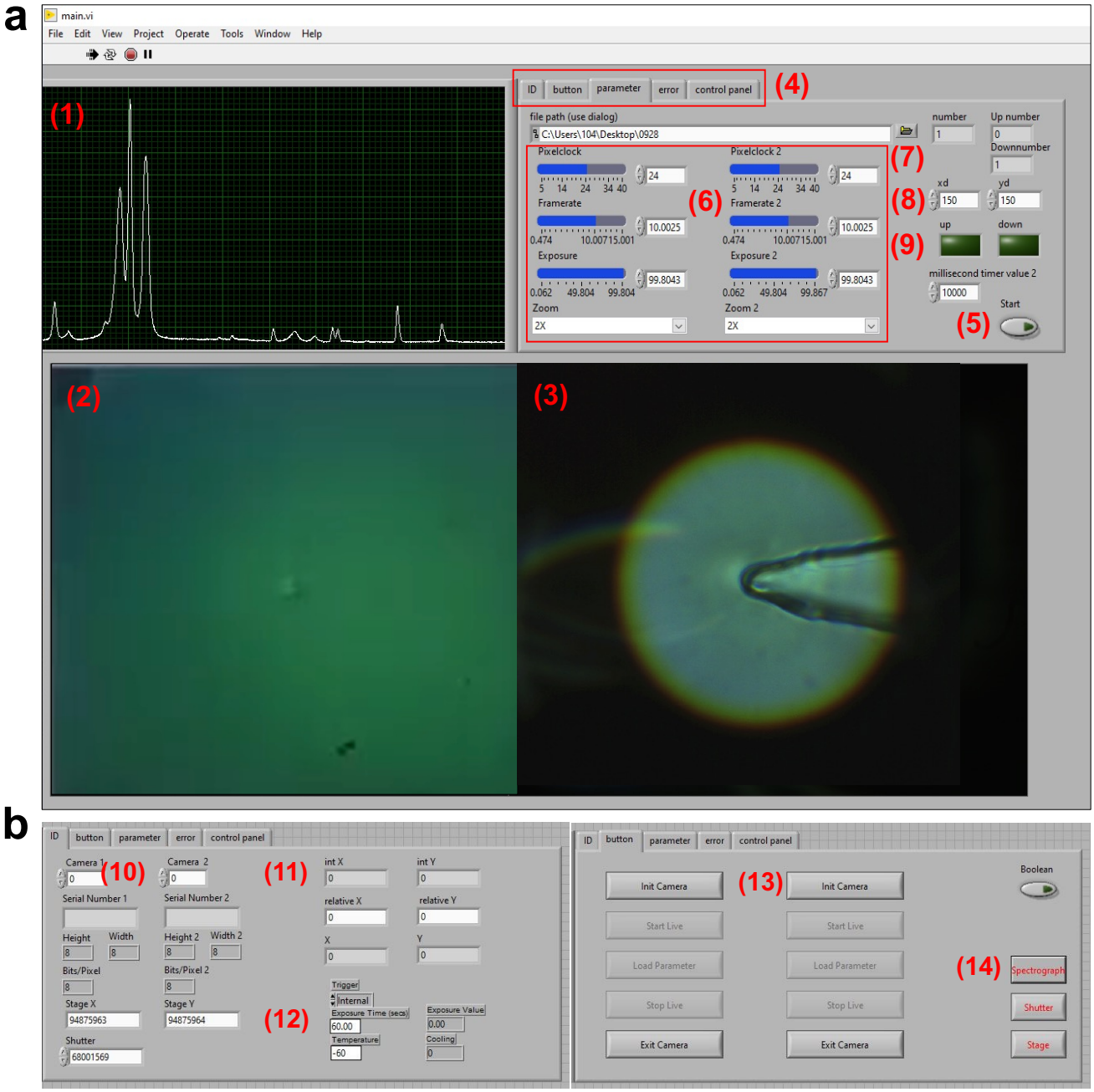

Figure 3.6 LabVIEW graphical user interface (GUI) to control the Raman optical tweezers system. (1) Real-time display of the Raman spectrum recorded; (2) Camera image with 100× magnification (CMOS 2 in **Figure 3.1**), a single cell is trapped; (3) Camera image with 20× magnification (CMOS 1 in **Figure 3.1**), the laser is focused in the middle of two chip outlets; (4) Tabs of the control panel (windows under Tab *ID* and *Button*) are shown in panel b); (5) Button to start the entire single cell sorting process; (6) Operation parameters of 2 cameras; (7) Number

of the cells analysed, selected or rejected; (8) Moving distance of the microscope stage; (9) Light indicator of moving direction; (10) Details of the 2 cameras; (11) Initial and current location of the microscope stage; (12) Exposure time for Raman spectral collection; (13) Buttons to control the cameras; (14) Buttons to start the spectrometer, stage and shutters.

3.3.3 Raman spectra of single bacterial cell

Campylobacter jejuni, a leading cause of human gastrointestinal diseases [29], was selected as a representative bacterial sample to test the performance of our Raman tweezers system. Phase-contrast images of the bacterial cells recorded in camera 2 are shown in **Figure 3.7ab**. Individual *C. jejuni* cells can be observed directly without staining and exhibit rod shape. When the laser is off, bacterial cells are suspended in fluid with various orientations, and some are slightly out of the imaging focal plane (**Figure 3.7a**). In comparison, the optically trapped cell (**Figure 3.7b**) is precisely on the imaging focus and appears a circular shape due to its lateral alignment within the optical trap.

Figure 3.7c shows a typical single-cell Raman spectrum of *C. jejuni*. The spectrum was acquired with a wavenumber range from 400 to 1800 cm^{-1}, the fingerprinting region containing comprehensive biochemical information of bacterial cells. The observed Raman peaks are mainly attributed to the biochemical compositions of bacterial cells, including nucleic acids, carbohydrates, proteins and lipids [3, 4]. Several peaks originating from the PDMS chip are indicated by the arrow and subtracted in the subsequent spectral analyses. Specific Raman peaks or the entire spectral profile can serve as intrinsic signatures of single bacterial cell, discriminating it from other cell populations. In this study, cells of interest are identified based on their unique Raman spectral patterns and sorted out using the optical tweezering. Furthermore, single-cell Raman spectra are potentially used to characterize the cells upon further

analyses, providing insights into bacterial compositions, metabolism and/or responses to environmental conditions.

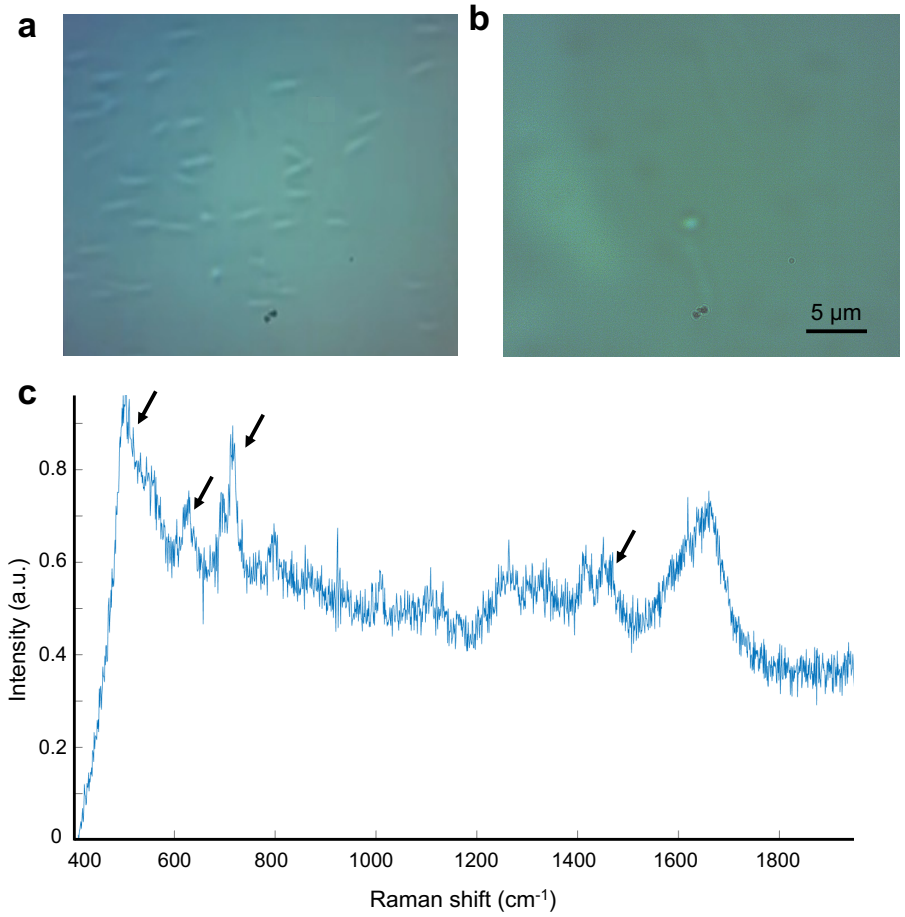

Figure 3.7 Phase-contrast images and Raman spectrum of the trapped single bacterial cell. (a) Image of *Campylobacter jejuni* cells in the solution under phase-contrast microscope. This view is captured by the camera 2 with 100× magnification. Bacterial cells display diverse alignments and positions in the solution, and some are slightly out of focus. (b) Phase-contrast image of a single *C. jejuni* cell trapped by optical tweezers. The trapped cell is positioned exactly on the imaging focus. The cell shows a circular appearance as it is laterally aligned within the optical trap and exhibits spontaneous random rotations. (c) A typical Raman spectrum of a trapped *C. jejuni* cell. The spectrum was acquired with ~25 mW laser power and 30-s exposure time. Raman peaks indicated by the arrow are attributed to the PDMS microfluidic chip and subtracted in the following analyses.

3.3.4 SRGAN to accelerate single-cell Raman spectroscopic analysis

In the proposed Raman tweezers system, identification and sorting criterion rely on the differences of Raman spectral features among tested samples. Thus, acquiring high-quality Raman spectra with high SNR is vital to enhancing the discriminatory power and identification accuracy. Prolonged integration time is usually required to improve the quality of Raman spectra. For the tested *C. jejuni* cells, the SNR of single-cell Raman spectra increased from 3.35 to 17.21 with an increasing integration time of 3 s, 5 s, 10 s, and 30 s **(Figure 3.8)**. However, extended integration times increase the risk of causing photodamage to live cells and decrease the speed for single-cell analysis. Thus, reliable processing methods are required in our system to improve the quality of single-cell Raman spectra with short integration time. In this study, we presented a deep learning technique SRGAN to transform noisy raw Raman spectra into high-quality spectra with improved SNRs. As SNR is positively correlated to integration time (**Figure 3.8**), improvement of SNR can lead to the reduction of spectral acquisition time and thus accelerate single-cell Raman spectroscopic analysis.

We evaluated the performance of SRGAN using single-cell Raman spectra from *C. jejuni*. Raw Raman spectra collected with an integration time of 3 s were used as input. Raman spectra acquired with an integration time of 30 s were employed as reference spectra as they have better spectral quality and have been commonly used in other single-cell Raman spectroscopic studies [30, 31]. As indicated in **Figure 3.9a**, raw single-cell Raman spectrum shows inferior spectral quality. Specifically, Raman peaks are overwhelmed by noise and no clear spectral features can be observed. In comparison, unique Raman spectral patterns can be identified in the spectra processed using SRGAN (**Figure 3.9c**). Compared to reference Raman spectra (**Figure 3.9b**),

the processed Raman spectra recover abundant peak information and the spectral patterns are mostly preserved without peak shift. The spectral quality was further quantitively evaluated based on SNR value, which is defined as the average peak intensity divided by the standard deviation of the background in this study. After spectral recovery using SRGAN, the SNR of 3 s-measurement was improved to 20.27, which was higher than that of the reference Raman spectra. Therefore, data acquisition time can be reduced at least 1 order of magnitude (i.e., from 30 s to 3 s), and enhanced spectral quality is achieved using SRGAN.

A comparative study was conducted between SRGAN and two other frequently used denoising methods, namely wavelet transformation and smoothing. The quality of processed Raman spectra (**Figure 3.9d and 3.9e**) was improved compared to the raw Raman spectra, but a considerable number of spectral features were still overwhelmed by the noise. The SNRs of the processed Raman spectra using wavelet transformation and smoothing were 8.50 and 8.43, respectively, which were lower than 17.21 of SRGAN (**Figure 3.9f**). Wavelet transformation and smoothing have been widely used for noise removal in a wide range of applications. However, they have limitations in certain situations. The challenges in selecting appropriate wavelet filters, wavelet threshold, and other parameters in wavelet transform may affect its denoising results [20]. For smoothing, there is a trade-off between spectral resolution and smoothing outcome as the weak spectral features might be distorted when the window size is large [18]. The superior performance of SRGAN might be attributed to its ability to learn and imitate the distribution of reference data and synthetically generate examples that optimally resemble the real data. Besides, multiple types of noise included in the training datasets contribute to the robustness of SRGAN for different applications. Taken together, SRGAN showed a better performance in

recovering Raman spectra with a low SNR than wavelet transformation and smoothing. Therefore, SRGAN has been adopted to couple with our Raman tweezers system to accelerate the data acquisition for single-cell analysis.

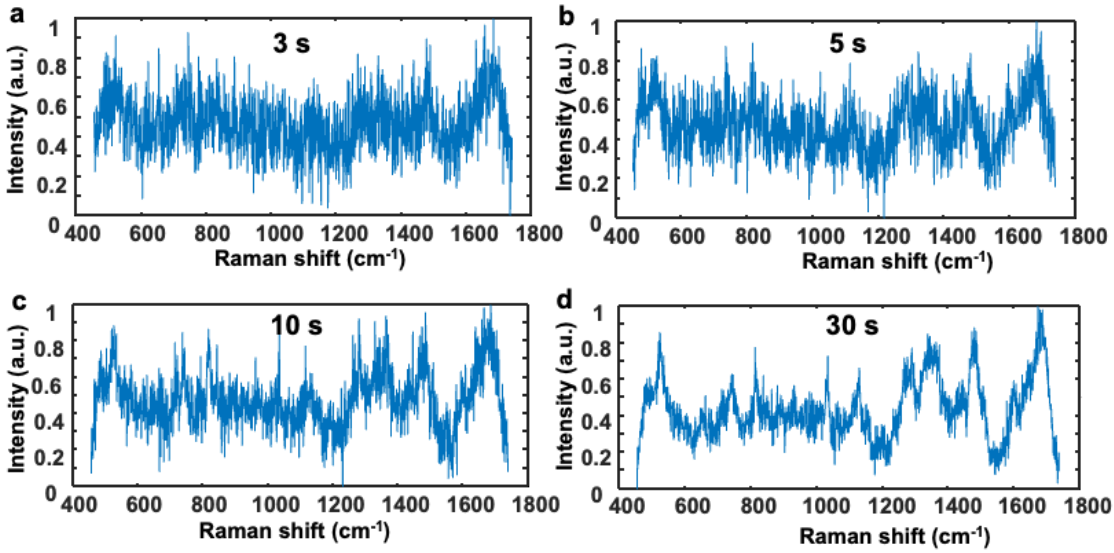

Figure 3.8 Single-cell Raman spectra of *Campylobacter jejuni* with integration time of 3 s (a), 5 s (b), 10 s (c) and 30 s (d). The signal-to-noise ratio (SNR) is 3.35, 5.86, 9.30 and 17.21, respectively.

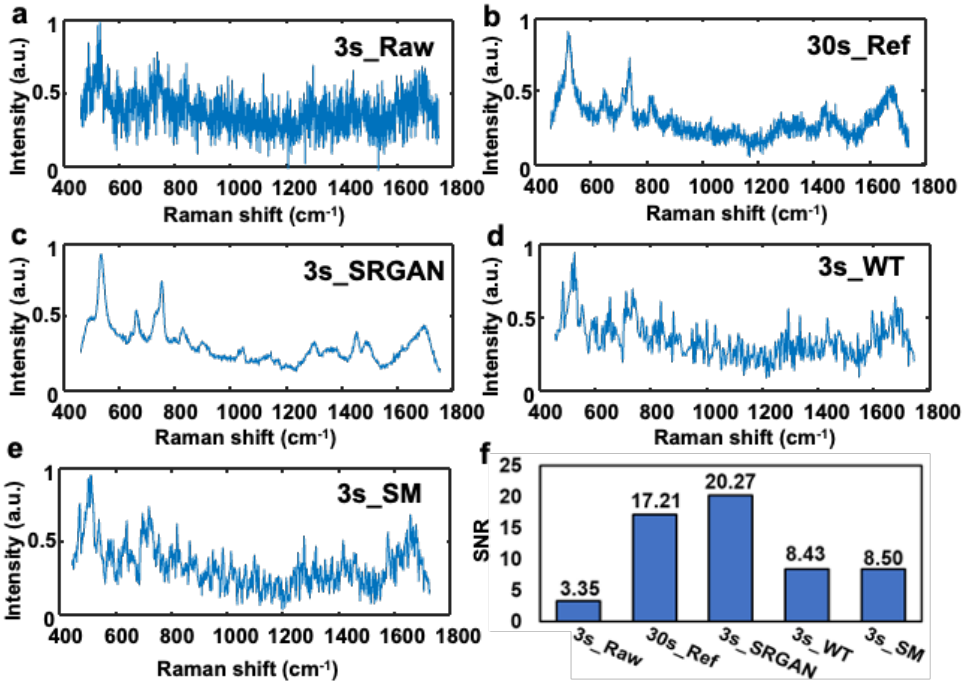

Figure 3.9 Average raw, reference and processed single-cell Raman spectra of *Campylobacter jejuni*. (a) Raw Raman spectra of *C. jejuni* with integration time of 3 s. (b) Reference Raman spectra with integration time of 30 s. (c) Processed Raman spectra using the proposed spectral recovery generative adversarial network (SRGAN). (d) Processed Raman spectra using wavelet transformation (WT). (e) Processed Raman spectra using smoothing (SM). (f) Signal-to-noise ratio (SNR) of all the raw, reference and processed Raman spectra.

3.3.5 Single-cell bacterial identification using Raman tweezers and machine learning

To test the performance of the Raman tweezers system incorporated with SRGAN, we performed the identification of various foodborne bacteria at the single-cell level. Rapid detection of bacteria at an early stage is crucial to ensure biomedical diagnostics and food safety. A total of 1000 single-cell Raman spectra from 5 leading foodborne bacteria, including *C. jejuni*, *Escherichia coli*, *Listeria monocytogenes*, *Staphylococcus aureus*, *Salmonella enterica* serovar Typhimurium, were collected using our Raman tweezers system combined with the microfluidic chip. These bacteria are responsible for a large number of food-associated events, such as

foodborne illnesses [32]. Average raw Raman spectra recorded from 5 bacterial genera with an integration time of 3 s are displayed in **Figure 3.10a**. After being recovered by SRGAN, the processed spectra indicated improved spectral quality (**Figure 3.10b**) and were used for the following identification.

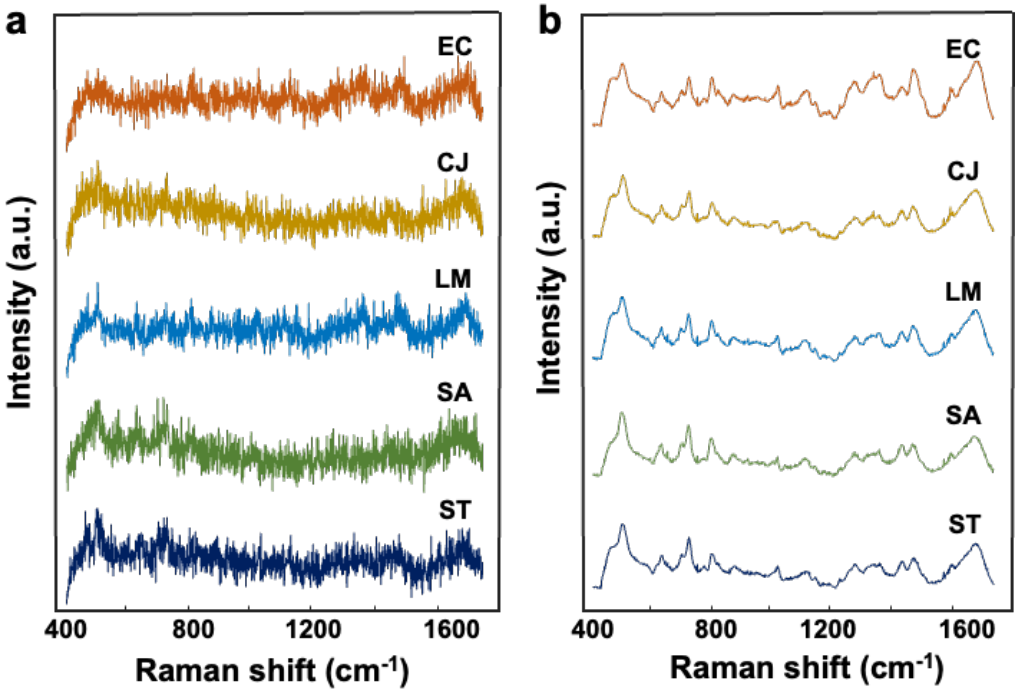

Figure 3.10 Single-cell Raman spectra of 5 leading foodborne bacteria collected using the Raman optical tweezers system. (a) Raw Raman spectra with integration time of 3 s. (b) Processed Raman spectra using SRGAN. CJ: *Campylobacter jejuni* F38011, EC: *Escherichia coli* K12, LM: *Listeria monocytogenes* ATCC19113, SA: *Staphylococcus aureus* Newman, ST: *Salmonella enterica* serovar Typhimurium SL1344.

We utilized a state-of-the-art deep learning technique named CNN to discriminate the bacteria based on the processed single-cell Raman spectra. The simplified architecture of CNN is displayed in **Figure 3.11.** Briefly, our CNN architecture includes four convolutional layers for feature extraction, followed by a fully connected layer to perform classification and an output layer. In the generated probability distribution, the one with the highest value among 5 bacterial species was taken as the predicted species. We conducted "10-fold" cross validation to test the stability of this CNN model utilizing all samples in an unbiased manner, and the identification accuracies are summarized in **Figure 3.11**. The values on the diagonal indicate the correct recognition rate for each strain while the incorrect predictions are exhibited in the off-diagonal area. The overall accuracy for the discrimination of 5 bacteria was 94.9%, with the accuracy ranging from 91.8% to 97.9% for individual bacterial species. These results demonstrated that our Raman tweezers system combined with CNN represents a reliable approach for bacterial identification at single-cell level.

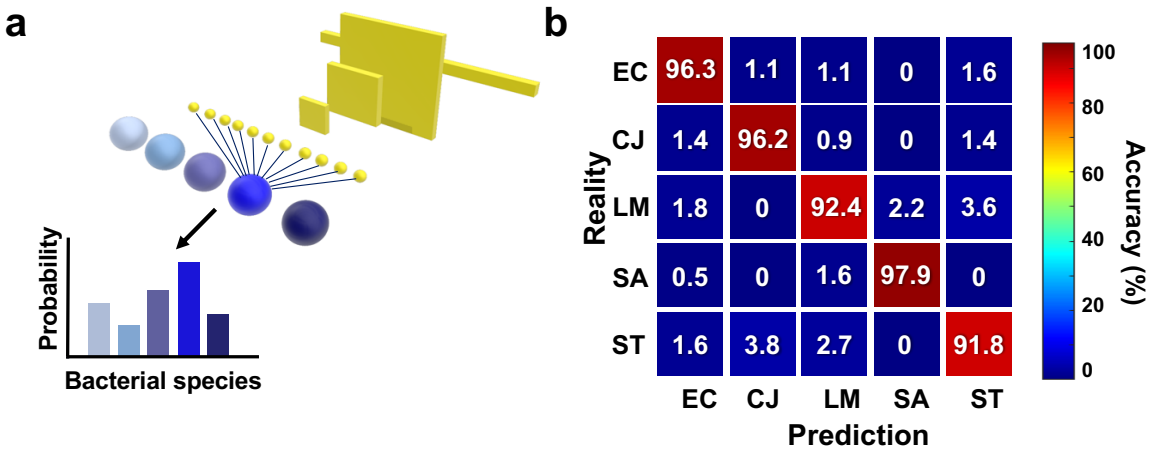

Figure 3.11 Identification results of 5 leading foodborne bacteria using a convolutional neural network (CNN). (a) Structure of the CNN model. It includes an input layer, 4 convolution layers with different numbers of kernels and kernel size for feature extraction, one

fully connected layer for classification and an output layer. (b) Confusion matrices for the classification of 5 bacteria using processed Raman spectra. The overall identification accuracy is 94.9%. CJ: *Campylobacter jejuni* F38011, EC: *Escherichia coli* K12, LM: *Listeria monocytogenes* ATCC19113, SA: *Staphylococcus aureus* Newman, ST: *Salmonella enterica* serovar Typhimurium SL1344.

Raman spectroscopy has been considered as a powerful tool for microbial identification as it is rapid, label-free, and easy to perform [3]. Combining the function of optical trapping, Raman optical tweezers enable the capture and analysis of single cells, significantly enhancing the sensitivity of Raman spectroscopic-based microbial detection. Raman tweezers also help minimize the background signals from the surrounding media by selectively analyzing cells of interest, which is valuable for the application in real environmental and clinical samples. In addition, employing CNN to interpret single-cell Raman spectroscopic data also improves the classification sensitivity. CNN is one of the most popular deep learning algorithms that has been extensively applied to image classification and voice recognition [33, 34]. It combines feature extraction and classification in one architecture that automatically learns the underlying relationship from the training datasets with little human supervision and accomplishes a high accuracy to predict the unknown samples. By integrating with machine learning algorithms, namely SRGAN and CNN, our Raman tweezers system could achieve rapid and accurate detection of various bacteria at single-cell level in real time.

3.3.6 Validation for the cell sorting capability

We further assessed the sorting capability of the proposed optofluidic platform for selectively isolating a specific bacterium within a microbial mixture. *C. jejuni* was selected as the target and the sorting criterion was based on the classification of different foodborne bacteria using the

CNN model as aforementioned. Bacterial solution containing *C. jejuni* and *S.* Typhimurium at equal concentration was injected into the microfluidic chip and the captured cells identified as *C. jejune* using the well-trained CNN model were sorted to the collection outlet. The sorted cells were then harvested and enumerated by the conventional plating assay. The recovery rate was defined as the number of single colonies on the agar plate out of the number of sorted cells as counted in the program. The single colonies were visually inspected and tested using *C. jejuni*-specific qPCR to confirm the identity and calculate the sorting accuracy. An average recovery rate of 80.3% was achieved and the cell loss might occur during optical moving from evaluation region to the collection region, in the collection stream to the outlet, and during transfer from the collection reservoir to the culture media. A comparable recovery rate of 82.1% was reported in a previous study for Raman-activated microbial cell sorting [24]. Within the recovered cells, the sorting accuracy for *C. jejuni* was 91.8%, indicating a reliable approach for isolating single cells from a mixed population. Various isolation accuracies have been reported ranging from ~90% to 98.3% for different targeted bacterial cells [10, 14, 24, 35]. The sorting accuracy not only relies on the experimental setup but is also related to the intrinsic Raman spectral variations among samples in specific applications. Besides bacterial identification and sorting, this platform can be customized to selectively characterize single cells based on other identification criteria, such as cells at unique physiological status or containing specific components. High sorting accuracy allows for a deep understanding of cellular heterogeneity especially for rare cell subpopulation.

3.3.7 Advantages of the Raman tweezers platform and automated pipeline

In this study, we demonstrated that Raman optical tweezers system is a promising technique to isolate and identify single microbial cells. An optical trap allows the isolation of a single

bacterial cell from a complex mixture without direct physical contact, and the cell can be identified by its distinct Raman spectral features simultaneously during the optical manipulation. This synergy of optical tweezering and Raman scattering significantly improves the sensitivity of Raman measurements to single-cell level, providing particularly advantages for studying heterogeneous samples with diverse cell subpopulations. Microfluidics incorporated to this platform could offer continuous and precise control over the sampling process to facilitate the analysis of specific cells in a dynamic manner.

Previously established Raman tweezers systems usually utilized two lasers (e.g., 1064 nm and 532 nm) [10, 24, 25], while a single 671-nm laser source was employed in the current study for both optical tweezering and Raman excitation. This reduces the overall cost and simplifies the optical setup, requiring relatively easy beam alignment and reduced space. Several previous studies were conducted in a static reservoir chamber (e.g., microscope slide or capillary glass tube) and individual cells were manually trapped and analyzed [9, 10, 36]. These processes are typically labor-intensive, time-consuming and the analytical reproducibility and reliability might be compromised by the human bias. With the elaborate microfluidic device and the home-designed software, automation was achieved at different steps in our approach, including 1) recognition of a trapped cell; 2) decision to accept or reject the cell; and 3) sorting the cell to defined locations. This is of great benefits for analyzing a large number of cells in practical applications. In the designed microfluidic chip, the trapped cell is displaced from the sample stream during spectral acquisition to ensure the surrounding cells do not interfere with the single-cell trapping and signal collection, thereby enhancing the efficiency and accuracy in the sorting process. Furthermore, this user-friendly program can be easily customized to sort bacterial cells

according to specific Raman spectral features. By using this approach, we can selectively isolate and analyze the cells of interest from complex microbial community *in situ*. Due to label-free and non-invasive properties of Raman tweezering, the identified cells are suitable for further single-cell characterizations, such as cultivation [37] and genomic sequence analysis [38]. This strategy promises to bridge the knowledge gap between phenotypic and genotypic properties and reveal the microbial diversity at the resolution of single-cell level.

This Raman-activated single-cell analytical approach indicates unique advantages compared to other common cell sorting techniques, such as flow cytometry. Flow cytometry usually relies on the size, shape, or fluorescence emission of the biological particles to perform identification and sorting [39, 40]. Therefore, fluorescence staining is generally needed in sample preparations for flow cytometry, and this might restrict the downstream characterization of the sorted cells. In comparison, the analysis of cells in Raman optical tweezers is based on the intrinsic molecular compositional properties and thus only minimal sample preparation is required. Additionally, a large sample number is usually demanded for flow cytometry while Raman optical tweezers allow precise manipulation of single cell within a small cell population. The choice between these two approaches depends on the specific research or diagnostic purposes.

Applications of advanced machine learning techniques amplify the efficiency of the proposed platform. CGAN is a relatively new deep learning technique that has been increasingly recognized in speech enhancement, image generation, and style transfer [41]. The main advantages of the proposed SRGAN for spectral processing are as follows: 1) The optimization process is rapid. Without an iterative optimization procedure, the entire enhancement process

usually takes less than a few milliseconds on a modern computer. 2) No parameter adjustment is required. All the parameters have been fixed in the training process, which can deal with various noise types in the training dataset. 3) It has a superior recovery capability for Raman spectra with a low SNR. SRGAN is more robust to extracting weak signals compared to the traditional noise removal methods. On the basis of these benefits, SRGAN can be integrated with our Raman optical tweezers for single cell sorting techniques to accelerate spectral acquisition and improve identification accuracy.

3.4 Conclusion

In summary, we introduced a Raman tweezers system combined with a microfluidic device and machine learning techniques for single-cell identification and sorting in a label-free and noninvasive manner. In the proposed scheme, individual bacterial cell in the microfluidic channel was captured by the optical tweezers, identified based on the Raman spectral features and then selectively sorted to the collection container. A user-friendly LabVIEW program was designed to control all the hardware and automatic operations were realized with little human supervision. We also developed a novel SRGAN to de-noise single-cell Raman spectra with a low SNR. This model increased the SNR of single-cell Raman spectra over 6 times and thus accelerated data acquisition by 10 times (i.e., 30 s vs. 3 s), significantly improving the analysis speed and throughput for single-cell analysis. Performance of the proposed optofluidic platform was verified by an overall accuracy of 94.9% for single-cell identification of 5 leading foodborne bacteria. Furthermore, selective isolation of *C. jejuni* from a bacterial mixture demonstrated a sorting accuracy of 91.8%. Single-cell analysis achieved in this work can aid in a better understanding of cellular heterogeneity and isolating specific subpopulations for further

characterization, such as single-cell genomic sequencing and transcriptomic sequencing. Multi-perspective analyses on a single cell might open new windows for microbiology, cancer diagnosis and drug screening.

3.5 Materials and methods

3.5.1 Construction of the home-built Raman optical tweezers system

A Raman optical tweezers system was constructed in our laboratory. **Figure 3.1** illustrates its schematic optical setup and the photographs of the hardware are shown in **Figure 3.2**. A diode laser (Optotronics, Chelmsford, USA) with a wavelength of 671 nm was selected as the light source for both optical trapping and Raman excitation. An optical beam shutter (SH1, Thorlabs, NJ, USA) was included as a switch to control the pass of the laser light. The laser beam was then expanded by lenses L1 and L2 in a telescopic arrangement. F1 is a laser line filter at 671 nm to make the light source more monochromatic. DM1 and DM2 are long-pass dichroic mirrors with cut-off wavelengths at 650 nm and 680 nm, respectively. Thus, the laser beam at 671 nm can pass through DM1 and reflected by DM2. The laser was focused on the sample within the microfluidic chip mounted on an inverted phase contrast microscope (IX71, Olympus, Tokyo, Japan) through a 60× objective (NA = 0.9, WD = 0.2 mm, UPLFLN, Olympus). The generated Raman scattering signals were collected by the same objective lens and eventually delivered to the spectrometer (Andor Kymera 328i-A, Oxford instruments, Abingdon, UK) equipped with a diffraction grating of 830-lines/mm. A confocal configuration was constructed with L3, L4 and a 40-μm pinhole to screen out the Rayleigh scattering and Raman signals from out-of-focus sample, followed by a notch filter F2 (cut-off wavelength: 671 nm) to further remove the undesirable background radiation and ambient lights. Raman signals entering the spectrometer

were measured using a CCD camera cooled at -60°C. Imaging signals are also collected by the objective and reflected by M4, M3, DM2 and DM1 to the beam splitter with a split ratio of 30: 70. Two CMOS cameras (DCC1645C, Thorlabs, USA) were adopted to record the microscopic imaging at different magnifications simultaneously to assist in the process of bacterial manipulation. COMS1 (30% of the imaging signals) with a 20× magnification was used to track the position of the laser beam within the microfluidic chip, while CMOS2 that can collect 100× magnified images received 70% of the imaging power to better visualize the captured bacterial cell. All the optical elements were purchased from Thorlabs unless specifically stated.

3.5.2 Design and fabrication of the microfluidic chip

The microfluidic chip was developed using soft lithography technique that comprises 4 major steps, including pattern design, mask and master fabrication, construction of the PDMS layer and assembly of the PDMS/glass-hybrid chip. Our microfluidic device consists of one bottom glass layer for sealing and support, and one top PDMS layer featured with the microfluidic pattern (**Figure 3.3**). The pattern was designed using AutoCAD (Version 2021; Autodesk, USA) as shown in **Figure 3.3a**, containing two inlet ports (Ø = 1 mm), an analysis region (1000 μm wide, 1000 μm long) and two outlet ports (Ø = 1 mm). The central analysis region was connected to the inlets and outlets with microchannels at different widths. This pattern was printed on a photomask at CAD/Art Services (Bandon, USA) for the following master microfabrication. Standard photolithography was conducted to fabricate the microfeatures on a silicon wafer (Ø = 100 mm; University Wafer, USA) for developing the master mold. Negative photoresist SU-8 2050 (Microchem, USA) was applied and the parameters were optimized to achieve a 50-μm thickness of chip pattern on the master. Once the silicon mold was obtained, PDMS replica could

be mass produced. Briefly, silicone elastomer and curing agent (Dow Sylgard 184 silicone encapsulant clear kit, Ellsworth Adhesives, USA) were mixed at the ratio of 10:1 (w/w) to form the PDMS prepolymer. The mixture was poured onto the silicon master and degassed in a vacuum desiccator, followed by curing on a hot plate at 80°C for 32 min. The cured PDMS slab was then carefully peeled off from the silicon mold, and the inlets/outlets were created using Miltex® biopsy punches (Ted Pella Inc., USA). Lastly, the PDMS/glass hybrid microfluidic device was assembled by bounding the PDMS slab and glass layer together after plasma treatment (plasma cleaner PDC32G; Harrick Plasma, USA) for 30 s. The glass layer is a regular coverslip (60 mm × 24 mm, No. 1, Fisher Scientific, Canada).

3.5.3 Operation of the microfluidic device

This microfluidic platform comprises two syringe pumps, syringes, PVC tubing, microfluidic chip and collection containers (**Figure 3.2c**). The fabricated microfluidic chip was fixed on the 3D scanning microscope stage (MZS500-E Z-Axis Piezo Stage and MLS203-1 XY Scanning Stage, Thorlabs) using a specimen clip holder and the fixation was reinforced by adhesive tape. Using syringes and pumps, sample solution and buffer were automatedly injected into two inlets, separately. Phosphate buffered saline (PBS) was used as the buffer to generate the sheath stream to push the sample stream to the waste outlet by default (**Figure 3.5a**). The flow rate for the sample fluid and PBS solution was set as 0.02 and 0.05 μL/min, respectively. To prevent the samples from accidently flowing into the collection outlet during initial stabilization, PBS was introduced first to fill the chip before injecting the sample solution. The waste outlet and collection outlet were connected to microcentrifuge tubes via tubing to collect the waste and

sorted bacterial cells, respectively. All components of the device were either autoclaved or sterilized under UV light for 30 min to reduce the risk of contamination.

3.5.4 Software program for automated single-cell identification

We developed an in-house software program using LabVIEW (National Instruments) to automatically operate the Raman tweezers system for single-cell identification and sorting. By using the LabVIEW-compatible software development kit and programming interfaces provided by the manufacturer, this program integrates the control of all hardware, including laser shutter, spectrometer, xyz scanning stage and 2 cameras. As shown in **Figure 3.6**, the main GUI window consists of 4 panels, including (1) display of the collected Raman spectrum; (2) image from 100× magnification camera; (3) image from 20× magnification camera and (4) a control panel with different tabs. Using this program, users are able to achieve the following functions: (5) start the identification process; (6) set the parameters of cameras to optimize the imaging speed and quality; (7) track the total number of captured cells, and the number of cells either selected or rejected; (8) set the moving distance of the microscope stage; (9) track the moving direction of the stage; (10) view the details of the cameras; (11) set the initial location and monitor the real-time position of stage; (12) set the spectral integration time; (13) control the working status of the cameras and (14) switch the on and off of spectrometer, microscope stage and shutters.

The automated single-cell sorting was operated using this software and the workflow is detailed in **Figure 3.5b**. Under the *Button* Tab, users can activate the spectrometer, stage, optical shutter and cameras. The laser beam can be visualized in the images window (2) and (3) to guide the focus. Once the laser spot was focused on the analysis region in the microfluidic chip, users

could click the start button (5) to initiate the automated identification process. Firstly, the program would recognize if any bacterial cell was optically captured under the laser focal point based on the image (2). Immediately after the capture, the trapped bacterial cell was moved by the optical tweezers to the evaluation region at a distance of 200 μm ('up' direction shown in the image). Raman spectrum of the trapped bacterial cell was then collected at this sample-free region to avoid the trapping of other coming cells and the loss of trapped cell due to the collision with other cells. The spectral integration time was 3 s and the collected spectrum was exhibited at window (1) in real time. The collected Raman spectra were fed into the pre-trained SRGAN model for preprocessing to improve the SNR, followed by a CNN model to perform the identification. Then, a decision was made according to the criteria defined by the user (e.g., if it is the bacterial species of interest). If the bacterial cell was selected based on the user-set criteria, the laser would move the cell to the collection region (up, 150 μm). The optical shutter was then closed to block the laser beam, and the captured bacterial cell was released and carried to the collection outlet by the sheath flow. The laser subsequently moved back to the initial capture region and optical shutter was opened to start the next round of cell capture, sorting and identification. When the bacterial cell was not the target of interest, the program directly returned to the capture location (down, 200 μm), released the cell to the waste outlet (shutter close), and started over (shutter open). All the spectra were automatically saved for future analysis. This Raman tweezers system was designed to be applied to diverse samples for different purposes so that the acquisition time, camera parameters, identification criteria and stage moving path are all adjustable based on the specific application.

3.5.5 Bacterial cultivation and sample preparation

The performance of the proposed Raman tweezers system was evaluated for bacterial identification at single-cell level. Five leading foodborne bacteria were investigated, including *Campylobacter jejuni* F38011, *Escherichia coli* K12, *Listeria monocytogenes* ATCC19113, *Staphylococcus aureus* Newman, and *Salmonella enterica* serovar Typhimurium SL1344. *C. jejuni* F38011 was routinely cultivated in Mueller-Hinton broth (Becton Dickinson, Franklin Lakes, NJ, US) at 37°C under microaerobic condition (10% CO_2) with constant shaking of 175 rpm for 16 h. All the other bacteria were grown in tryptic soy broth (Becton Dickinson, NJ, US) aerobically at 37°C for 12 h. Overnight bacterial culture was individually harvested, and the concentration was adjusted to ~10^8 CFU/mL. After centrifugation at 15,000 ×*g* for 3 min, the supernatant was discarded, and the cell pellet was washed for another two times with sterile PBS to remove the residue of the growth media. Finally, the resultant bacterial cell pellet was individually resuspended in PBS for Raman spectral collection.

3.5.6 Raman spectral collection

Spectral collection was carried out using Andor Solis software (Oxford Instruments, USA). The laser power of ~25 mW was focused on the sample with a laser spot size of ~1 μm. Raman spectra were recorded with a spectral resolution of 2 cm^{-1} in the wavenumber range of 1,800 to 400 cm^{-1}. For establishing the training dataset for the proposed SRGAN, single-cell Raman spectra with low SNR were collected with an integration time of 3 s. Another set of Raman spectra of the same cells were integrated for 30 s and used as the reference spectra with a high SNR. For each bacterial sample tested, ~200 individual single cells were measured from three

independent batches to minimize the influence of biological variability, environmental noise and experimental operations.

3.5.7 Construction of SRGAN model for spectral preprocessing

We introduced SRGAN as a general-purpose solution to improve the SNR of single-cell Raman spectra [22, 42]. The SRGAN included a generator (G) and a discriminator (D) (**Figure 3.12**). Raw spectra collected with an integration time of 3 s were used as the input data. The objective of G was to generate processed Raman spectra with an improved SNR from the input data so that it became challenging for D to distinguish the generated spectra from the corresponding real spectra (30-s integration time). Then, D and G were trained jointly and gradually with the training datasets. Briefly, G combined an encoder and a decoder structure with skip layers. The encoder was composed of 5 blocks that contained a one-dimensional convolutional layer (Conv) with a filter size of 5 × 1 and a sinusoidal activation function (Sine). The stride was set to 2 with padding and the number of the extracted feature maps in each layer is shown in **Figure 3.12**. The decoder of G had the same number of blocks as the encoder. It reversed the down-sampling process and output a processed spectrum of the same size as that of the input spectrum. The skipping connections could directly send the information (e.g., the spectral energy distribution) to the decoder.

The discriminator D was trained to differentiate the processed spectrum (generated by G) and the input reference spectrum. D started with five Conv-batch normalization layer and leaky rectified linear unit (Conv+BN+LeakyReLU) blocks, followed by a fully-connected layer. The loss functions in the SRGAN were defined as:

$$L_G = \frac{1}{N}\sum_{n=1}^{N}(D(G(s^n), s^n) - 1)^2 + \lambda\|G(s^n) - x^n\|_1 \quad (1)$$

$$L_D = \frac{1}{N}\sum_{n=1}^{N}(D(x^n, s^n) - 1)^2 + \left(D(G(s^n), s^n)\right)^2 \quad (2)$$

where s^n is the raw spectrum, x^n is the reference spectrum with $n \in \mathbb{N}_N$, N is the number of training spectra, and λ is the hyper-parameter for the magnitude of the *L1* norm. We selected *L1* norm as it could improve the SNR of the processed spectra [43]. The least-squares function with binary coding was introduced to resolve the vanishing gradient problem [44]. The model was trained using RMSprop for 100 epochs with a learning rate of 0.0001 and an effective batch size of 50. Python was used to run SRGAN.

A large and comprehensive training dataset increases the robustness and stability of the model. In this study, the training dataset consists of three parts:

1) Spectral database for organic compounds

A total of 600 Raman spectra of organic compounds were randomly selected from Spectral Database for Organic Compounds [45] to represent abundant organic compositions of bacterial cells. We artificially added different types of noise to those spectra following the procedures mentioned in a previous study [46] to mimic the background noises found in the real-world spectra. These spectra with noises serve as the input dataset for G, and the corresponding clean spectra are used as the reference dataset for D.

2) Real-world dataset

Single-cell Raman spectra were collected from bacteria using our homebuilt Raman spectrometer as aforementioned, including all types of noises in our experimental settings.

3) Simulated dataset

Due to the difficulty in obtaining a high number of standard spectra, we also constructed a large synthetic dataset to extend the diversity of the training dataset. The simulated spectra consist of Lorentz and Gaussian peaks with random intensity, linewidth, peak number, and distribution. The simulated spectra were also artificially degraded with multiple types of noises.

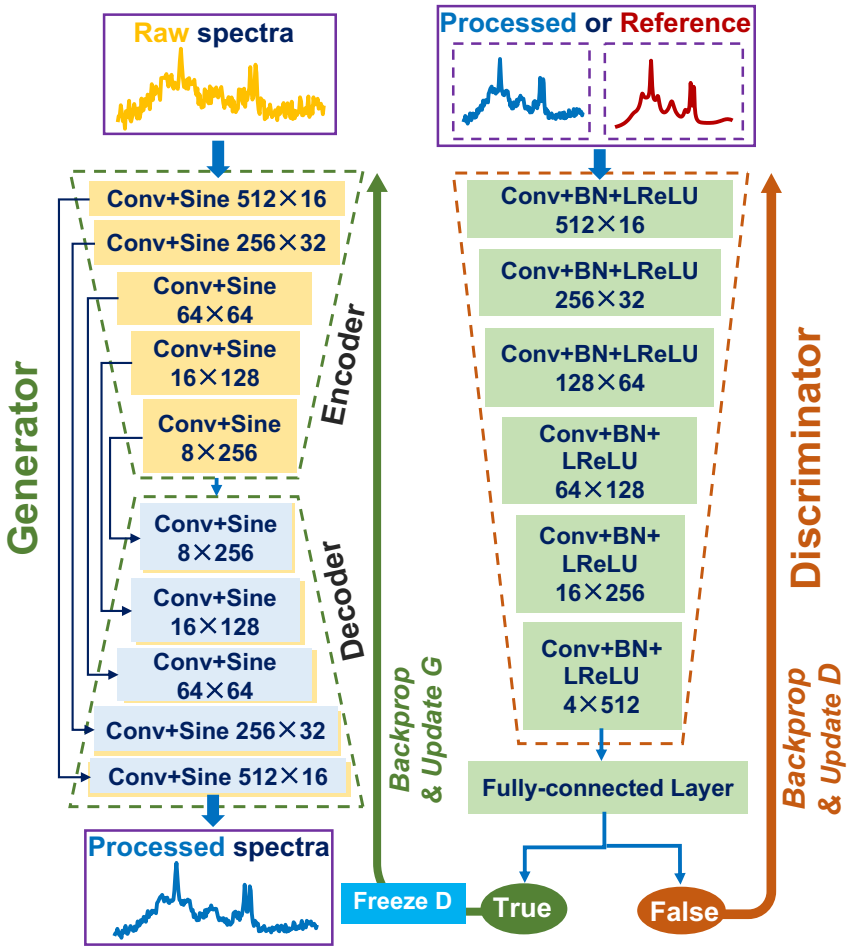

Figure 3.12 Architecture of the proposed conditional generative adversarial network for spectral recovery (SRGAN). A generator (G) and a discriminator (D) are trained jointly and gradually in SRGAN. G serves as a mapping function to recover a processed Raman spectrum from an input raw spectrum, while D is trained to differentiate the processed spectrum (generated by G) from the corresponding reference spectrum. G includes an encoder and a decoder structure, and each has 5 blocks. Each block contains a one-dimensional convolutional layer (Conv), a sinusoidal activation function (Sine) and different numbers of extracted feature maps. D consists of 6 blocks with a conv-batch normalization layer and leaky rectified linear unit (Conv+BN+LReLU), followed by a fully-connected layer.

3.5.8 Classification of different bacterial species using CNN

CNN was used to discriminate different bacteria based on their single-cell Raman spectra. Four convolutional layers, one fully connected layer and one output layer were included in our CNN architecture (**Figure 3.11a**). All the parameters of CNN were tuned using grid search algorithm. In the probability distribution generated by output layer, the species with the highest value among 5 bacteria was considered as the predicted species. "Ten-fold" cross validation was conducted to evaluate the stability of the CNN model for bacterial classification. In this strategy, 10% sample was randomly selected as the test dataset and the remaining 90% samples as the training dataset. The validation process was repeated until all the samples have been tested and the average accuracy over all the validations was defined as the overall accuracy of the CNN.

3.5.9 Testing of sorting capability

We further performed isolation of *C. jejuni* within a bacterial mixture using the proposed platform to evaluate its sorting efficiency. Bacterial solution was prepared by mixing *C. jejuni* and *S.* Typhimurium at 1:1 ratio by concentration and injected into the microfluidic chip. The well-trained CNN model (**Figure 3.11**) was integrated with the customized software to conduct the identification of each captured bacterial cell and guide the selective sorting. The cells

identified as *C. jejuni* were manipulated to the collection outlet and the total number was recorded in the program. The sorted cells in the collection tube were then cultivated on Mueller–Hinton blood agar. Single colonies formed on the agar were counted and the recovery rate was calculated as the number of single colonies on the agar plate divided by the number of collected *C. jejuni* cells reported in the program. The single colonies were visually examined and confirmed using qPCR developed in a previous study [47] to verify if the recovered cells were *C. jejuni* or not. Sorting accuracy was defined as the percentage of confirmed *C. jejuni* cells out of all the recovered cells. Three biological replicates were carried out with ~200 individual single cells tested in total.

3.6 References

[1] Y. He, X. Wang, B. Ma, J. Xu, Ramanome technology platform for label-free screening and sorting of microbial cell factories at single-cell resolution, Biotechnology Advances, 37 (2019) 107388.

[2] Y. Zhou, S. Bian, X. Zhou, Y. Cui, W. Wang, L. Wen, L. Guo, W. Fu, F. Tang, Single-cell multiomics sequencing reveals prevalent genomic alterations in tumor stromal cells of human colorectal cancer, Cancer Cell, 38 (2020) 818-828. e815.

[3] H.J. Butler, L. Ashton, B. Bird, G. Cinque, K. Curtis, J. Dorney, K. Esmonde-White, N.J. Fullwood, B. Gardner, P.L. Martin-Hirsch, Using Raman spectroscopy to characterize biological materials, Nature Protocols, 11 (2016) 664.

[4] A.C.S. Talari, Z. Movasaghi, S. Rehman, I.u. Rehman, Raman spectroscopy of biological tissues, Applied Spectroscopy Reviews, 50 (2014) 46-111.

[5] W. Liu, Z. Sun, J. Chen, C. Jing, Raman spectroscopy in colorectal cancer diagnostics: Comparison of PCA-LDA and PLS-DA models, Journal of Spectroscopy, 2016 (2016).

[6] K. Wang, L. Chen, X. Ma, L. Ma, K.C. Chou, Y. Cao, I.U.H. Khan, G. Golz, X. Lu, *Arcobacter* identification and species determination using Raman spectroscopy combined with neural networks, Applied Environmental Microbiology, 86 (2020).

[7] J.W. Chan, Recent advances in laser tweezers Raman spectroscopy (LTRS) for label-free analysis of single cells, Journal of Biophotonics, 6 (2013) 36-48.

[8] A. Ashkin, J.M. Dziedzic, J.E. Bjorkholm, S. Chu, Observation of a single-beam gradient force optical trap for dielectric particles, Optics Letters, 11 (1986) 288-290.

[9] W.E. Huang, A.D. Ward, A.S. Whiteley, Raman tweezers sorting of single microbial cells, Environmental Microbiology Reports, 1 (2009) 44-49.

[10] T. Fang, W. Shang, C. Liu, J. Xu, D. Zhao, Y. Liu, A. Ye, Nondestructive identification and accurate isolation of single cells through a chip with Raman optical tweezers, Analytical Chemistry, 91 (2019) 9932-9939.

[11] A. Grünberger, W. Wiechert, D. Kohlheyer, Single-cell microfluidics: opportunity for bioprocess development, Current Opinion in Biotechnology, 29 (2014) 15-23.

[12] A. Reece, B. Xia, Z. Jiang, B. Noren, R. McBride, J. Oakey, Microfluidic techniques for high throughput single cell analysis, Current Opinion in Biotechnology, 40 (2016) 90-96.

[13] A.Y. Lau, L.P. Lee, J.W. Chan, An integrated optofluidic platform for Raman-activated cell sorting, Lab on a Chip, 8 (2008) 1116-1120.

[14] X. Wang, L. Ren, Y. Su, Y. Ji, Y. Liu, C. Li, X. Li, Y. Zhang, W. Wang, Q. Hu, Raman-activated droplet sorting (RADS) for label-free high-throughput screening of microalgal single-cells, Analytical Chemistry, 89 (2017) 12569-12577.

[15] S. Dochow, C. Krafft, U. Neugebauer, T. Bocklitz, T. Henkel, G. Mayer, J. Albert, J. Popp, Tumour cell identification by means of Raman spectroscopy in combination with optical traps and microfluidic environments, Lab on a Chip, 11 (2011) 1484-1490.

[16] D.I. Ellis, R. Goodacre, Metabolic fingerprinting in disease diagnosis: biomedical applications of infrared and Raman spectroscopy, Analyst, 131 (2006) 875-885.

[17] Z. Wang, M. Zhang, P.d.B. Harrington, Comparison of three algorithms for the baseline correction of hyphenated data objects, Analytical Chemistry, 86 (2014) 9050-9057.

[18] G. Vivó-Truyols, P.J. Schoenmakers, Automatic selection of optimal Savitzky-Golay smoothing, Analytical Chemistry, 78 (2006) 4598-4608.

[19] Y. Xie, L. Yang, X. Sun, D. Wu, Q. Chen, Y. Zeng, G. Liu, An auto-adaptive background subtraction method for Raman spectra, Spectrochimica Acta Part A: Molecular and Biomolecular Spectroscopy, 161 (2016) 58-63.

[20] F. Ehrentreich, L. Sümmchen, Spike removal and denoising of Raman spectra by wavelet transform methods, Analytical Chemistry, 73 (2001) 4364-4373.

[21] I. Koo, X. Zhang, S. Kim, Wavelet-and Fourier-transform-based spectrum similarity approaches to compound identification in gas chromatography/mass spectrometry, Analytical Chemistry, 83 (2011) 5631-5638.

[22] P. Isola, J.-Y. Zhu, T. Zhou, A.A. Efros, Image-to-image translation with conditional adversarial networks, Proceedings of the IEEE conference on computer vision and pattern recognition, 2017, pp. 1125-1134.

[23] R. Smith, K.L. Wright, L. Ashton, Raman spectroscopy: an evolving technique for live cell studies, Analyst, 141 (2016) 3590-3600.

[24] K.S. Lee, M. Palatinszky, F.C. Pereira, J. Nguyen, V.I. Fernandez, A.J. Mueller, F. Menolascina, H. Daims, D. Berry, M. Wagner, An automated Raman-based platform for the sorting of live cells by functional properties, Nature Microbiology, 4 (2019) 1035-1048.

[25] H. Mao, P. Luchette, An integrated laser-tweezers instrument for microanalysis of individual protein aggregates, Sensors and Actuators B: Chemical, 129 (2008) 764-771.

[26] A. Ashkin, J.M. Dziedzic, Optical trapping and manipulation of viruses and bacteria, Science, 235 (1987) 1517-1520.

[27] M. El-Desouki, M.J. Deen, Q. Fang, L. Liu, F. Tse, D. Armstrong, CMOS image sensors for high speed applications, Sensors, 9 (2009) 430-444.

[28] G. Giridhar, R. Manepalli, G. Apparao, Confocal Raman spectroscopy, Spectroscopic methods for nanomaterials characterization, Elsevier2017, pp. 141-161.

[29] P.M. Burnham, D.R. Hendrixson, *Campylobacter jejuni*: collective components promoting a successful enteric lifestyle, Nature Reviews Microbiology, 16 (2018) 551-565.

[30] T. Fang, W. Shang, C. Liu, Y. Liu, A. Ye, Single-cell multimodal analytical approach by integrating Raman optical tweezers and RNA sequencing, Analytical Chemistry, 92 (2020) 10433-10441.

[31] M. Li, J. Xu, M. Romero-Gonzalez, S.A. Banwart, W.E. Huang, Single cell Raman spectroscopy for cell sorting and imaging, Current Opinion in Biotechnology, 23 (2012) 56-63.

[32] S. Yan, S. Wang, J. Qiu, M. Li, D. Li, D. Xu, D. Li, Q. Liu, Raman spectroscopy combined with machine learning for rapid detection of food-borne pathogens at the single-cell level, Talanta, 226 (2021) 122195.

[33] J. Gu, Z. Wang, J. Kuen, L. Ma, A. Shahroudy, B. Shuai, T. Liu, X. Wang, G. Wang, J. Cai, Recent advances in convolutional neural networks, Pattern Recognition, 77 (2018) 354-377.

[34] Z. Li, F. Liu, W. Yang, S. Peng, J. Zhou, A survey of convolutional neural networks: analysis, applications, and prospects, IEEE transactions on neural networks and learning systems, (2021).

[35] C. Lin, X. Li, T. Wu, J. Xu, Z. Gong, T. Chen, B. Li, Y. Li, J. Guo, Y. Zhang, Optofluidic identification of single microorganisms using fiber-optical-tweezer-based Raman spectroscopy with artificial neural network, BMEMat, 1 (2023) e12007.

[36] B. Zhou, L. Sun, T. Fang, H. Li, R. Zhang, A. Ye, Rapid and accurate identification of pathogenic bacteria at the single-cell level using laser tweezers Raman spectroscopy and deep learning, Journal of Biophotonics, 15 (2022) e202100312.

[37] D. Anggraini, N. Ota, Y. Shen, T. Tang, Y. Tanaka, Y. Hosokawa, M. Li, Y. Yalikun, Recent advances in microfluidic devices for single-cell cultivation: methods and applications, Lab on a Chip, 22 (2022) 1438-1468.

[38] C. Gawad, W. Koh, S.R. Quake, Single-cell genome sequencing: current state of the science, Nature Reviews Genetics, 17 (2016) 175-188.

[39] K.M. McKinnon, Flow cytometry: an overview, Current Protocols in Immunology, 120 (2018) 5-1.

[40] A. Adan, G. Alizada, Y. Kiraz, Y. Baran, A. Nalbant, Flow cytometry: basic principles and applications, Critical Reviews in Biotechnology, 37 (2017) 163-176.

[41] S. Kench, S.J. Cooper, Generating three-dimensional structures from a two-dimensional slice with generative adversarial network-based dimensionality expansion, Nature Machine Intelligence, 3 (2021) 299-305.

[42] I. Goodfellow, J. Pouget-Abadie, M. Mirza, B. Xu, D. Warde-Farley, S. Ozair, A. Courville, Y. Bengio, Generative adversarial nets, Advances in Neural Information Processing Systems, 27 (2014).

[43] D. Pathak, P. Krahenbuhl, J. Donahue, T. Darrell, A.A. Efros, Context encoders: feature learning by inpainting, Proceedings of the IEEE conference on computer vision and pattern recognition, 2016, pp. 2536-2544.

[44] X. Mao, Q. Li, H. Xie, R.Y. Lau, Z. Wang, S. Paul Smolley, Least squares generative adversarial networks, Proceedings of the IEEE international conference on computer vision, 2017, pp. 2794-2802.

[45] Spectral Database for Organic Compounds. Retrieved from http://sdbs.db.aist.go.jp/sdbs/cgi-bin/cre_index.cgi

[46] J.M. Smulko, N.C. Dingari, J.S. Soares, I. Barman, Anatomy of noise in quantitative biological Raman spectroscopy, Bioanalysis, 6 (2014) 411-421.

[47] R. Lv, K. Wang, J. Feng, D.D. Heeney, D. Liu, X. Lu, Detection and quantification of viable but non-culturable *Campylobacter jejuni*, Frontiers in Microbiology, 10 (2020) 2920.

Connecting Text

Chapter 3 introduced a Raman tweezers system combined with a microfluidic device and machine learning techniques for single-cell identification and nondestructive sorting. This optofluidic platform achieved a high accuracy of 94.9% for the identification of 5 leading foodborne bacteria including *C. jejuni* at single-cell level. In Chapter 4, this platform was further utilized to identify and discriminate *C. jejuni* cells in the VBNC state from their culturable counterparts at single-cell resolution. The influence of induction stresses or induction durations on the formed VBNC cells was also investigated. Furthermore, we applied a gradient-weighted class activation mapping technique to visualize the spectral regions that contributed most to the identification of VBNC *C. jejuni*. This provided insights to the molecular mechanisms of VBNC formation.

Chapter 4: Single-cell identification and characterization of viable but non-culturable *Campylobacter jejuni* using Raman tweezers system coupled with machine learning

4.1 Abstract

Campylobacter jejuni is a leading foodborne pathogen and it can enter a viable but non-culturable (VBNC) state to survive under environmental stresses, posing a significant health concern. In this study, we developed a culture-independent approach to identify and characterize VBNC *C. jejuni* at single-cell level using Raman tweezers system coupled with machine learning. Two representative *C. jejuni* strains were induced into the VBNC state under osmotic pressure (7% w/v NaCl solution) and aerobic stress (atmospheric condition), respectively. Images of phase-contrast microscopy and transmission electron microscopy revealed the morphological alterations of VBNC cells, such as the transformation from rod to coccus shape and the uneven distribution of cell content. Raman spectra were automatically collected from individual *C. jejuni* cells using an in-house Raman tweezers system combined with a microfluidic device. Based on the single-cell Raman spectra and convolutional neural network (CNN), VBNC *C. jejuni* cells could be successfully distinguished from their culturable counterparts with high accuracies ranging from 91.7% to 93.4%. In addition, there were no significant spectral changes between the VBNC cells formed under different stressors or with different induction periods. Furthermore, we utilized a gradient-weighted class activation mapping to highlight the spectral regions that contribute most to the CNN-based classification of culturable and VBNC cells. Molecular changes in proteins, nucleic acids, lipids and

peptidoglycan were identified in the VBNC cells, providing insights into the formation mechanism of VBNC state of *C. jejuni*. This approach holds the promise to study other unculturable bacterial populations in the environment and to advance our knowledge of microbial diversity and ecology.

4.2 Introduction

Campylobacter jejuni is a Gram-negative foodborne pathogen and considered as the leading bacterial cause of human gastroenteritis worldwide. *Campylobacter* was estimated to cause approximately 145,000 illnesses and 565 hospitalizations in Canada every year (1). Campylobacteriosis also affects 14.3 per 100,000 population in the U.S. (2), leading to an annual healthcare cost of ~$1.56 billion (3). Consumption of contaminated food, such as undercooked poultry and unpasteurized milk, is one of the major transmission routes of *C. jejuni* infections (4). Despite being considered as a fastidious bacterium (e.g., microaerophilic, 30-42°C), *C. jejuni* is prevalently spread in the environment and agri-food systems (5). Entering viable but non-culturable (VBNC) state is a survival strategy adopted by *C. jejuni* to combat adverse conditions, including extreme pH, oxidative stress, temperature fluctuation, osmotic pressure and limited nutrients (6). VBNC cells are unable to grow on the conventional culture media but maintain the membrane integrity and basic metabolic activity (7). VBNC *C. jejuni* can evade the routine culture-based detection and survive for extended periods under harsh environment due to the enhanced stress tolerance. It also possesses the ability to resuscitate and regain the virulence under favorable environment, posing a significant risk to food safety and public health (8).

Conventional detection methods for *C. jejuni* are mostly culture-dependent that significantly underestimate the presence of VBNC cells. Several viability-based assays have been applied to identify VBNC cells, such as direct viable count based on the absorption ability of antibiotics, detection of respiratory activity using 5-cyano-2,3-ditolyl tetrazolium chloride (CTC), and the LIVE/DEAD fluorescence staining methods that assess the cell membrane integrity (9). Molecular-based approaches have also been established for detecting VBNC *C. jejuni* based on

the evaluation of gene expression or selective DNA amplifications, such as reverse transcription quantitative polymerase chain reaction (RT-qPCR) (10) and the combination of qPCR with DNA-intercalating dyes (11). However, most of these methods are restricted by relatively low sensitivity, non-specificity, high cost or technical challenges (7, 9). Besides, the detection of VBNC *C. jejuni* typically requires an initial step of using the conventional plating assay to confirm the cells in a non-culturable state (12). This process is time-consuming (~48 h) and labor-intensive. Therefore, a sensitive and easy-to-use approach is demanded for the rapid diagnostics of *C. jejuni* in the VBNC state.

Raman spectroscopy has emerged as a non-destructive and label-free tool for bacterial identification and characterization (13). Raman spectra describe the vibrational signatures of diverse molecules, thereby deciphering the comprehensive molecular compositions of the entire bacterial cell. However, most Raman spectra acquired from microorganisms represent the averaged Raman signals of bulk population, hampering the detailed and accurate investigation of individual cells due to the population heterogeneity. Raman optical tweezers system, combining optical tweezers and Raman spectroscopy, can overcome this issue via the ability to collect Raman spectra from single bacterial cell (14). Optical tweezers can trap and manipulate an individual cell in the focused laser beam and then Raman spectra can be acquired simultaneously (15). Based on the single-cell analytical resolution, Raman optical tweezers system represents a promising approach for the identification of unculturable bacteria especially from a mixed microbial population. VBNC bacterial cells usually exhibit distinct compositional properties compared to their culturable counterparts (8), potentially serving as biomarkers for selective detection of VBNC cells using Raman tweezers. Moreover, the “fingerprinting” of Raman

spectra might help decipher the biochemical features of VBNC cells and reveal the underlying mechanism of VBNC formation.

Raman spectra are high-dimensional data and the spectral variations among different bacterial samples are generally subtle, especially for single-cell Raman spectra with relatively low signal-to-noise ratio (SNR) (16). Therefore, reliable and advanced classification techniques are required to retrieve the intricate characteristics from complex Raman spectra. Conventional multivariate methods, such as principal component analysis (PCA), linear discriminant analysis (LDA) and support vector machine (SVM), have been frequently utilized for the classification of Raman spectra (17). However, their applications are usually hindered by the restricted capability for non-linear tasks, limited robustness, and challenge in handling large-scale datasets. Convolutional neural networks (CNNs) have emerged as powerful tools for Raman spectroscopic based analyses (18, 19). CNNs enable the automatic feature extraction and demonstrate high robustness to noise, thereby significantly enhancing the classification accuracy using single-cell Raman spectra. For examples, CNN was combined with Raman spectroscopy to discriminate methicillin-resistant and -susceptible *Staphylococcus aureus* strains and achieved an accuracy of 89.1% (20). In another study, an average accuracy of 95.64% was obtained for the CNN-based classification of 14 microbial species based on single-cell Raman spectra (21). Therefore, CNN has the potential to assist in the examination of VBNC *C. jejuni* at single-cell level using Raman optical tweezers.

Although CNNs generally achieve superior accuracy compared to the traditional machine learning algorithms, their “black-box” operation and “end-to-end” working mode make it

challenging to comprehend the decision-making process (22). Understanding the spectral regions responsible for CNN-based classifications in biological studies is critical to both model verification and data interpretability. Recently, gradient-weighted class activation mapping (Grad-CAM) has been proven to be a valuable technique for visual explanation of CNN models in various applications (23). Grad-CAM can generate a heatmap based on the weighted sum of features maps in a convolutional layer to demonstrate the contribution of each spectral feature to the classification. For Raman spectroscopic based classifications of bacteria, a reliable localization of the influential spectral regions can help ensure that the identification is based upon the signals from the sample rather than background noises. The recognized Raman features can also provide insights into the molecular compositions that drive the classification, facilitating a further interpretation of the bacterial samples.

In this study, we proposed a novel culture-free approach of employing Raman optical tweezers and machine learning algorithms for the identification of VBNC *C. jejuni* at single-cell level. Two *C. jejuni* strains were induced into the VBNC state under different adverse conditions (i.e., osmotic pressure and aerobic atmosphere). Single-cell Raman spectra of culturable and VBNC *C. jejuni* were automatedly collected with our home-built Raman optical tweezers platform integrated with a microfluidic device. A CNN model was used to differentiate the culturable and VBNC cells and Grad-CAM was further conducted to understand the compositional changes during VBNC formation. To the best of our knowledge, this is the first study of utilizing Raman tweezers combined with neural networks for the single-cell identification and characterization of VBNC *C. jejuni*.

4.3 Materials and methods

4.3.1 Bacterial cultivation

Two *C. jejuni* strains, namely F38011 (human isolate) and ATCC33560 (bovine feces isolate) were included in this study. Both *C. jejuni* strains were routinely cultivated on Mueller–Hinton (MH) blood agar (5% sheep blood supplement; BD Difco, Waltham, USA) under microaerobic condition (10% CO_2) at 37°C. Overnight culture of *C. jejuni* was prepared by transferring several single colonies into the MH broth (BD Difco, Waltham, USA) and incubated with a constant shaking of 175 rpm. Bacterial culture was harvested after 16-18 h and diluted to an initial optical density at 600 nm (OD_{600}) of 0.3, equivalent to ~10^9 CFU/mL. Both strains were kept in glycerol (20% v/v) at −80°C for long-term storage.

4.3.2 Induction and characterization of VBNC *C. jejuni*

C. jejuni strains were induced into the VBNC state under osmotic stress and aerobic condition, respectively, following the procedures described in our previous studies (11, 24). Sodium chloride (NaCl) solution at 7% (w/v) was used to generate high osmotic pressure. Overnight culture of *C. jejuni* was centrifuged to remove the growth media and resuspended into the NaCl solution to a final concentration of 8 log CFU/mL. The bacterial suspension was then incubated at microaerobic condition for 24 h. For the induction under aerobic stress, overnight culture was diluted to 8 log CFU/mL in MH broth, followed by incubation under atmospheric condition for 48 h. Samples were kept at 37°C with a constant shaking at 175 rpm under both conditions. To compare the VBNC cells at different dormancy levels, *C. jejuni* F38011 was also induced at hyperosmotic and aerobic condition for extended period of 48 h and 72 h, respectively.

At the end of the induction, the absence of culturable cells in the treated bacterial sample was confirmed using the plating assay. Briefly, 3 mL of the induced samples were separately transferred onto MH blood agar plates and the detection limit was defined as 0.3 CFU/mL. In the meanwhile, the formation of VBNC population was determined by propidium monoazide combined with real-time polymerase chain reaction (PMA-qPCR) as aforementioned with minor modifications (11). PMA is a DNA-intercalating dye that can bind to the DNA from dead cells with compromised cell membrane and prevent the subsequent amplification, enabling the selective quantification of viable cells. Bacterial culture was treated with 15 μM of PMA to quench the DNA from dead cells, followed by DNA extraction and qPCR amplification. Primers (5′-GAGTAAGCTTGCTAAGATTAAAG-3′ and 5′-AAGAAGTTTTAGAGTTTCTCC-3′) targeting the *rpoB* gene were used in the *C. jejuni*-specific qPCR analysis. When no culturable cells were detected (i.e., <0.3 CFU/mL), all the viable cells determined using PMA-qPCR were considered as VBNC cells.

4.3.3 Phase-contrast imaging and transmission electron microscopy

We investigated the morphological differences between normal culturable cells and VBNC cells of *C. jejuni* using phase-contrast microscopy (PCM) and transmission electron microscopy (TEM), respectively. Culturable cells at the exponential phase were collected from overnight culture after incubation for 16 h. VBNC cells were harvested at the end of the induction as aforementioned. PCM images of the samples were captured using the microscope (IX71, Olympus, Tokyo, Japan) included in our Raman optical tweezers system (see details in the following section). To visualize the internal structures of *C. jejuni* cells using TEM, bacterial cell pellets were harvest by centrifugation (15,000 ×*g*, 3 min) and resuspended in phosphate buffered

saline (PBS). Bacterial suspensions were applied onto a glow-discharged and carbon-coated grid and incubated for 3 min, followed by staining with 1% uranyl acetate for 30 s. Images of the stained samples were acquired with 20,000× and 50,000× magnification using a FEI Tecnai Spirit TEM (FEI, Hillsboro, USA) operating at 80 kV.

4.3.4 Setup of Raman tweezers system and automatic Raman spectral collection

Single-cell Raman spectra of culturable and VBNC cells were acquired using our home-built Raman optical tweezers system combined with a microfluidic chip. Schematic illustration of our Raman tweezers system is displayed in **Figure 4.1a**. This system consists of a 671-nm diode laser (Optotronics, Chelmsford, USA), a confocal Raman spectrometer (Andor Kymera 328i-A, Oxford instruments, Abingdon, UK), an inverted phase-contrast microscope (IX71, Olympus, Tokyo, Japan), and other optical apparatuses (Thorlabs, Newton, USA). The single laser serves as the source for both Raman excitation and optical tweezering. The laser beam (red) is guided through dichroic mirrors (DM1, DM2), and mirrors (M1-2) to a 60× objective lens (NA = 0.9; UPLFLN, Olympus) and focused on samples in the microfluidic chip. An optical trap is formed at the highly focused laser beam to capture bacterial cells at focal spot and Raman scattering of the trapped cell was generated simultaneously (**Figure 4.1b**). Raman scattering signals (green beam) pass through the pinhole (40 μm) and enter the spectrometer equipped with an 830 lines/mm grating. Dispersed Raman signals were finally recorded by a thermoelectric-cooled charge-coupled device (CCD) camera to generate Raman spectra. Two cameras (20× and 100×, Thorlabs, USA) were used to collect imaging signals (blue beam) emitted from the phase-contrast microscope and monitor the single-cell manipulation process under different magnifications.

A polydimethylsiloxane (PDMS)-based microfluidic chip was integrated with Raman tweezers for single-cell analysis. **Figure 4.1c** shows the Y-shape chip layout that comprises two inlets, a main analysis channel and one outlet for waste collection. This PMDS chip was fabricated using standardized soft lithography technique as described in our previous study (25). The microfluidic chip was mounted onto the x/y/z motorized microscope stage to achieve 3-dimensional cell manipulation using optical tweezers. Single-cell spectral collection was automatically operated using an in-house LabVIEW (National Instruments) software program. This program integratedly controls all the hardware in the system, including laser shutter, spectrometer, microscope scanning stage, and cameras. Bacterial suspension was pumped into the microfluidic chip via sample inlet and PBS buffer was injected via buffer inlet. Sample stream was pushed to one side of the channel by the buffer sheath flow, forming an evaluation region without samples. The focused laser beam could randomly capture an individual cell in the sample flow and move it to the evaluation region for spectral acquisition. This precautionary measure was implemented to prevent the capture of other surrounding cells during spectral acquisition, ensuring the spectrum was collected from a single cell. This can also minimize the risk of the trapped cell being lost due to cell collisions, improving the analysis efficiency. Approximately 25 mW of laser power was focused on the bacterial cell to generate a stable optical trap without significant photodamage. Each Raman spectrum was integrated for 30 s over the wavenumber region from 750 to 1,800 cm^{-1} with a resolution of 2 cm^{-1}. The analyzed cell was released to the sample stream by blocking the laser beam with optical shutter and the entire process was then repeated for the subsequent cells. With this automated process, ~200 single-cell Raman spectra were obtained for each VBNC and culturable *C. jejuni* sample in 3 biological replicates.

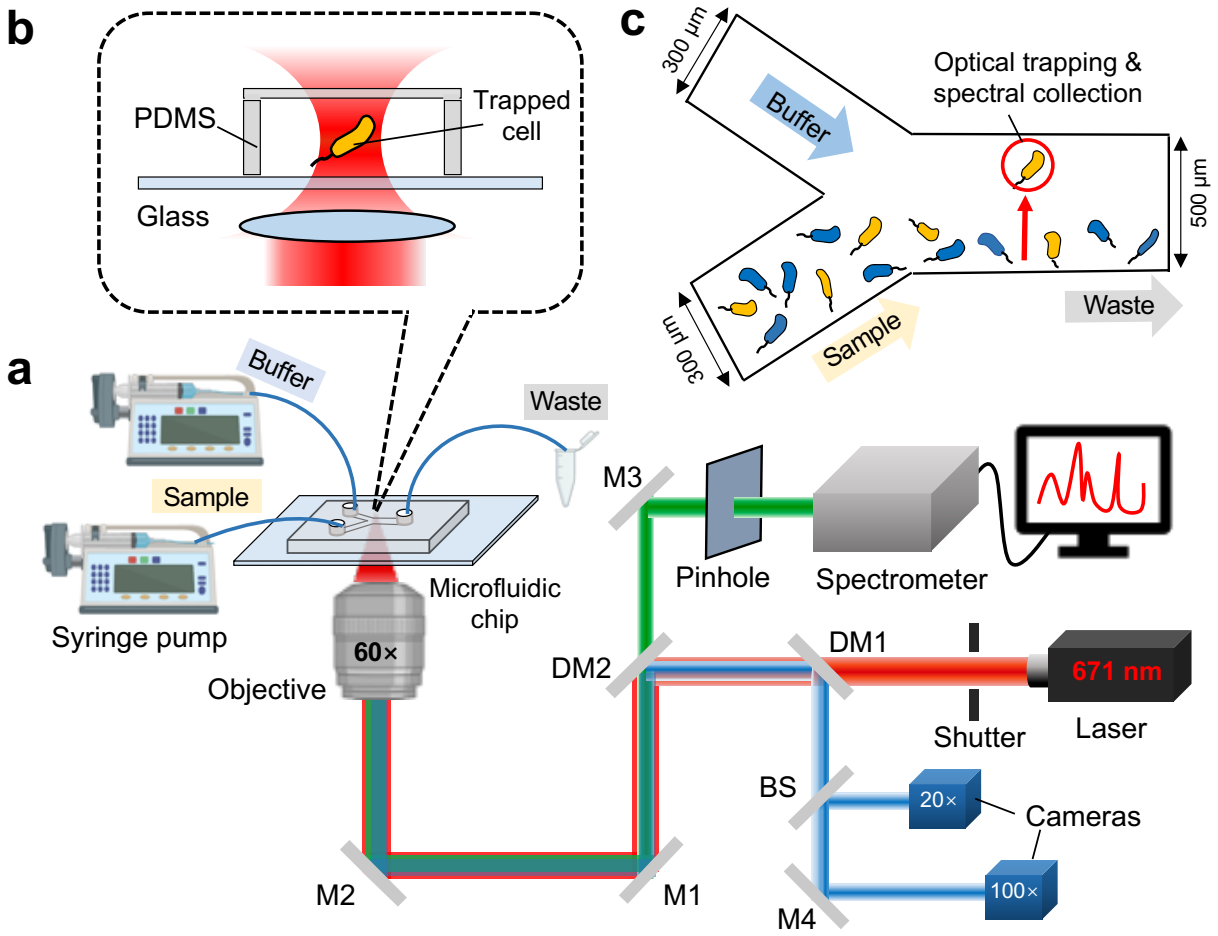

Figure 4.1 Schematic illustration of Raman optical tweezers combined with microfluidic device. (a) Simplified optical configuration of the Raman optical tweezers system. Laser beam (red path) from a 671-nm laser source is focused on the sample in a microfluidic chip via a 60× objective (NA = 0.9). The generated Raman scattering signal (green beam) is directed to the spectrometer for Raman spectral collection. Imaging signals (blue beam) from the phase-contrast microscope are separated by a beam splitter to both cameras (20× and 100× magnifications, respectively) for real-time monitoring of the single-cell manipulation. M: mirror; DM: dichroic mirror; BS: beam splitter. (b) Optical tweezering of bacterial cell within the polydimethylsiloxane (PDMS)-based microfluidic channel. (c) Working principle of the Raman tweezers-based optofluidic platform. Individual bacterial cell is randomly captured by the optical tweezers and immediately moved to the evaluation region (red circle) to collect single-cell Raman spectra.

4.3.5 Raman spectral preprocessing

Spectral preprocessing is a primary and inevitable step for Raman spectra to improve the spectral quality and enhance the accuracy for the subsequent data analyses. Median filtering was applied to remove cosmic rays and other noises, followed by vector normalization to minimize the instrumental variations. Raman scattering signals generated from the PDMS microfluidic chip were subtracted from the Raman spectra. All the spectral preprocessing steps were carried out using MATLAB (R2021b, MathWrorks).

4.3.6 Classification using CNN

A CNN was developed and employed for the discrimination between culturable and VBNC *C. jejuni* cells based on the single-cell Raman spectra. The architecture of the proposed CNN comprised an input layer, 6 convolutional layers to extract the features, 2 fully connected layers to perform the classification, and an output layer to generate the identification results. One-dimensional single-cell Raman spectra of *C. jejuni* were utilized as the input. Six convolutional layers contained 256, 512, 128, 64, 32 and 16 filters, respectively. These filters had a kernel size of 3×1 and a Rectified Linear Unit (ReLU) activation function. Following the convolution, the extracted features were then flattened and analyzed by 2 fully connected layers with 128 and 64 neurons, respectively. Softmax activation function was adopted in the output layer. The tested cell would be classified as either culturable or VBNC cell based on the generated probability distribution.

Raman spectra of each bacterial group were randomly divided into two subsets: 1) training data set (80% of the entire data) and 2) validation data set (the remaining 20%). The CNN was firstly

trained on the training set for 500 epochs with an initial learning rate of 0.0001. Validation set was then used to evaluate the overfitting and tune model hyperparameters via grid search. Finally, the performance of the optimized CNN was verified using a holdout test data set collected from an independent biological batch, including ~30 spectra for each bacterial group. Identification accuracies for all the three data sets were separately generated. All the algorithms were conducted using Python 3.7.

We further assessed the robustness of the CNN model using receiver operating characteristic (ROC) curve. It was created by plotting the true-positive rate (sensitivity) over the false positive rate (1-specificity) across various threshold values. The calculations were carried out according to the equations below:

$$\text{True positive rate} = \frac{\text{TP}}{\text{TP+FN}}$$

$$\text{False positive rate} = \frac{\text{FP}}{\text{FP+TN}}$$

, where TP, FP, TN, FN represent true positive, false positive, true negative and false negative, respectively. The area under the curve (AUC) values (0-1) were also calculated to quantify the overall performance of the classifier. Specifically, a higher AUC value indicates a better discrimination between positive and negative instances, with the best performance at 1.

To compare the performance of different classifiers, another commonly used machine learning algorithm, SVM, was also applied for the single-cell identification of VBNC *C. jejuni*. Sigmod

kernel function and c value of 0.95 were utilized. The SVM model was trained and assessed on the same training, validation and test data set as aforementioned.

4.3.7 Features visualization using Grad-CAM

Interpretability in CNN-based spectral analysis is crucial to understanding the classification process and verifying whether the predictions rely on characteristic peaks rather than background noises. In this study, Grad-CAM was utilized to identify and visualize the Raman spectral features that play an important role in the classification between VBNC and culturable bacterial cells. The computation of Grad-CAM involves calculating the gradients of the predicted class score with respect to the feature maps of a convolutional layer and then obtaining a weighted sum of these feature maps (23).

Key equations used in calculating Grad-CAM scores are described below.

$$\alpha_k^c = \frac{1}{Z}\sum_i\sum_j \frac{\partial y^c}{\partial A_{ij}^k}$$

, where α_k^c represents the importance weight of the k^{th} feature map in the convolutional layer concerning the target class c; $\frac{\partial y^c}{\partial A_{ij}^k}$ calculates the gradient of class c with respect to the k^{th} feature map; $\frac{1}{Z}\sum_i\sum_j(\cdot)$ represents global average pooling, where Z is the total number of spatial locations in the feature map.

$$L_{Grad-CAM}^c = \mathrm{Re}\,LU\left(\sum_k \alpha_k^c A^k\right)$$

, where $L^c_{Grad-CAM}$ represents the class-discriminative localization heatmap generated for class *c*; $\sum_k \alpha_k^c A^k$ calculates the weighted sum of the features maps; $\mathrm{Re}LU(\cdot)$ is the rectified linear unit activation function.

The generated Grad-CAM heatmap reveals the contribution of different spatial locations in the input Raman spectra to the classification results, where colors ranging from blue to red correspond to values between 0 to 1. Region with a larger value indicates a higher impact on the decision-making of the CNN model. Top 10 spectral regions with the highest contribution were highlighted in the heatmap while all other regions were displayed in blue for a better visualization.

4.3.8 Statistical analysis

Means and standard deviations of PMA-qPCR results were calculated using Excel (Microsoft, Seattle, WA, USA). Statistical significance tests were performed with analyses of variance (ANOVA) using SPSS Statistics (IBM, Armonk, NY, USA) ($P < 0.05$).

4.4 Results and discussion

4.4.1 Induction and morphological characterization of VBNC *C. jejuni*

C. jejuni is able to enter the VBNC state to survive under adverse conditions, such as nutrient deficiency, osmotic pressure, oxidative stress and temperature shift (6). In this study, VBNC cells of *C. jejuni* were prepared under osmotic stress and aerobic condition to mimic the common stressors encountered during food harvest, processing, and storage. As no culturable cells were

detected using the plating assay (i.e., <0.3 CFU/mL) at the end of the indication, all the viable cell counts quantified using PMA-qPCR were considered as VBNC cells. As shown in **Figure S4.1**, *C. jejuni* strains were completely induced into the VBNC state under both conditions with a final concentration of ~log 6-log 7 CFU/mL, representing ~1%-10% of the initial population.

The morphologies of the normal culturable and VBNC *C. jejuni* cells were examined using PCM equipped in our Raman tweezers system and TEM (**Figure 4.2**). PCM can directly visualize transparent live cells without staining and reveal the optical density and refractive index within the cells (26). TEM are based on the electron density of the cell contents and usually provide a higher resolution of images than light microscopes. Culturable *C. jejuni* cells at the exponential phase indicate a typical rod shape in both PCM and TEM images, and cell contents are uniformly distributed (**Figure 4.2**). In comparison, VBNC cells induced under osmotic pressure exhibit reduced cell size in a coccoid form. The cell shrinkage is probably attributed to the efflux of water from bacterial cells, driven by the need to equalize the osmotic pressure in a high-concentration salt solution. For the VBNC cells formed in aerobic condition, they maintain the rod shape but the chromosomal DNA and other cytoplasmic components (e.g., ribosomes) show less density and uneven distribution (**Figure 4.2bc**), indicating low metabolic activities and potential protein aggregation. These alterations are also revealed in the PCM images (**Figure 4.2a**), where aerobically induced VBNC cells show less prominent appearance compared to their culturable counterparts. Fewer intracellular components cause less optical density and affect their refractive properties, reducing the phase contrast and visibility of the cells. Both types of VBNC cells demonstrate intact cell membranes that verify their viability.

The morphological transition from rod to coccoid shape of VBNC *C. jejuni* was also reported in other previous studies (10, 27). Alterations in cellular shapes might be resulted from the changes in cell membrane compositions, water content, and other cellular activities. For example, peptidoglycans in the cell membrane demonstrated a high degree of cross-linking when bacterial cells entered the VBNC state (28). Extensive protein aggregation was observed in the VBNC *E. coli* O157:H7, while absent in exponential and resuscitated cells (29). These morphological variations indicate the adaptions employed by VBNC cells in response to adverse conditions, while more detailed molecular changes during VBNC formation need further exploration.

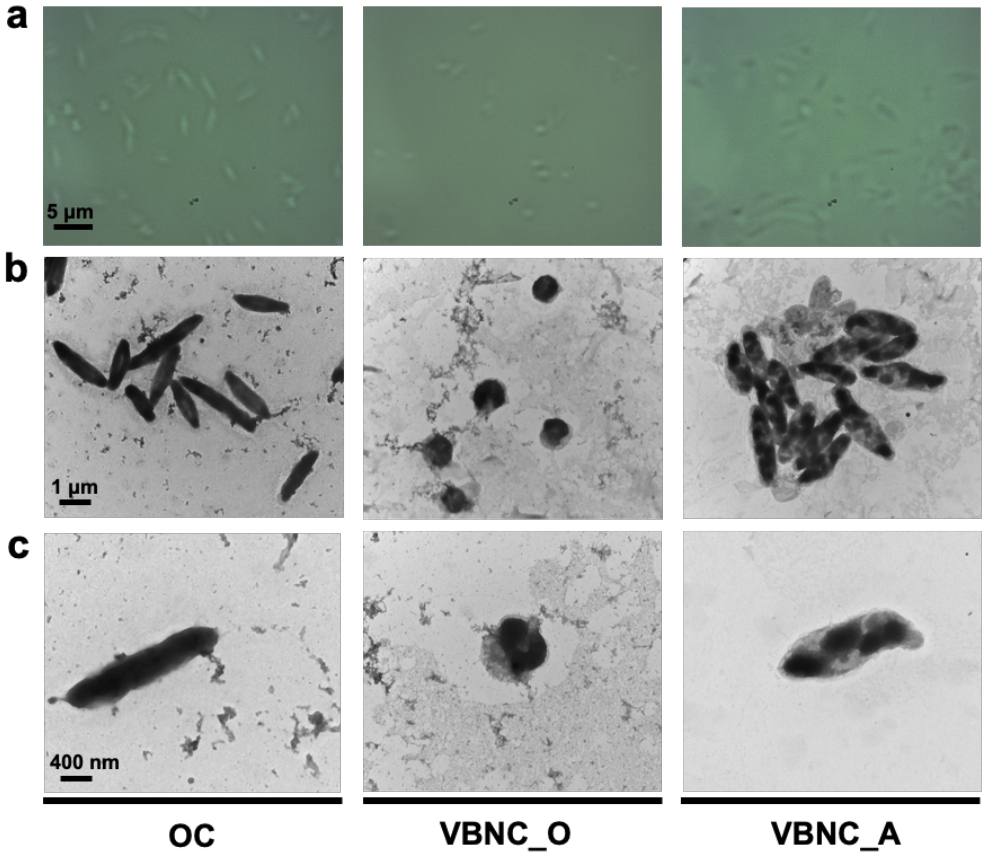

Figure 4.2 Morphological characterizations of VBNC *C. jejuni* using phase-contrast microscopy (a) and transmission electron microscopy with 20,000× (b) and 50,000× (c) magnifications, respectively. Culturable cells were harvested from overnight culture (OC) after

16-h incubation when cells were at the exponential growth phase. VBNC cells were induced under osmotic pressure (VBNC_O) and aerobic condition (VBNC_A), respectively. Culturable cells show typical rod shapes and uniform distribution of cell contents. Coccoid shapes are observed in osmotic-induced VBNC cells, and aerobic-induced VBNC cells exhibit less cellular content and uneven density.

4.4.2 Single-cell Raman spectra of culturable and VBNC *C. jejuni*

Raman optical tweezers system has been proven to be a powerful tool to non-destructively monitor the physiological dynamics of single bacterial cells (14). To collect the single-cell Raman spectra of VBNC *C. jejuni* cells, we constructed an in-house Raman tweezers system, compromising optical tweezers, a confocal Raman spectroscopy, an inverted phase-contrast microscope, and a PDMS-based microfluidic chip. **Figure 4.1** shows the simplified schematic diagram of this Raman tweezers system and more details regarding the instrument construction and operation are provided in our previous study (**Chapter 3** in this thesis).

Raman spectra of culturable and VBNC cells of *C. jejuni* were automatically collected from individual cells (see details in **Section 4.3.4**). Average single-cell Raman spectra calculated from each bacterial group are displayed in **Figure 4.3**. All Raman spectra were acquired in the wavenumber region from 750 to 1800 cm^{-1}, representing the "fingerprinting" spectral features of bacterial cells. Although single-cell Raman spectra generally demonstrate relatively low SNR, diverse Raman peaks were observed for each bacterial type. Most characteristic peaks were attributed to the major components of *C. jejuni* cells, including carbohydrates (860 cm^{-1}, 1576 cm^{-1}), lipids (1256 cm^{-1}, 1448 cm^{-1}), nucleic acids (785 cm^{-1}, 1098 cm^{-1}, 1320 cm^{-1}) and proteins (756 cm^{-1}, 1004 cm^{-1}, 1320 cm^{-1}, 1648 cm^{-1}) (30).

For both *C. jejuni* strains, culturable and VBNC cells induced under different stresses indicate slightly different Raman spectral patterns in terms of relative intensity of specific peaks (e.g., 1098 cm^{-1}, 1320 cm^{-1}). Due to the intrinsic complexity of Raman spectral features and inferior quality of single-cell Raman spectra, it is challenging to visually discern the subtle spectral variations among different groups. Raman spectra obtained from individual cells within the same bacterial group may also exhibit considerable variability. Therefore, advanced analytical tools are demanded to accurately distinguish VBNC and culturable *C. jejuni* at single-cell level and to interpretate these intricate spectral variations.

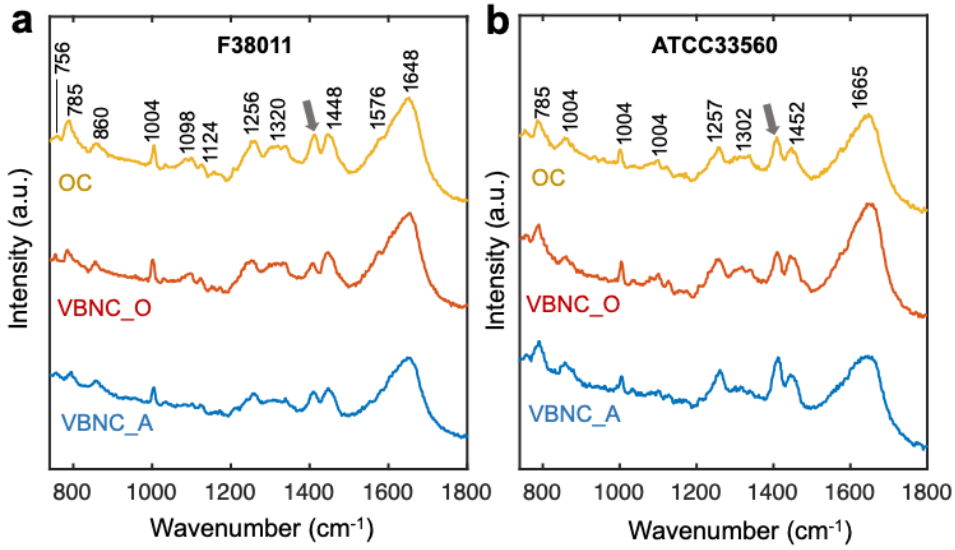

Figure 4.3 Average single-cell Raman spectra of culturable and VBNC *C. jejuni* cells. Two *C. jejuni* strains F38011 (a) and ATCC 33560 (b) were utilized. Culturable cells were collected from the overnight culture (OC) of *C. jejuni* after 16-h incubation. VBNC cells were induced under osmotic pressure for 24 h (VBNC_O) and aerobic condition for 48 h (VBNC_A), respectively. Each single-cell Raman spectrum was acquired with an integration time of 30 s. Average Raman spectrum was calculated from all the spectra collected for each bacterial group. Raman peak indicated by the black arrow is attributed to the PDMS layer of the microfluidic chip.

4.4.3 Classification of culturable and VBNC *C. jejuni* at single-cell level

CNN was utilized to discriminate the Raman spectra of VBNC cells and culturable cells of *C. jejuni*. CNN is a state-of-the-art machine learning algorithm that can automatically learn hierarchical features and achieve high performance on complex non-linear tasks (31). Our CNN contains 6 convolutional layers to capture features from input spectra and 2 fully connected layers to conduct the classification (**Figure 4.4a**). As Raman spectra are one-dimensional data, pooling layers commonly used in image classifications were excluded to reduce the computational cost and the potential loss of spectral details.

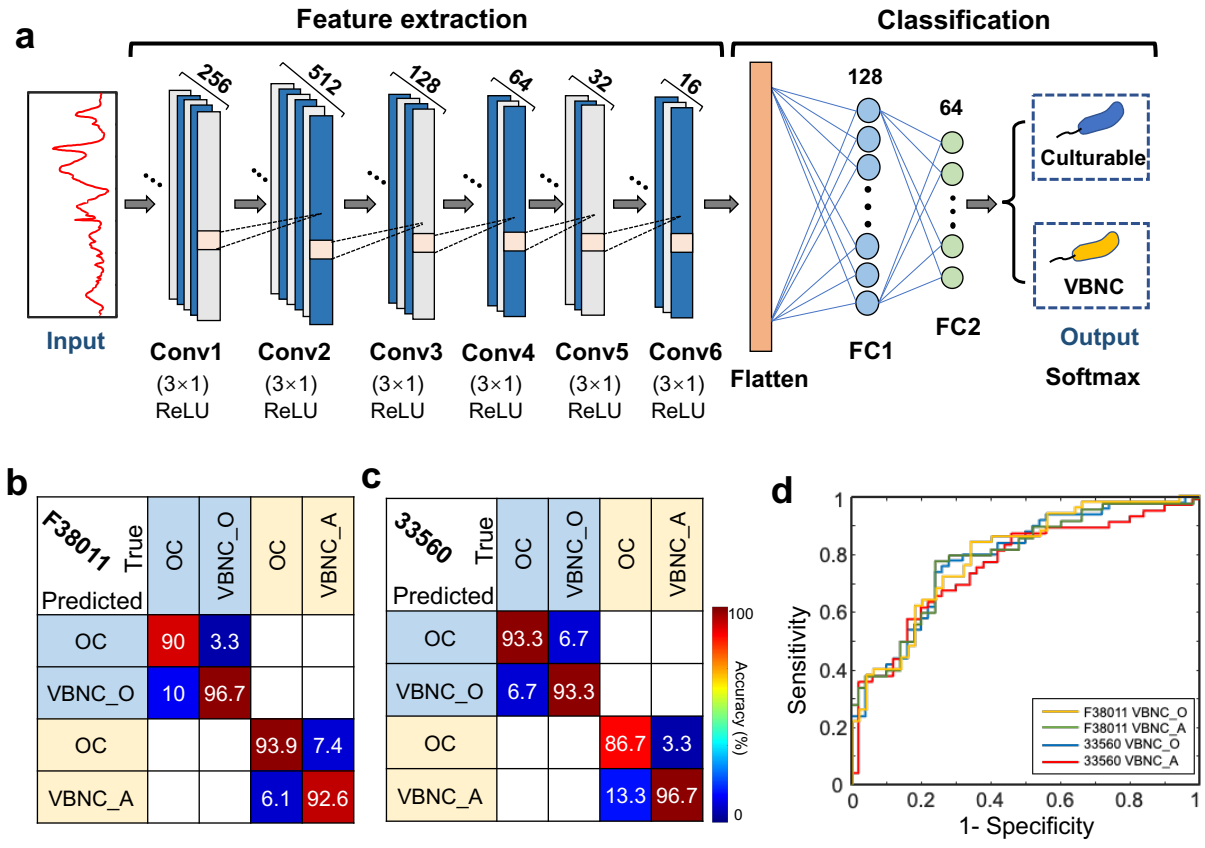

Figure 4.4 Raman spectroscopic based single-cell identification of VBNC *C. jejuni* using convolutional neural network (CNN). (a) Structure of the proposed CNN model. This model

consists of 6 convolutional layers for feature extraction and 2 fully connected layers for classification. The tested sample is predicted as either culturable cell or VBNC cell based on the input single-cell Raman spectrum. (b-c) Classification results between culturable and VBNC cells of *C. jejuni* F38011 and ATCC33560, respectively. OC: culturable cells collected from fresh overnight culture; VBNC_O: VBNC cells induced under osmotic stress; VBNC_A: VBNC cells induced under aerobic condition. Values on the diagonal regions indicate the identification accuracy for each bacterial type on the test data set. The average accuracies are summarized in Table 4.1. (d) The ROC curve for the classification of culturable and VBNC *C. jejuni* cells using CNN with the test data set. The AUC values are summarized in Table S4.1.

For each *C. jejuni* strain, we compared the culturable cell at the exponential growth phase with VBNC cells induced under osmotic pressure and aerobic condition, respectively. We trained the CNN model on the training set (80% of the total data) and verified its classification accuracy on the validation set (20% of the total data) to optimize the parameters and avoid overfitting. The performance of the optimized CNN was further unbiasedly evaluated on an independent test data set collected from a separate bacterial batch including 30 spectra per bacterial group. **Table 4.1** summarizes the average classification accuracies achieved for each data set, and the detailed prediction results on the test data set are displayed in the confusion matrices (**Figure 4.4bc**). For the VBNC cells of *C. jejuni* F38011 induced under osmotic pressure, the average identification accuracy for the test set was 93.4% (**Table 4.1**) and only 3.3% of the spectra were mistakenly predicted as culturable cells. Similar accuracy of 93.3% was achieved to differentiate aerobically induced VBNC cells from their culturable counterparts. For *C. jejuni* ATCC 33560, the discrimination between culturable cells from osmotic-induced and aerobic-induced VBNC cells reached an accuracy of 93.3% and 91.7% (**Table 4.1**), respectively. We further assessed the sensitivity and specificity of the CNN model using the ROC curve (**Figure 4.4d**). The AUC value ranged from 0.7668 to 0.7948 (**Table S4.1**), suggesting that Raman tweezers system

combined with CNN represents a reliable approach to identify VBNC *C. jejuni* at single-cell resolution.

Table 4.1 Identification accuracy (%) for VBNC *C. jejuni* using single-cell Raman spectra coupled with machine learning algorithms.

Strain	Classification groups		CNN			SVM		
			Training	Validation	Test	Training	Validation	Test
F38011	OC	VBNC_O	93.4	91.7	93.4	84.1	80.3	83.3
	OC	VBNC_A	94.5	92.0	93.3	85.9	83.2	85.0
ATCC 33560	OC	VBNC_O	92.8	91.1	93.3	83.2	83.1	83.3
	OC	VBNC_A	94.2	93.3	91.7	86.3	84.4	81.7

OC: culturable cells collected from fresh overnight culture; VBNC_O: VBNC cells induced under osmotic stress; VBNC_A: VBNC cells induced under aerobic condition; CNN: convolutional neural network; SVM: support vector machine.

In addition, we compared the performance of the proposed CNN with SVM, another popular machine learning algorithm. SVM was applied to the same tasks of identifying VBNC cells formed under different conditions from their culturable counterparts. The classification accuracies ranged from 81.7%-85.0% on the holdout test data set (**Table 4.1**). CNN outperformed SVM in terms of accuracy for all the classification tasks involving different bacterial groups, indicating that CNN is more suitable for the analysis of single-cell Raman spectra with relatively low SNR in the current study.

Identification of *C. jejuni* among other major foodborne pathogens was achieved in our recent study using single-cell Raman spectroscopic analysis (32). The current study steps forward to propose a culture-free approach for discriminating *C. jejuni* at different physiological states, namely VBNC and culturable cells, at the single-cell level. Rapid and accurate diagnostics of VBNC cells is critical to mitigate the foodborne diseases and allow effective clinical therapies. Raman spectroscopy coupled with stable isotope probing was recently applied to study the metabolic events of VBNC bacteria, as incorporation of isotope in VBNC cells could lead to specific Raman peak shifts (33-35). For example, D_2O-labeled Raman spectroscopy revealed that UV-treated VBNC *E. coli* cells demonstrated treatment dose- and incubation time-dependent metabolic activities (35). However, this method was unable to distinguish the VBNC and culturable cells in a mixed population and the isotope labeling might introduce artifacts that hamper potential further analyses. In the current study, the single-cell identification and characterization of VBNC cells were based on the intrinsic Raman features without any labeling requirement. Furthermore, the entire Raman spectra were taken into consideration rather than focusing on a single Raman peak shift, providing enhanced discriminatory power and molecular insights. Matrix-assisted laser desorption ionization time-of-flight (MALDI-TOF) mass spectrometry was used to differentiate *E. faecalis* in culturable, VBNC and resuscitated state based on the peptide mass fingerprints (36). However, this approach could not be carried out at the single-cell resolution and thus usually requires time-consuming culturing to get sufficient biomass. It is challenging to be utilized to evaluate the nonculturable bacteria with relatively low concentrations in real-world samples. By using the Raman tweezers system combined with CNN in our study, VBNC *C. jejuni* cells were accurately identified at single-cell level in a culturable-

independent and non-destructive manner, offering benefits for studying nonculturable cells *in situ* in heterogeneous microbial populations.

4.4.4 Discrimination of VBNC *C. jejuni* induced with different conditions

We further explored the influence of induction methods and induction periods on the formed VBNC cells. To investigate the cellular compositional variations upon exposure to different stressors, classifications were conducted between osmotic-induced and aerobic-induced VBNC cells of both *C. jejuni* strains. As shown in **Table 4.2**, the classification accuracy was 73.7% for F38011 and 73.2% for ATCC 33560, indicating that there were no significant spectral differences among VBNC cells formed under different conditions.

Bacteria possess complex stress regulatory systems to effectively adapt to various harsh environments. General stress responses may be activated by different stressors to achieve cross-protection of bacteria from these stress conditions (37). For example, upregulation of oxidative stress genes, such as *katA* and *sodB*, was observed in *C. jejuni* exposed to hyperosmotic condition (38), suggesting that oxidative stress defense is also involved in the response to osmotic pressure. Therefore, similar compositional changes might occur in the VBNC cells formed under different stresses (i.e., hyperosmolarity and oxidative stress) and thus they were unable to be distinguished based on single-cell Raman spectra.

We further assessed the stability of VBNC cells upon extended exposure to the stressors. As aforementioned, *C. jejuni* cells completely entered VBNC state (i.e., no culturable cells) after incubation under osmotic pressure for 24 h or under aerobic stress for 48 h. We extended the

treatment time for another 24 h (i.e., 48 h and 72 h, respectively) and then determined the VBNC concentrations and collected the single-cell Raman spectra. Under both conditions, no significant differences in VBNC cell counts were observed between the samples with different induction times (**Figure 4.5a**), suggesting that VBNC cells could survive in unfavorable environments for prolonged periods. Similar spectral features were displayed in the VBNC cells with various induction durations (**Figure 4.5bc**) and the classification accuracy was only 68.5% and 71.4% (**Table 4.2**), respectively. The challenges in distinguishing their spectral variations suggest that VBNC cells did not undergo substantial compositional alterations during the prolonged induction.

Bacterial cells can maintain a stable physiological status for an extended period once they enter the VBNC state. Similar results were reported that the number of VBNC *C. jejuni* cells remained constant during the longer exposure to chlorine, osmotic stress and aerobic atmosphere (39). In another study, Raman spectra generated from VBNC *E. coli* induced via chlorination for 0.5 h and 2 h demonstrated high similarity and could not be discriminated using PCA (40). While in some other cases, prolonged exposure to stressors may lead to further adaptations and changes in the VBNC state (7, 41). The persistence of VBNC cells under harsh conditions depends on various factors, such as the type and severity of the adverse stresses, the induction process and the distinctive characteristics of bacterial species (12). Understanding these diverse factors is essential for a comprehensive assessment of the persistence and behavior of bacteria in the VBNC state.

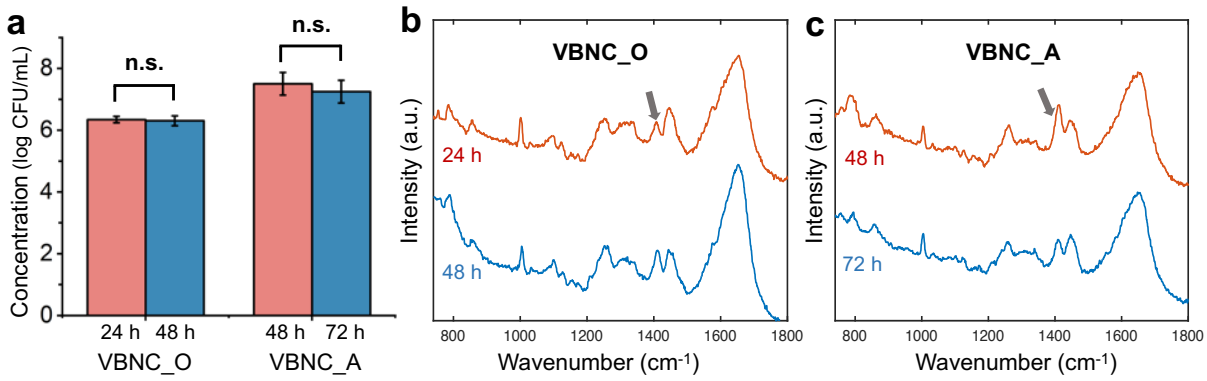

Figure 4.5 Influence of induction time on the VBNC *C. jejuni* cells. (a) Concentration of VBNC cells in the induced samples with different treatment periods. Error bars represent the standard deviations calculated from three biological replicates. n.s.: no significant difference ($P > 0.05$). (b) Average single-cell Raman spectra of VBNC *C. jejuni* F38011 induced under osmotic pressure for 24 h and 48 h, respectively. (c) Average single-cell Raman spectra of VBNC *C. jejuni* F38011 induced under aerobic condition for 48 h and 72 h, respectively. Raman peak indicated by the black arrow is attributed from the PDMS layer of the microfluidic chip.

Table 4.2 Identification accuracy (%) for VBNC *C. jejuni* induced under different adverse conditions or with different induction time periods.

Factor	Strain	Classification groups		Accuracy (%)		
				Training	Validation	Test
Induction method	F38011	VBNC_O	VBNC_A	78.1	74.3	73.7
	ATCC33560	VBNC_O	VBNC_A	77.5	73.9	73.2
Induction time	F38011	VBNC_O48	VBNC_O72	73.6	69.7	68.5
	F38011	VBNC_A24	VBNC_A48	72.3	70.5	71.4

VBNC_O: VBNC cells induced under osmotic stress; VBNC_A: VBNC cells induced under aerobic condition; Numbers of 24, 48 and 72 indicate the induction duration (h) under stresses.

4.4.5 Interpretation of Raman features that contribute to VBNC identification

As Raman spectral features represent comprehensive compositional information of bacterial cells, it is crucial to uncover the spectral regions that contribute significantly to the CNN-based classification of VBNC and culturable cells. Interpretability has been considered as a controversial issue of CNNs due to their inherent "black-box" nature. In this study, we employed a Grad-CAM technique to better understand the decision-making process of CNN. Grad-CAM can generate a heatmap to visualize the impact of Raman spectral regions on the CNN-based classifications (23). As shown in **Figure 4.6**, the color indicates the contribution (values ranging from 0-1) of the corresponding spectral features to the identification of VBNC cells. We selected the top 10 responsible spectral regions based on their contribution values, and the tentative assignments of these Raman peaks are summarized in **Table 4.3**.

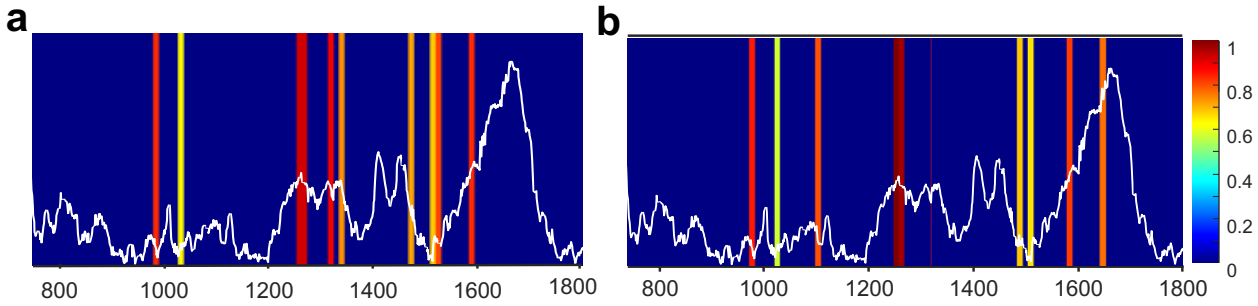

Figure 4.6 Visualization of the contribution of Raman spectral features to the identification of VBNC *C. jejuni* cells induced under osmotic pressure (a) or aerobic condition (b). Colors ranging from blue to red, corresponding to values between 0 to 1, represent the significance of the Raman spectral regions for the classification, with 1 indicating the highest impact. For a better visualization, only the top 10 regions with the highest contribution values were selected while all other regions were displayed in blue.

Table 4.3 Tentative assignments of Raman spectral regions that contribute most to the identification of VBNC cells **(Figure 4.6).**

Spectral regions (cm^{-1})	Functional groups or compounds	Molecular components	Note
1248-1267	α-helix of amide III	Proteins	
	Ring breathing modes of guanine, cytosine and adenine	Nucleic acids	
	Phospholipids	Nucleic acids	
	C=C groups in unsaturated fatty acids	Lipids	
	Triglycerides	Lipids	
	C-O vibration mode	Peptidoglycan	
1308-1317	CH_3/CH_2 twisting or bending mode	Lipids	
	Ring breathing mode of guanine	Nucleic acids	
	Amide III	Proteins	
968-977	Ethers	Lipids	
	Phosphate monoester groups	Proteins/nucleic acids	
	C-C stretching	Proteins	
1568-1578	Guanine, adenine	Nucleic acids	
	C-O vibration mode	Peptidoglycan	
1508-1517	Cytosine, adenine	Nucleic acids	Fig. 4.6a
1328-1337	Phospholipids, guanine	Nucleic acids	Fig. 4.6a
	Tryptophan	Proteins	
	CH_3CH_2 wagging, twisting and deforming modes	Nucleic acids	

1458-1467	Deoxyribose	Nucleic acids	Fig. 4.6a
	CH_2/CH_3 deformation	Lipids	
1098-1107	PO^{2-} group	Nucleic acids	Fig. 4.6b
	Phenylalanine	Protein	
	C-C vibration mode	Lipids/fatty acids	
1628-1637	C=O stretching, α-helix and β-structure in amide I	Proteins	Fig. 4.6b
1478-1487	Amide II	Proteins	Fig. 4.6b
	Guanine, adenine	Nucleic acids	
1498-1507	C-C stretching in benzenoid ring	Proteins	
	N-H bending	Proteins	
1018-1027	Glycogen	Carbohydrates	
	Ribose	Nucleic acids	

The order of spectral regions is based on the contribution values.

The spectral regions without note are shown in both **Figure 4.6a** and **Figure 4.6b**.

Assignments are referred to a review paper (30) and the references involved.

Among them, most Raman signals originate from amide III in proteins and ring breathing modes of nucleotides in nucleic acids, including 1248-1267, 1308-1317, 1508-1517, 1568-1578 cm^{-1} (30). Extensive syntheses of protein and nucleic acids are generally regarded as the indicators for active bacterial growth. In VBNC cells, the concentration of total proteins is usually reduced compared to the normal culturable cells due to the minimized metabolic activities at this dormancy state. For example, the expression of virulence-associated proteins (e.g., flaA, ciaB

and cdtB) were significantly downregulated in the VBNC *C. jejuni* cells (42), leading to a diminished virulence potential. The synthesis of nucleic acids is also typically downregulated in VBNC cells. DNA replication and transcription are energy-consuming processes. In the VBNC state, cells conserve energy by minimizing these activities. Maalej and coauthors analyzed the nucleic acids in culturable and VBNC cells using flow cytometry and a large amount of VBNC populations demonstrated reduced nucleic acids contents (43). Production of nucleic acid is closely related to cell division and growth. In response to stresses, VBNC cells might prioritize the essential functions for survival rather than growth-related activities. The decrease in nucleic acid content may contribute to elucidating the loss of culturability of VBNC cells.

On the other hand, certain proteins can be upregulated in VBNC cells to maintain the viability and essential cellular functions under harsh environments. For example, overexpression of OmpW on cell membranes plays a critical role in the stress tolerance of VBNC cells when exposed to oxidative stress (44). Enhanced synthesis of a regulatory enzyme PPK1 facilitated the transition of *C. jejuni* into the VBNC state by increasing the accumulation of polyphosphate (45). These upregulated proteins might also contribute to the variations in proteins-related Raman spectral features (e.g., 1248-1267, 1098-1107, 1478-1487 cm^{-1}) in VBNC cells (**Figure 4.6**).

Besides proteins and nucleic acids, Raman peaks at 1248-1257 and 1568-1578 cm^{-1} might also be attributed to the C-O mode of peptidoglycan (46, 47). Berezin and coworkers characterized the compositions of bacterial cell walls using tip-enhanced Raman spectroscopy and identified enhanced Raman signals at 1250 cm and 1578 cm^{-1} arising from carbohydrate and polypeptides

of the peptidoglycan layer (47). These results indicated that the peptidoglycans of cell wall might undergo modifications during the transition into the VBNC state, such as the changes in molecular compositions or cross-linking patterns of peptidoglycan strands (12). A thicker peptidoglycan layer could provide enhanced protection against external stresses and help maintain the structural integrity of cell wall. The alterations in cellular shapes of VBNC cells (**Figure 4.2**) also indicated the compositional changes in the cell wall.

Raman peaks at wavenumber region of 1248-1267 cm^{-1} are partially generated from C=C groups in unsaturated fatty acids (48) and there are also other Raman signals associated with lipids, such as those at 968-977, 1458-1467, 1098-1107 cm^{-1} (30). The high contribution values of these regions to the CNN-based classification suggest a prominent change of lipid compositions between VBNC and culturable cells. We hypothesize that the ratio of unsaturated fatty acids in the cell membranes of VBNC cells might decrease, potentially resulting in a more rigid cell membrane structure. Cell membrane fluidity and stability are crucial to the cellular physiological processes. In the VBNC state, adjustments in membrane fluidity may occur to cope with environmental stress (49). A previous study reported that *C. jejuni* could reduce cell membrane fluidity by decreasing the proportion of unsaturated fatty acids and increasing the content of cyclopropane fatty acids, as an adaptive response to undesirable environments (50).

Most influential spectral regions are the same for the identification of VBNC cells induced under osmotic pressure and aerobic condition (**Figure 4.6ab**). This agrees with the aforementioned results that VBNC cells induced with different conditions did not demonstrate significant spectral variations (**Table 4.1**). There are several Raman spectral regions showing varied impacts

on the classification of different types of VBNC cells. Specifically, Raman peaks at 1508-1517, 1328-1337 and 1458-1467 cm^{-1} were exclusively important for identifying osmotic-induced VBNC cells, while peaks at 1098-1107, 1628-1637 and 1478-1487 cm^{-1} play a critical role in the classification of aerobic-induced VBNC cells. These peaks are all attributed to nucleic acids, proteins and lipids (30). The slight variations in the spectral regions might be due to the adoption of distinct stress response strategies upon exposure to different stressors. When treated with oxidative stress, various antioxidant defence enzymes were overexpressed in *C. jejuni*, such as KatA, AhpC and SodB, leading to a long-term aerobic adaptation (51). Under hyperosmotic pressure, *C. jejuni* exhibited enhanced expression of transporters for K^+ and increased the synthesis of other potential osmoprotectants (38). Upregulation of capsule export gene *kpsM* might also contribute to the hyperosmotic resistance (38). These biochemical compositional changes under different adaptive strategies are reflected by the variations in their Raman spectral patterns.

4.5 Conclusion

This study proposed a culture-independent approach of using Raman optical tweezers system combined with machine learning to identify VBNC *C. jejuni* at single-cell level. Based on the variations in the single-cell Raman spectra, VBNC *C. jejuni* cells induced under osmotic pressure and aerobic condition were successfully discriminated from their culturable counterparts with high accuracies (i.e., 91.7% to 93.4%) by using CNN. This approach represents a promising tool for identifying VBNC bacteria at the single-cell resolution from heterogeneous samples in food industry, environmental studies and clinical settings. Furthermore, the major spectral

regions that are responsible for the CNN-based classification were deciphered using Grad-CAM, providing insights into the molecular mechanism underlying the VBNC formations.

In this study, single-cell Raman spectra were automatically collected using the homebuilt Raman tweezers system without the need of human intervention. This automation substantially decreased the workload for operators and enhanced overall throughput. Due to the rapid and non-destructive characteristics, Raman tweezers system also holds the potential for real-time monitoring of the molecular dynamics in individual *C. jejuni* cells during the transition from normal state to VBNC state. In future work, the identified VBNC cells can be selectively isolated from the population using the optical tweezers and subjected to other molecular analysis (e.g., single-cell RNA sequencing) for downstream characterization. This approach has the potential to investigate other nonculturable microorganisms in natural environments and facilitate a better understanding of microbial diversity and ecological processes.

4.6 References

1. Thomas MK, Murray R, Flockhart L, Pintar K, Fazil A, Nesbitt A, Marshall B, Tataryn J, Pollari F. 2015. Estimates of foodborne illness-related hospitalizations and deaths in Canada for 30 specified pathogens and unspecified agents. Foodborne Pathogens and Disease 12:820-827.
2. Crim SM, Iwamoto M, Huang JY, Griffin PM, Gilliss D, Cronquist AB, Cartter M, Tobin-D'Angelo M, Blythe D, Smith K. 2014. Incidence and trends of infection with pathogens transmitted commonly through food-Foodborne Diseases Active Surveillance Network, 10 US sites, 2006-2013. Morbidity and Mortality Weekly Report 63:328.
3. Devleesschauwer B, Bouwknegt M, Mangen M-JJ, Havelaar AH. 2017. Health and economic burden of *Campylobacter*, p 27-40, Campylobacter. Elsevier.
4. Jacobs-Reitsma W, Lyhs U, Wagenaar J. 2008. *Campylobacter* in the food supply. Campylobacter:625-644.
5. Kaakoush NO, Castaño-Rodríguez N, Mitchell HM, Man SM. 2015. Global epidemiology of *Campylobacter* infection. Clinical Microbiology Reviews 28:687-720.
6. Kim S-H, Chelliah R, Ramakrishnan SR, Perumal AS, Bang W-S, Rubab M, Daliri EB-M, Barathikannan K, Elahi F, Park E. 2021. Review on stress tolerance in *Campylobacter jejuni*. Frontiers in Cellular and Infection Microbiology 10:596570.
7. Ramamurthy T, Ghosh A, Pazhani GP, Shinoda S. 2014. Current perspectives on viable but non-culturable (VBNC) pathogenic bacteria. Frontiers in Public Health 2:103.
8. Zhao X, Zhong J, Wei C, Lin C-W, Ding T. 2017. Current perspectives on viable but non-culturable state in foodborne pathogens. Frontiers in Microbiology 8:580.

9. Gao R, Liao X, Zhao X, Liu D, Ding T. 2021. The diagnostic tools for viable but nonculturable pathogens in the food industry: current status and future prospects. Comprehensive Reviews in Food Science and Food Safety 20:2146-2175.
10. Santos LS, Rossi DA, Braz RF, Fonseca BB, Guidotti–Takeuchi M, Alves RN, Beletti ME, Almeida-Souza HO, Maia LP, Santos PdS. 2023. Roles of viable but non-culturable state in the survival of *Campylobacter jejuni*. Frontiers in Cellular and Infection Microbiology 13:315.
11. Lv R, Wang K, Feng J, Heeney DD, Liu D, Lu X. 2020. Detection and quantification of viable but non-culturable *Campylobacter jejuni*. Frontiers in Microbiology 10:2920.
12. Dong K, Pan H, Yang D, Rao L, Zhao L, Wang Y, Liao X. 2020. Induction, detection, formation, and resuscitation of viable but non-culturable state microorganisms. Comprehensive Reviews in Food Science and Food Safety 19:149-183.
13. Stöckel S, Kirchhoff J, Neugebauer U, Rösch P, Popp J. 2016. The application of Raman spectroscopy for the detection and identification of microorganisms. Journal of Raman Spectroscopy 47:89-109.
14. Chan JW. 2013. Recent advances in laser tweezers Raman spectroscopy (LTRS) for label-free analysis of single cells. Journal of Biophotonics 6:36-48.
15. Ashkin A, Dziedzic JM, Bjorkholm JE, Chu S. 1986. Observation of a single-beam gradient force optical trap for dielectric particles. Optics Letters 11:288-290.
16. Wang D, He P, Wang Z, Li G, Majed N, Gu AZ. 2020. Advances in single cell Raman spectroscopy technologies for biological and environmental applications. Current Opinion in Biotechnology 64:218-229.

17. Butler HJ, Ashton L, Bird B, Cinque G, Curtis K, Dorney J, Esmonde-White K, Fullwood NJ, Gardner B, Martin-Hirsch PL. 2016. Using Raman spectroscopy to characterize biological materials. Nature Protocols 11:664-687.
18. Wang K, Chen L, Ma X, Ma L, Chou KC, Cao Y, Khan IUH, Golz G, Lu X. 2020. *Arcobacter* identification and species determination using Raman spectroscopy combined with neural networks. Applied Environmental Microbiology 86.
19. Kazemzadeh M, Hisey CL, Zargar-Shoshtari K, Xu W, Broderick NG. 2022. Deep convolutional neural networks as a unified solution for Raman spectroscopy-based classification in biomedical applications. Optics Communications 510:127977.
20. Ho C-S, Jean N, Hogan CA, Blackmon L, Jeffrey SS, Holodniy M, Banaei N, Saleh AA, Ermon S, Dionne J. 2019. Rapid identification of pathogenic bacteria using Raman spectroscopy and deep learning. Nature Communications 10:4927.
21. Lu W, Chen X, Wang L, Li H, Fu YV. 2020. Combination of an artificial intelligence approach and laser tweezers Raman spectroscopy for microbial identification. Analytical Chemistry 92:6288-6296.
22. Alzubaidi L, Zhang J, Humaidi AJ, Al-Dujaili A, Duan Y, Al-Shamma O, Santamaría J, Fadhel MA, Al-Amidie M, Farhan L. 2021. Review of deep learning: Concepts, CNN architectures, challenges, applications, future directions. Journal of Big Data 8:1-74.
23. Selvaraju RR, Cogswell M, Das A, Vedantam R, Parikh D, Batra D. Grad-cam: Visual explanations from deep networks via gradient-based localization, p 618-626. *In* (ed),
24. Zhang J, Lu X. 2023. Susceptibility of *Campylobacter jejuni* to stressors in agrifood systems and induction of a viable-but-nonculturable state. Applied and Environmental Microbiology 89:e00096-23.

25. Ma L, Petersen M, Lu X. 2020. Identification and antimicrobial susceptibility testing of *Campylobacter* using a microfluidic lab-on-a-chip device. Applied and environmental microbiology 86:e00096-20.
26. Kong L, Zhang P, Wang G, Yu J, Setlow P, Li Y-q. 2011. Characterization of bacterial spore germination using phase-contrast and fluorescence microscopy, Raman spectroscopy and optical tweezers. Nature Protocols 6:625-639.
27. Lázaro B, Cárcamo J, Audícana A, Perales I, Fernández-Astorga A. 1999. Viability and DNA maintenance in nonculturable spiral *Campylobacter jejuni* cells after long-term exposure to low temperatures. Applied and Environmental Microbiology 65:4677-4681.
28. Signoretto C, Lleò MdM, Canepari P. 2002. Modification of the peptidoglycan of *Escherichia coli* in the viable but nonculturable state. Current Microbiology 44:125-131.
29. Fu Y, Jia Y, Fan J, Yu C, Yu C, Shen C. 2020. Induction of *Escherichia coli* O157: H7 into a viable but non-culturable state by high temperature and its resuscitation. Environmental Microbiology Reports 12:568-577.
30. Talari ACS, Movasaghi Z, Rehman S, Rehman Iu. 2014. Raman spectroscopy of biological tissues. Applied Spectroscopy Reviews 50:46-111.
31. Gu J, Wang Z, Kuen J, Ma L, Shahroudy A, Shuai B, Liu T, Wang X, Wang G, Cai J. 2018. Recent advances in convolutional neural networks. Pattern Recognition 77:354-377.
32. Ma X, Wang K, Chou KC, Li Q, Lu X. 2022. Conditional generative adversarial network for spectral recovery to accelerate single-cell Raman spectroscopic analysis. Analytical Chemistry 94:577-582.

33. Guo L, Ye C, Cui L, Wan K, Chen S, Zhang S, Yu X. 2019. Population and single cell metabolic activity of UV-induced VBNC bacteria determined by CTC-FCM and D_2O-labeled Raman spectroscopy. Environment International 130:104883.
34. Qi Z, Huang Z, Liu C. 2022. Metabolism differences of biofilm and planktonic Pseudomonas aeruginosa in viable but nonculturable state induced by chlorine stress. Science of The Total Environment 821:153374.
35. Zhang S, Guo L, Yang K, Zhang Y, Ye C, Chen S, Yu X, Huang WE, Cui L. 2018. Induction of *Escherichia coli* into a VBNC state by continuous-flow UVC and subsequent changes in metabolic activity at the single-cell level. Frontiers in Microbiology 9:2243.
36. Kuehl B, Marten S-M, Bischoff Y, Brenner-Weiß G, Obst U. 2011. MALDI-ToF mass spectrometry-multivariate data analysis as a tool for classification of reactivation and non-culturable states of bacteria. Analytical and Bioanalytical Chemistry 401:1593-1600.
37. Kim J-C, Oh E, Kim J, Jeon B. 2015. Regulation of oxidative stress resistance in *Campylobacter jejuni*, a microaerophilic foodborne pathogen. Frontiers in Microbiology 6:751.
38. Cameron A, Frirdich E, Huynh S, Parker CT, Gaynor EC. 2012. Hyperosmotic stress response of *Campylobacter jejuni*. Journal of Bacteriology 194:6116-6130.
39. Yagi S, Okada A, Inoshima Y. 2022. Role of temperature, nutrition, oxygen, osmolality, and bacterial strain in inducing a viable but non-culturable state in *Campylobacter jejuni*. Journal of Microbiological Methods 195:106456.
40. Chen S, Li X, Wang Y, Zeng J, Ye C, Li X, Guo L, Zhang S, Yu X. 2018. Induction of *Escherichia coli* into a VBNC state through chlorination/chloramination and differences in characteristics of the bacterium between states. Water Research 142:279-288.

41. Morishige Y, Fujimori K, Amano F. 2013. Differential resuscitative effect of pyruvate and its analogues on VBNC (viable but non-culturable) *Salmonella*. Microbes and Environments 28:180-186.
42. Chaisowwong W, Kusumoto A, Hashimoto M, Harada T, Maklon K, Kawamoto K. 2012. Physiological characterization of *Campylobacter jejuni* under cold stresses conditions: its potential for public threat. Journal of Veterinary Medical Science 74:43-50.
43. Maalej S, Denis M, Dukan S. 2004. Temperature and growth-phase effects on *Aeromonas hydrophila* survival in natural seawater microcosms: role of protein synthesis and nucleic acid content on viable but temporarily nonculturable response. Microbiology 150:181-187.
44. Asakura H, Kawamoto K, Haishima Y, Igimi S, Yamamoto S, Makino S-i. 2008. Differential expression of the outer membrane protein W (OmpW) stress response in enterohemorrhagic *Escherichia coli* O157: H7 corresponds to the viable but non-culturable state. Research in Microbiology 159:709-717.
45. Gangaiah D, Kassem II, Liu Z, Rajashekara G. 2009. Importance of polyphosphate kinase 1 for *Campylobacter jejuni* viable-but-nonculturable cell formation, natural transformation, and antimicrobial resistance. Applied and Environmental Microbiology 75:7838-7849.
46. de Siqueira e Oliveira FS, Giana HE, Silveira Jr L. 2012. Discrimination of selected species of pathogenic bacteria using near-infrared Raman spectroscopy and principal components analysis. Journal of Biomedical Optics 17:107004-107004.
47. Berezin S, Aviv Y, Aviv H, Goldberg E, Tischler YR. 2017. Replacing a century old technique-modern spectroscopy can supplant Gram staining. Scientific Reports 7:3810.

48. Krafft C, Neudert L, Simat T, Salzer R. 2005. Near infrared Raman spectra of human brain lipids. Spectrochimica Acta Part A: Molecular and Biomolecular Spectroscopy 61:1529-1535.
49. Yoon Y, Lee H, Lee S, Kim S, Choi K-H. 2015. Membrane fluidity-related adaptive response mechanisms of foodborne bacterial pathogens under environmental stresses. Food Research International 72:25-36.
50. Martinez-Rodriguez A, Mackey B. 2005. Physiological changes in *Campylobacter jejuni* on entry into stationary phase. International Journal of Food Microbiology 101:1-8.
51. Oh E, McMullen L, Jeon B. 2015. Impact of oxidative stress defense on bacterial survival and morphological change in *Campylobacter jejuni* under aerobic conditions. Frontiers in Microbiology 6:295.

4.7 Supplementary information

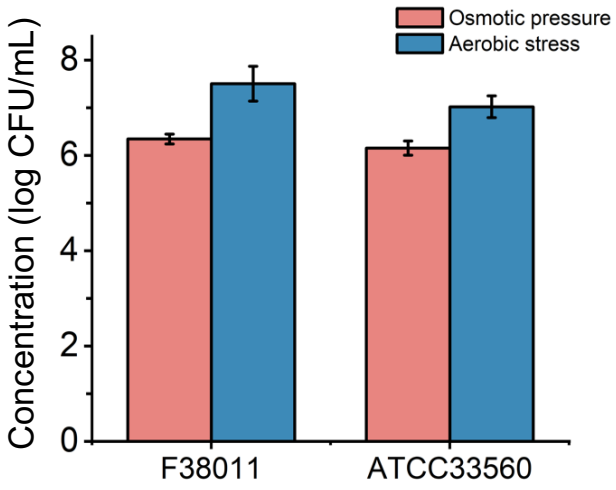

Figure S4.1 Concentration of VBNC *C. jejuni* cells inducted at osmotic pressure and aerobic stress, respectively.

Table S4.1 The area under the curve (AUC) value in the receiver operating characteristic (ROC) curve (Figure 4.4d) for the classification of culturable and VBNC *C. jejuni* cells using CNN.

Strain	Classification groups		AUC value
F38011	OC	VBNC_O	0.7948
	OC	VBNC_A	0.7840
ATCC33560	OC	VBNC_O	0.7916
	OC	VBNC_A	0.7668

OC: culturable cells collected from fresh overnight culture; VBNC_O: VBNC cells induced under osmotic stress; VBNC_A: VBNC cells induced under aerobic condition.

Connecting Text

Single-cell identification and characterization of VBNC *C. jejuni* was achieved in Chapter 4, facilitating a better understanding of the formation mechanisms of VBNC *C. jejuni*. VBNC cells can retrieve cultivability and virulence under favorable conditions, posing a high risk to food safety and public health. Therefore, it is crucial to investigate the resuscitation requirements of VBNC *C. jejuni* and elucidate the underlying mechanism. In Chapter 5, we induced VBNC *C. jejuni* cells at low temperature (4°C) and tested their resuscitation in embryonated chicken eggs. Eggs at different embryonic stages demonstrated varied capabilities of resuscitating VBNC *C. jejuni*. We further conducted untargeted metabolomics to identify the major compounds in eggs that potentially contributed to the resuscitation of VBNC *C. jejuni.*

Chapter 5: Resuscitation of viable but non-culturable *Campylobacter jejuni* in embryonated chicken eggs and metabolomic profiling to identify the potential resuscitation stimuli

5.1 Abstract

Campylobacter jejuni can enter a viable but non-culturable (VBNC) state in response to adverse conditions, but resuscitation of VBNC *C. jejuni* is poorly understood. We investigated the resuscitation of VBNC *C. jejuni* in embryonated chicken eggs and identified the potential resuscitation stimuli using untargeted metabolomics and lipidomics. Four *C. jejuni* strains were induced into the VBNC state at low temperature (4°C). Resuscitation of VBNC *C. jejuni* cells was achieved following passage through the embryonated chicken eggs. We further assessed the resuscitation rates of VBNC *C. jejuni* in eggs at different embryonic days (D) ranging from D1 to D11. Eggs at relatively late embryonic stages (i.e., D9 and D11) demonstrated superior capabilities of promoting the resuscitation of VBNC *C. jejuni* compared to the early-stage eggs (i.e., D1 and D3). Metabolites and lipids with significantly higher abundance in late-stage eggs were identified using mass spectrometry-based approach. Among them, several essential amino acids and citric acid intermediates were potentially associated with the energy production of *C. jejuni* and might contribute to the resuscitation of VBNC *C. jejuni.* This study sheds lights on the resuscitation mechanisms of VBNC *C. jejuni*. Identification of the potential resuscitation stimuli provides valuable insights on developing novel cultivation media to detect VBNC pathogens.

5.2 Introduction

Campylobacter is one of the most common causes of human diarrheal illnesses, with *C. jejuni* being responsible for the majority of the infections (> 90%) (1). It is estimated that approximately 400-500 million cases of campylobacteriosis occur worldwide each year (2), leading to a significant economic burden and heath concern. The main symptoms of campylobacteriosis are diarrhea, abdominal pain, fever and nausea, while severe and prolonged post-infection complications have also been reported, such as reactive arthritis and Guillain Barré syndrome (3). *C. jejuni* is prevalent in food-producing animals and food processing environments, although it generally requires fastidious growth conditions. One hypothesis to interpret this contradiction is that *C. jejuni* can survive under adverse conditions by entering a viable-but-non-culturable (VBNC) state (4).

The formation of VBNC *C. jejuni* can be triggered by various stressors during food processing and food preservation, such as extreme temperatures, starvation, oxidative stress and low pH (5). VBNC cells maintain the intact cell membrane and fundamental metabolisms but are unable to multiply on the routine culture media, and thus can evade the conventional culture-based detection (6). Although bacterial pathogens in the VBNC state are generally considered to be avirulent, they demonstrate the capability of resuscitating under favorable conditions (7). Resuscitation refers to the process where VBNC cells recover to a culturable state with active gene expression and metabolic activities (8). Virulence retention from the resuscitated cells can potentially cause human infections, posing a severe risk to food safety and public health.

Resuscitation of VBNC cells depends on diverse factors. As the VBNC state is usually induced by harsh conditions, eliminating the external stress is the most common method to promote the resuscitation (7). For example, VBNC bacteria formed at low or high temperature restored the culturability after incubation at the optimal temperature (9-11). Cultivation in nutrient-rich media enabled the resuscitation of VBNC *Escherichia coli* induced by starvation (12). Nevertheless, simple reversal of the VBNC-inducing conditions was insufficient to achieve the resuscitation of certain bacterial species (8, 11). The presence of specific stimuli is another critical factor to facilitate the resuscitation, such as physical triggers (e.g., heat shock), chemicals (e.g., sodium pyruvate, Tween 20, amino acids and vitamins) and active proteins (e.g., Rpfs, and catalase, YeaZ) (7, 8, 13). In addition, VBNC cells exhibit the capability of resuscitating within biological hosts. For instance, Senoh and coauthors discovered that VBNC cells of *Vibrio cholerae* reverted to a culturable state after co-cultivation with eukaryotic cells (14). Resuscitation of VBNC *C. jejuni* was reported to occur *in vivo* in the intestinal track of mice (15) and 1-day-old chicks (16).

Embryonated chicken egg has been considered as a potential biological host to enable the resuscitation of VBNC bacterial cells. It is a self-sufficient host system containing a comprehensive and well-balanced supply of nutrients required for embryonic development (17). These nutrients may also support the metabolic activity and growth of VBNC *Campylobacter*. Besides, the immune system in the embryonated eggs is not well developed (18), thereby reducing the possibility of immune clearance and facilitate the colonization of the inoculated VBNC cells. Resuscitation of VBNC *Listeria monocytogenes* was previously confirmed after incubation in the embryonated eggs (19). Therefore, embryonated chicken eggs might represent a suitable environment for supporting the resuscitation of VBNC *C. jejuni*.

The mechanisms of VBNC resuscitation have not been well explored. Most previous studies on resuscitation mechanisms focused on the role of a specific compound or pathway in the resuscitation process (12, 13, 20, 21). It would be valuable to systematically investigate how the components in the biological host impact the resuscitation of VBNC bacterial cells. With the advancement of high-throughput technologies, metabolomic analysis has emerged as a powerful tool for discerning the metabolite profiles of a biological sample. Conducting qualitative and quantitative analysis of all the metabolites in the embryonated eggs via metabolomics might help identify the compounds that potentially contribute to the VBNC resuscitation.

Low temperature (4°C) is commonly employed during food processing, transportation, and storage. Various major foodborne pathogens were reported to enter the VBNC state when exposed to refrigeration temperature (9, 11, 21). In this study, different *C. jejuni* strains were induced into VBNC state at 4°C and their resuscitation in embryonated chicken eggs was investigated. Eggs at different embryonic stages demonstrated varied capabilities of supporting the resuscitation of VBNC *C. jejuni*. We further performed metabolomics and lipidomics to compare the compositional variations among the eggs to identify the potential resuscitation stimuli. This study provides insights on the mechanism underlying VBNC resuscitation and further exploration can be conducted to develop novel cultivation media for recovering VBNC pathogens.

5.3 Materials and methods

5.3.1 Bacterial strains and cultivation

Four *C. jejuni* strains including two reference strains ATCC 33560^T (bovine source) and NCTC 11168 (human source), and two clinical isolates F38011 and 81-116 were used in this study. Bacterial stocks were preserved at -80°C containing 40% (v/v) glycerol and 20% (v/v) defibrinated sheep blood. *C. jejuni* strains were routinely grown on Mueller-Hinton (MH) agar (BD Difco, NJ, USA) supplemented with 5% defibrinated sheep blood (Cedarlane, ON, Canada) at 37°C under microaerobic condition (10% CO_2) for 48 h. To prepare overnight culture, several *C. jejuni* colonies on the agar plates were transferred into MH broth (MHB) and incubated with a constant shaking of 175 rpm for 16-18 h to reach a late exponential phase.

5.3.2 Induction of VBNC *C. jejuni* at low temperature

C. jejuni was induced to VBNC state by incubation at low temperature (4°C). Fresh overnight culture of *C. jejuni* was diluted to a final concentration of ~log 8 CFU/mL (equivalent to OD_{600} = 0.03) in MHB and incubated at 4°C under atmospheric conditions to mimic the real food storage conditions. The concentration of culturable cells was monitored over time using the standard plating assay. Briefly, bacterial samples were 10-fold serially diluted in phosphate-buffered saline (PBS) and streaked on MH blood agar to enumerate the colonies formed after incubation. The limit of detection (LOD) of the plating assay was determined to be 0.1 CFU/ml based on the presence of one colony on the MH blood agar using 10 mL of bacterial sample (Silvestri et al., 2017). Specifically, 10-mL aliquot of the sample was concentrated by centrifugation and streaked on MH blood agar to test the culturability. When the culturable cell concentration was lower than the LOD (i.e., 0.1 CFU/mL), the induced sample was transferred into the fresh MHB

and incubated under optimum conditions for 72 h to further validate that no culturable cells existed.

Two different assays were conducted in parallel to test the viable cells in the induced sample, when there was no culturable cell. Firstly, the viable cell count was determined by propidium monoazide (PMA) coupled with quantitative polymerase chain reaction (qPCR) following the protocol described in a previous study (22) with minor modifications. PMA is a DNA intercalating dye that can selectively penetrate the dead cells with compromised cell membrane integrity and covalently bond to DNA after photoactivation. The amplification of PMA-bound DNA is inhibited during the following qPCR, enabling the quantification of viable cells only. More details of the PMA-qPCR assay are available in the supplementary information (SI). As the culturable cell counts were decreased to an undetectable level, the viable cells quantified by the PMA-qPCR were considered as VBNC cells. The presence of VBNC cells was further verified using LIVE/DEAD™ *Bac*Light™ bacterial viability kit (Invitrogen, Carlsbad, USA) combined with fluorescence microscopy. This kit contains a green-fluorescent dye SYTO 9 and a red-fluorescent dye propidium iodine (PI). SYTO 9 can stain all the cells with both intact and compromised membranes, whereas PI only penetrates dead cells with damaged membranes. Therefore, viable cells and dead cells are stained in green and red under fluorescence microscopy, respectively. This assay was performed according to the manufacturer's protocol. Briefly, 3 μL of the dye mixture (1:1 v/v) was added into 1 mL of bacterial culture, followed by incubation in the dark for 15 min. The stained bacterial suspension was added to a glass slide and examined using a fluorescence microscope (Axio Imager Z1; Carl Zeiss, Germany). For each sample, at least 5 pictures were taken on different fields to confirm the presence of VBNC cells.

5.3.3 Resuscitation of VBNC *C. jejuni* in embryonated chicken eggs

VBNC *C. jejuni* were injected into embryonated chicken eggs to test the resuscitation capability. Fresh fertilized eggs from chicken breed Plymouth Rock Barred were purchased from a local farm DC Heritage Poultry (Shawville, QC, Canada). Eggs were incubated at 37.5°C with relative humidity of 50-55% to mimic the conditions at the commercial hatchery. All the eggs were candled to check the embryo development and the confirmed unfertilized eggs were removed (**Figure S5.1**). We selected 9-day-old embryonated eggs for testing the VBNC resuscitation. Eggshell was thoroughly disinfected with 75% (v/v) ethanol before injection to avoid contamination. A hole was punched on the eggshell from the air cell side and 100 μL of VBNC bacterial suspension was aseptically injected into the embryonated egg using a sterile syringe and a needle with length of 25 mm and diameter of 0.9 mm (Fisher Scientific, Hampton, USA). Negative and positive control groups were included by inoculating eggs with sterilized PBS and culturable *C. jejuni* (i.e., overnight culture), respectively. The injection hole was sealed with tape and the inoculated eggs were incubated at 37.5°C in aerobic atmosphere for 3 days. To test the resuscitation of the inoculated VBNC cells, the egg was gently opened from the air cell end using sterile scissor and tweezer, and all the egg contents were collected into a stomacher bag, followed by homogenization for 1 min. The egg homogenate was streaked onto MH blood agar and incubated at 37°C under microaerobic condition for 2 days to determine if there is any culturable cell grown. The colonies grown on agar plates were subjected to PCR and 16S rRNA sequencing (see details below) to validate whether they were the inoculated *C. jejuni* stain or contamination. To evaluate the resuscitation capability of each *C. jejuni* strain, three independent biological replicates were conducted with 6 to 7 eggs per replicate. The resuscitation rate (%)

was calculated as the ratio of the eggs that could support the resuscitation out of the total number of the eggs being tested.

5.3.4 Identification of the resuscitated bacterial cells

The resuscitated cells were identified at the strain level using PCR and 16S rRNA sequencing. DNA was extracted from the resuscitated colonies and subjected to PCR amplification as previously described by Bang and others (23). Primers targeted on the 16S rRNA gene of *C. jejuni* were utilized and the amplified PCR products (1495 bp) were sequenced using Sanger technique at CHU de Québec-Université Laval research center (Quebec City, Canada). The 16S rRNA sequences of the recovered cells were compared to those accessed from GenBank using nucleotide BLAST to confirm they were identical to the inoculated *C. jejuni* strains (i.e., ATCC 33560^{T}, NCTC 11168, F38011 and 81-116).

5.3.5 Resuscitation capability of eggs at different embryonic stages

As the compositional profiles in the embryonated eggs change along with the embryonic development, eggs at different embryonic stages may demonstrate varied capability of facilitating the resuscitation of VBNC *C. jejuni*. VBNC cells of *C. jejuni* ATCC 33560 and F38011 were injected into eggs at different embryonic days (D) of 1, 3, 5, 7, 9 and 11, respectively, to investigate their resuscitation potential. Injection of VBNC cells and testing of resuscitation were performed as aforementioned. A total of ~15 eggs at each day were used in three independent experiments.

5.3.6 Metabolomics and lipidomics of egg samples

5.3.6.1 Chemicals and reagents

Methanol, isopropanol, acetonitrile, methyl tert-butyl ether (MTBE) and H_2O were all OmniSolv® LC/MS grade and purchased from Sigma-Aldrich (Alabaster, USA). Ammonium formate and ammonium acetate powder (LC/MS grade) with purity ≥99.0% were obtained from Thermo Fisher Scientific (Waltham, USA). Formic acid and acetic acid (Optima™ LC/MS) used for pH adjustment were also purchased from Thermo Fisher Scientific.

5.3.6.2 Sample preparation

For metabolomic and lipidomic analyses, five embryonated chicken eggs were randomly selected at each embryonic day of D1, D3, D9 and D11 as biological replicates. Eggs at D1 and D3 represent the early-stage eggs with limited capability of supporting the resuscitation of VBNC *C. jejuni*, while eggs at D9 and D11 are late-stage eggs exhibiting enhanced VBNC resuscitation capability. Egg homogenates were collected as aforementioned and kept at -80°C before the extraction of metabolites. Dual extraction was applied to extract hydrophilic metabolites and hydrophobic lipids from the egg samples simultaneously. Briefly, 50 μL of egg homogenates was added into 400 μL ice-cold methanol and vortexed for 10 s, followed by sonication in ice water for 15 min. The mixtures were then stored at -20°C overnight for protein precipitation. Next, the samples were mixed with 900 μL of MTBE and vortexed for 2 min at room temperature to extract hydrophobic molecules (lipids). After adding 315 μL of cold H_2O, samples were centrifuged at 21,300 ×*g* for 10 min to achieve a clear phase separation between the MTBE layer (top, lipids) and methanol/H_2O layer (bottom, metabolites). Two layers were separately collected and dried using a SpeedVac vacuum concentrator (SPD120, ThermoFisher).

The MTBE layer was reconstituted with 300 µL of isopropanol alcohol/acetonitrile (1:1 v/v), and the methanol/H_2O layer was reconstituted with 900 µL of H_2O/acetonitrile (1:1 v/v). The reconstituted samples were centrifuged at either 4°C (metabolites) or 10°C (lipids) to collect the supernatant for further metabolomic and lipidomic analysis, respectively. Quality control (QC) sample was prepared by mixing equal volume (10 µL) of each sample extracts. For the negative controls, a method blank sample was prepared using 50 µL of H_2O and subjected to all the extraction procedures, and the reconstitution solvent was used as a solvent blank sample. All the samples were stored at -80°C until further analysis.

5.3.6.3 Liquid chromatography and mass spectrometry analysis

Metabolomic and lipidomic analyses of samples were conducted using an Agilent 1290 infinite II ultra-high performance liquid chromatography (UHPLC) system coupled with an Agilent 6546 quadrupole-time-of-flight (Q-TOF) mass spectrometer (Agilent Technologies, Santa Clara, USA). An aliquot of 50 µL of the sample was injected into the HPLC vial with insert. Method blank sample was used for the first 2 injections, followed by the solvent blank to stabilize the system. QC sample was run twice before the samples and between every six samples throughout the process to ensure the consistency of the system. The method blank sample was analyzed twice at the end of the batch.

Chromatographic separation of hydrophilic metabolites was carried out using a XBridge BEH Amide column (2.1 × 100 mm, 2.5 µm, 130 Å) (Waters, Milford, USA) with a KrudKatcher ULTRA HPLC In-Line Filter (0.2 µm). Mobile phase A was H_2O containing 10 mM ammonium acetate (pH 4.8) and mobile phase B was acetonitrile. Sample elution was achieved with a flow

rate of 0.5 mL/min and a linear gradient as follows: 0-16 min, 95% to 85% A; 16-24 min, 85% to 70% A; 24-28 min, 70% to 5% A; 28-30.5 min, 5% A; 30.5-30.6 min, 5% to 95% A; 30.6-38 min, 95% A. The column and autosampler were kept at 35°C and 4°C, respectively. Sample injection volume was optimized as 5 µL to achieve maximum spectral intensity without signal saturation.

Lipidomic profiling was investigated using reverse-phase chromatography on a XBridge BEH C_{18} column (2.1 × 100 mm, 2.5 µm, 130 Å) (Waters, Milford, USA). Mobile phase A consisted of 2 mM ammonium formate in acetonitrile/H_2O (6:4 v/v) with pH of 4.8 and B was isopropanol alcohol/acetonitrile (9:1 v/v). The column was maintained at 25°C with a flow rate of 0.48 mL/min. The solvent gradient was set as follows: 0-5 min, 80% to 27% A; 5-26 min, 27% to 24.5% A; 26.1-29.9 min, 0% A; 29.9-30 min, 0%-80% A; 30-35 min, 80% A. Injection volume was 2 µL for positive mode and 5 µL for negative mode.

An electrospray ionization (ESI) source was applied to ionize metabolites under both positive (Pos) and negative (Neg) polarity mode. Full scan MS (MS1) and data-dependent MS/MS (auto MS/MS) spectra were acquired with a spectra rate of 8 Hz over m/z range from 50 to 1,000. The optimal settings for the ESI source were as follows: voltage was 3500 V, drying gas temperature was 200°C and flow rate was 10 L/min, sheath gas temperature was 300°C and flow rate was 12 L/min, and nebulizer gas pressure was 50 psi. A stepping collision energy (5.6 to 10.5 eV) was employed for the auto MS/MS acquisition with an intensity threshold of 300.

5.3.6.4 Data analysis

Raw data generated from UHPLC-MS/MS analyses were pre-processed using MS-DIAL 3.52 (RIKEN, Kanagawa, Japan) for spectral deconvolution, peak detection and alignment. Features of QC samples with relative standard deviation (RSD) >30% were discarded. Missing values were replaced by minimum imputation values for the downstream statistical analysis. Features were normalized by sum and logarithmic transformation was performed to generate normally distributed data. Identification of the features in metabolomic and lipidomic profiles were conducted using MS-Finder 3.20 (RIKEN) and Agilent Lipid Annotator (Agilent Technologies) with an m/z tolerance of 5 ppm, respectively. The molecular formula and chemical structures were determined based on adducts types, MS1 peaks, and MS/MS fragments. Statistical analysis was performed using a web-based tool MetaboAnalyst 5.0 (Pang et al., 2021). Multivariate analysis is a crucial strategy to decipher the complicated dataset and identify the potential marker compounds. Unsupervised models, principal component analysis (PCA) and hierarchical cluster analysis (HCA), were used to visualize the variations of metabolites profiles among eggs at different embryonic days. Orthogonal partial least squares-discriminant analysis (OPLS-DA) was further applied to classify different egg groups in a supervised manner and the Variable Importance in the Projection (VIP) values were calculated to indicate the contribution of each feature to the classification. Fold change (FC) and t-test were computed for each feature to demonstrate its abundance difference between each pair of the compared egg groups. The criteria of FC >2 or <0.5, *P*-value <0.05 and VIP value >1 were employed to select the compounds with significantly different abundance between early- and late-stage eggs. We also conducted enrichment analysis and pathway analysis on the selected metabolites by searching Kyoto

Encyclopedia of Genes and Genomes (KEGG) database to explore the potentially influenced metabolic pathways.

5.3.7 Statistical analysis.

One-way analysis of variance (ANOVA) followed by Tukey's post hoc test were performed for multiple comparisons among different groups. Significance tests were carried out using SPSS Statistics 19.0 (IBM SPSS Inc.) and the significant level was defined as 0.05. Error bars in the figures represent the standard deviations (SD) of all the replicates.

5.4 Results and discussion

5.4.1 Induction of *C. jejuni* strains into the VBNC state

Processing and preservation of perishable food products (e.g., poultry, milk, and other meat products) at low temperature (4°C) is a common practice in food industry to inhibit bacterial growth and maintain food quality. Exposure to the refrigeration temperature represents a cold stress to *C. jejuni* and may induce the formation of VBNC population. In this study, we first investigated the transition of four *C. jejuni* strains from the culturable state to the VBNC state at low temperature (**Figure 5.1**), namely ATCC 33560, NCTC 11168, F38011 and 81-116. All *C. jejuni* strains were incubated in MHB at 4°C with an initial concentration of 8 log CFU/mL, and the dynamics of culturable cells were monitored over time. As shown in **Figure 5.2a**, the culturable cell counts of different strains gradually decreased to an undetectable level (<0.1 CFU/mL) at day 35, 24, 42 and 32 during the incubation, respectively. When there was no culturable cell detected, the presence of viable cells was examined using the LIVE/DEAD bacterial viability assay. Viable cells stained in green verified the formation of VBNC cells

(**Figure 5.2b**). The final concentration of VBNC *C. jejuni* cells was quantified using the PMA-qPCR assay (**Figure 5.2c**), revealing that ~1% to 10% of the original bacterial population entered the VBNC state at low temperature.

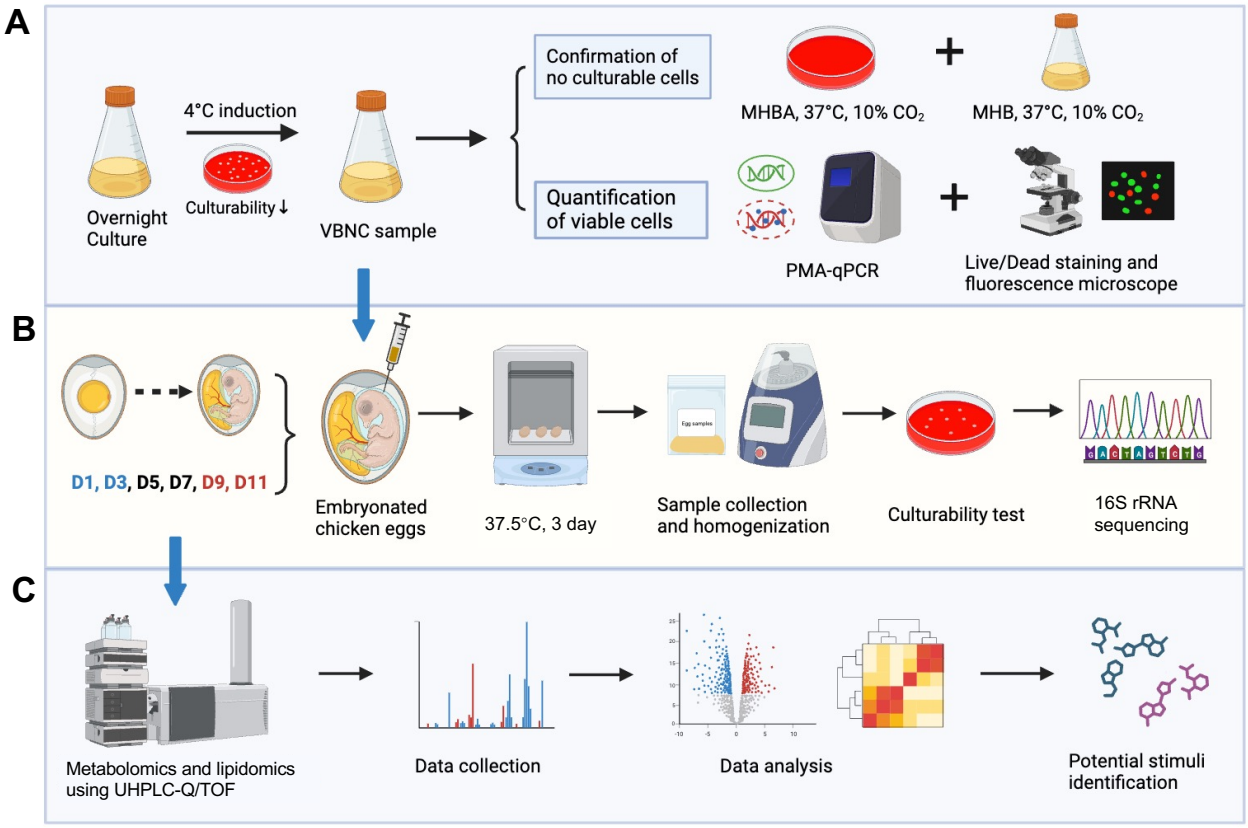

Figure 5.1 Schematic workflow of the metabolomics-based approach to investigate the resuscitation of VBNC *C. jejuni* in embryonated chicken eggs. (A) Induction of VBNC *C. jejuni*. Overnight culture of *C. jejuni* was stored in Mueller-Hinton broth (MHB) at 4°C over time to induce the VBNC state. At the end of the induction, the absence of culturable cells was confirmed when no bacterial growth was detected in both MH blood agar (MHBA) and MHB at the optimal cultivation condition. The presence of viable cells (i.e., VBNC cells) was visualized using Live/Dead bacterial staining assay and quantified using PMA-qPCR. (B) Resuscitation of VBNC *C. jejuni* in embryonated chicken eggs. VBNC *C. jejuni* cells were aseptically injected into embryonated chicken eggs. Following incubation, the egg content was collected and streaked on MHBA to test the regrowth of VBNC *C. jejuni* cells. The identity of the formed bacterial colonies was verified using 16S rRNA sequencing. (C) Untargeted metabolomic and

lipidomic analyses. Eggs at different embryonic days ranging from D1 to D11 indicated enhanced capability of facilitating the resuscitation of VBNC *C. jejuni.* The profiles of metabolites and lipids in the eggs at early embryonic stages (D1 and D3) and late stages (D9 and D11) were investigated using UHPLC-Q/TOF-based approach. Compounds with significantly higher abundance in late-stage eggs were identified and some might potentially contribute to the resuscitation of VBNC *C. jejuni*.

The formation of VBNC *C. jejuni* at low temperature was also investigated in a previous study, where *C. jejuni* completely lost culturability after 50 days at 4°C while maintained the viability for up to 7 months, indicating a prolonged survival of VBNC *C. jejuni* under cold stress (24). In another study, ten *C. jejuni* strains were induced into the VBNC state in artificial seawater at 4°C after 12 to 35 days, with the final VBNC concentration of ~5 log CFU/mL (15). The variations in the induction durations and final VBNC concentrations among different studies might be attributed to the differences in *C. jejuni* strains, initial bacterial concentration, atmospheric condition, and nutrient levels used in each study (25). *C. jejuni* lacks the cold-shock proteins that are commonly present in other foodborne pathogens, such as CspA (26). Entering the VBNC state is the survival strategy of *C. jejuni* to cope with cold stress (27). As food products are important vehicles of *C. jejuni* and low temperature is extensively employed in food processing and storage, the formation of VBNC *C. jejuni* at low temperature poses a high risk to food safety. Further exploration of its resuscitation potential is therefore warranted.

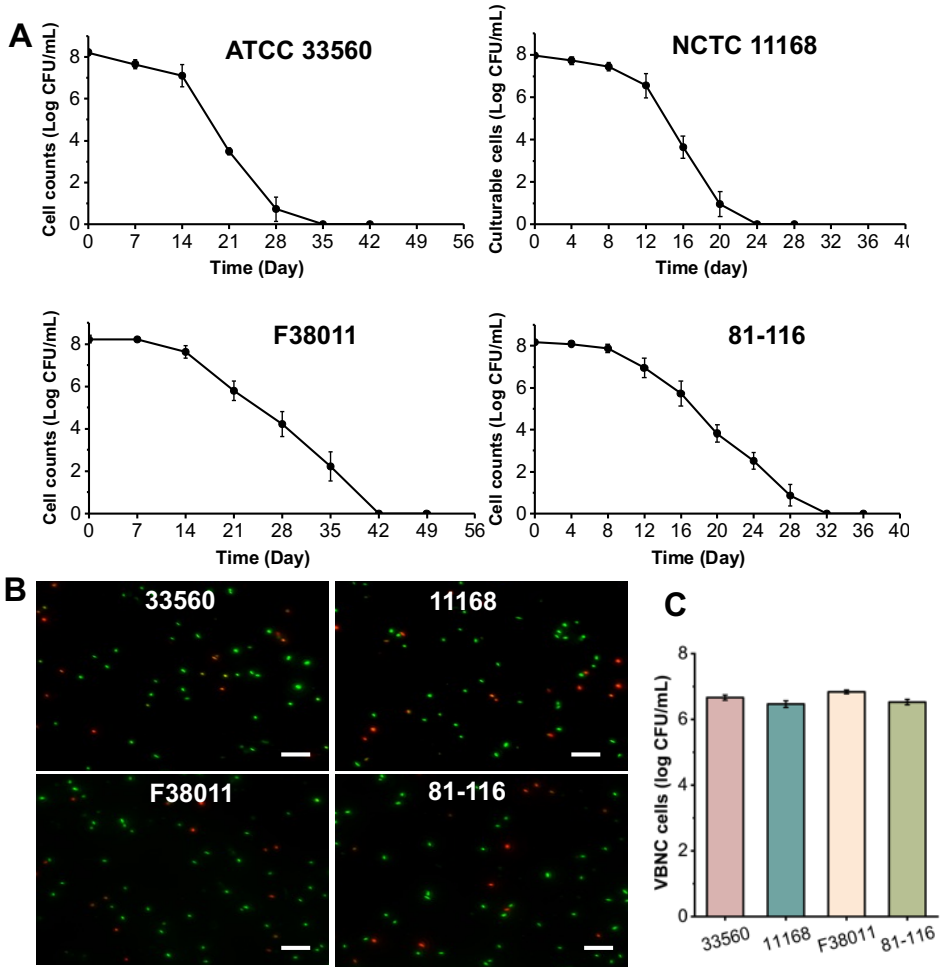

Figure 5.2 Induction of four *C. jejuni* strains into the VBNC state at low temperature (4°C). (A) Dynamics of culturable cell counts in the bacterial samples during the induction. (B) Representative images of VBNC *C. jejuni* cells stained using a LIVE/DEAD BacLight bacterial viability kit under fluorescence microscopy (N=6). Cells stained in green represented the VBNC cells, while dead cells were strained in red. Scale bar: 10 μm (C) Final concentration of VBNC *C. jejuni* cells determined using the PMA-qPCR assay at the end of the induction. The error bars represent the standard deviations among all the replicates.

5.4.2 Resuscitation of VBNC *C. jejuni* strains in embryonated chicken eggs

To evaluate the potential risk posed by VBNC *C. jejuni* cells, we assessed their resuscitation capabilities in embryonated chicken eggs (**Figure 5.1b**). VBNC cells of four *C. jejuni* strains

were individually harvested at the end of the induction (i.e., when no culturable cell was detected) and then aseptically inoculated into the embryonated chicken eggs. The egg content was separately collected after incubation for 3 days, followed by testing on MH blood agar. Uniform bacterial colonies were formed on the agar plates with *Campylobacter*-like morphological characteristics, such as greyish, non-haemolytic, smooth and relatively small in size. These colonies were subsequently confirmed to be identical to the inoculated *C. jejuni* strains using PCR and 16S rRNA sequencing (**Figure S5.2**). In comparison, the VBNC bacterial samples incubated in MH broth under optimal condition showed no bacterial growth, ruling out the possibility that the recovered *C. jejuni* colonies resulted from the remaining culturable cells in the sample. Furthermore, no *C. jejuni* cell was detected in the negative control eggs without VBNC inoculum, indicating that the formed *C. jejuni* colonies were not due to the original *Campylobacter* colonization in the eggs. Collectively, these results demonstrated that VBNC *C. jejuni* cells were successfully resuscitated after passage through the embryonated chicken eggs. Resuscitation in eggs was observed for all four *C. jejuni* strains, with strain-specific resuscitation rates ranging from 68.4% for strain 11168 to 90.5% for strain F38011 (**Figure 5.3a**). We also determined the concentration of the resuscitated *C. jejuni* cells in the eggs and the average concentrations were all >8 log CFU/mL **(Figure 5.3b)**. These were higher than the initially inoculated VBNC bacterial concentrations, indicating proliferation of the resuscitated *C. jejuni* cells within eggs during the 3-day incubation. No significant difference in the resuscitated concentration was observed among the four *C. jejuni* strains.

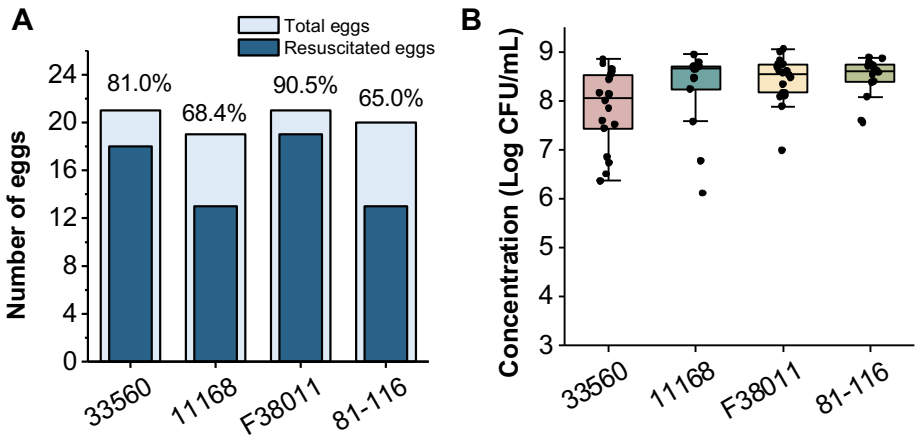

Figure 5.3 Resuscitation capability of different VBNC *C. jejuni* strains in embryonated chicken eggs. (A) Resuscitation rate (%) of each VBNC *C. jejuni* strain in the eggs. Resuscitation rate was determined by dividing the number of eggs capable of facilitating VBNC resuscitation by the total number of eggs tested. (B) Concentration of the resuscitated *C. jejuni* cells in the eggs after 3-d incubation.

Although the existence of VBNC *C. jejuni* was indicated by the maintenance of cell membrane integrity when culturability was lost (**Figure 5.2**), resuscitation serves as definitive evidence that these nonculturable cells were indeed dormant cells rather than dead cells. Various methods have been applied to resuscitate VBNC cells of other pathogenic bacteria. For instance, VBNC *E. coli* O157:H7 and *S.* Typhimurium were recovered to culturable state by supplementing Tween 80 (28) and by heat shock (29), respectively. The quorum sensing autoinducer (AI-2) collected from the cell-free supernatant of culturable cells promoted the resuscitation of VBNC *V. vulnificus* (30). However, all these stimuli were unable to trigger the resuscitation of VBNC *C. jejuni* in the current study (data not shown). Recovery of VBNC *C. jejuni* from dormancy was previously described after intestinal passage in one-day-old chicks (16, 31), mice (15, 31) and rats (32), while contrary results were reported by others that resuscitation was unsuccessful in these animal models (33-35). Our study offers an alternative approach to investigate the

resuscitation of VBNC *C. jejuni* in embryonated chicken eggs. Compared to the *in vivo* animal models, injection into fertilized eggs is cost-effective, less labor-intensive and does not require highly trained personnel. Higher resuscitation rates (i.e., 68-90.5%) were obtained in this study compared to the study conducted by Baffone and coauthors (15), where less than 44.4% of the VBNC *C. jejuni* samples were resuscitated in the mice intestine. Thus, the proposed egg model could be a preferable approach to the recovery of VBNC *C. jejuni*. As no *C. jejuni* resuscitation was observed in the unfertilized chicken eggs (data not shown), the presence of embryogenesis might be a crucial factor to enable the resuscitation. This hypothesis was reinforced by a previous study that resuscitation of *Helicobacter polyri* was achieved in a liquid media supplemented with foetal calf serum (36). Embryo development is a dynamic process, implying that the resuscitation capability of fertilized chicken eggs at different embryonic stages may vary and requires further investigation.

5.4.3 Resuscitation of VBNC *C. jejuni* in eggs at different embryonic stages

The embryonated chicken egg is a comprehensive system with dynamic molecular compositions to meet diverse nutritional requirements throughout the embryonic development. Thus, we hypothesized that chicken eggs at different embryonic stages may exhibit varying capabilities of promoting the resuscitation of VBNC *C. jejuni*. To test this hypothesis, embryonated eggs collected at D1, D3, D5, D7, D9 and D11 were individually subjected to VBNC resuscitation (**Figure S5.3**), and the results are summarized in **Figure 5.4**. For both *C. jejuni* ATCC 33560 and F38011 strains, the resuscitation rates gradually increased along with the embryonic periods. Specifically, no resuscitation was observed in the eggs at D1 for both strains. The resuscitation rate reached 90% in both D9- and D11-eggs for strain ATCC 33560. For strain F38011, the

highest resuscitation rate (i.e., 90%) was also achieved in eggs at D9, while it slightly decreased to 84% in D11-eggs. Overall, eggs at later embryonic stages exhibited a higher resuscitation rate compared to those at earlier stages.

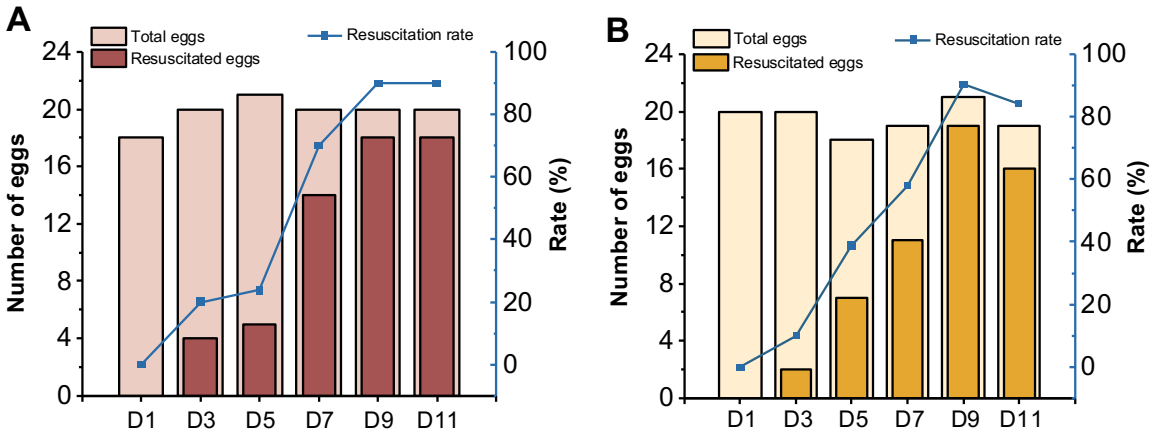

Figure 5.4 Resuscitation rate of VBNC *C. jejuni* ATCC33560 (A) and F38011 (B) in chicken eggs at different embryonic days ranging from D1 to D11. The values of resuscitation rates are presented on the right axis.

In previous studies that investigated the VBNC bacterial resuscitation in embryonated eggs, eggs at the same embryonic age (i.e., D7 or D9) were utilized (37-39). The influence of egg embryonic stages on the resuscitation of VBNC bacterial cells has not been investigated yet. In the current study, C. *jejuni* strains displayed an increasing trend in the resuscitation rates when tested in eggs at embryonic days ranging from D1 to D11. Embryonic development of chicken requires a total of 21 days from a fertilized egg to a hatched chick (40). This dynamic process is usually divided into 3 major phases: germ establishment (D1-D7), embryo completion (D8-D14) and preparation for hatching (D15-D21) (17). In the first phase of embryogenesis, digestion of nutrients commenced from the yolk and albumen to support the initial development of the germ. For example, albumen proteins were hydrolyzed to polypeptides and amino acids to facilitate

their absorption by the cells (41). The absence or low resuscitation rates in eggs at D1-D7 might be due to the limited nutritional level at the beginning of embryo development, which was insufficient to support the recovery of VBNC bacterial cells. The resuscitation rates increased in correlation with the accumulation of the nutrients in eggs at later stages.

For the eggs tested at late embryonic stages of D9 and D11, comparably high resuscitation rates (i.e., 84 to 90%) were obtained for both *C. jejuni* strains. The slight decrease in the resuscitation rate in D11-eggs for strain F38011 might result from the biological variations of the eggs used in the current study. During the second embryogenic phase (D8-D14), there are intensive absorption, digestion, and transportation of nutrients in the eggs to support the rapid growth of embryo (17). Metabolic activities of proteins, lipids, carbohydrates, and minerals increase significantly to provide energy and building blocks for the development of various tissues and organs (42-45). Based on these findings, we speculated that the enhanced metabolisms and enriched nutrient profiles in the eggs at late embryonic stages (D9 and D11) may play a crucial role in stimulating the resuscitation of VBNC *C. jejuni*. Further investigations are required to identify these potential stimuli that contribute to the VBNC resuscitation.

5.4.4 Metabolomics and lipidomics to investigate the potential resuscitation stimuli

To identify the potential contributing compounds to the resuscitation of VBNC *C. jejuni*, we assessed the compositional variations between the eggs at early (i.e., D1 and D3) and late embryonic stages (i.e., D9 and D11) using untargeted metabolomic and lipidomic analyses. Hydrophilic metabolites and hydrophobic lipids were extracted from the egg samples simultaneously and separately analyzed using UHPLC-Q/TOF.

For metabolomic analysis of the hydrophilic metabolites, after removing the features with RSD value of QC samples >0.3, 650 and 901 metabolites with MS2 spectra were identified in the positive and negative ion mode, respectively. Unsupervised PCA was applied to these metabolites from all samples to evaluate the reproducibility of the analytical platform and visualize the overall metabolic variations among different samples. As shown in **Figure 5.5a**, the tight clustering of all the QC samples indicates good repeatability and stability of the UHPLC-Q/TOF-based metabolomics. Eggs at early stages of D1 and D3 were noticeably separated from late-stage eggs of D9 and D11, demonstrating that they exhibited distinct metabolite profiles. The cluster overlap between eggs at D1 and D3, as well as between D9 and D11, suggested similar metabolic characteristics among them. Supervised PLS-DA was further utilized and the separation among 4 egg groups was observed in both modes (**Figure 5.5b**). Eggs from early stages (D1 and D3) and late stages (D9 and D11) were more distinctively segregated, indicating significant differences in their metabolomes. Relative abundances of the metabolites in each egg sample were visualized using an HCA-based heatmap (**Figure S5.4**). Most metabolites showed increased concentrations in eggs at D9 and D11, confirming that the rapid embryonic development in late-stage eggs lead to an enriched metabolite profile. These metabolites might provide essential nutrients or other stimuli to trigger the resuscitation of VBNC *C. jejuni*.

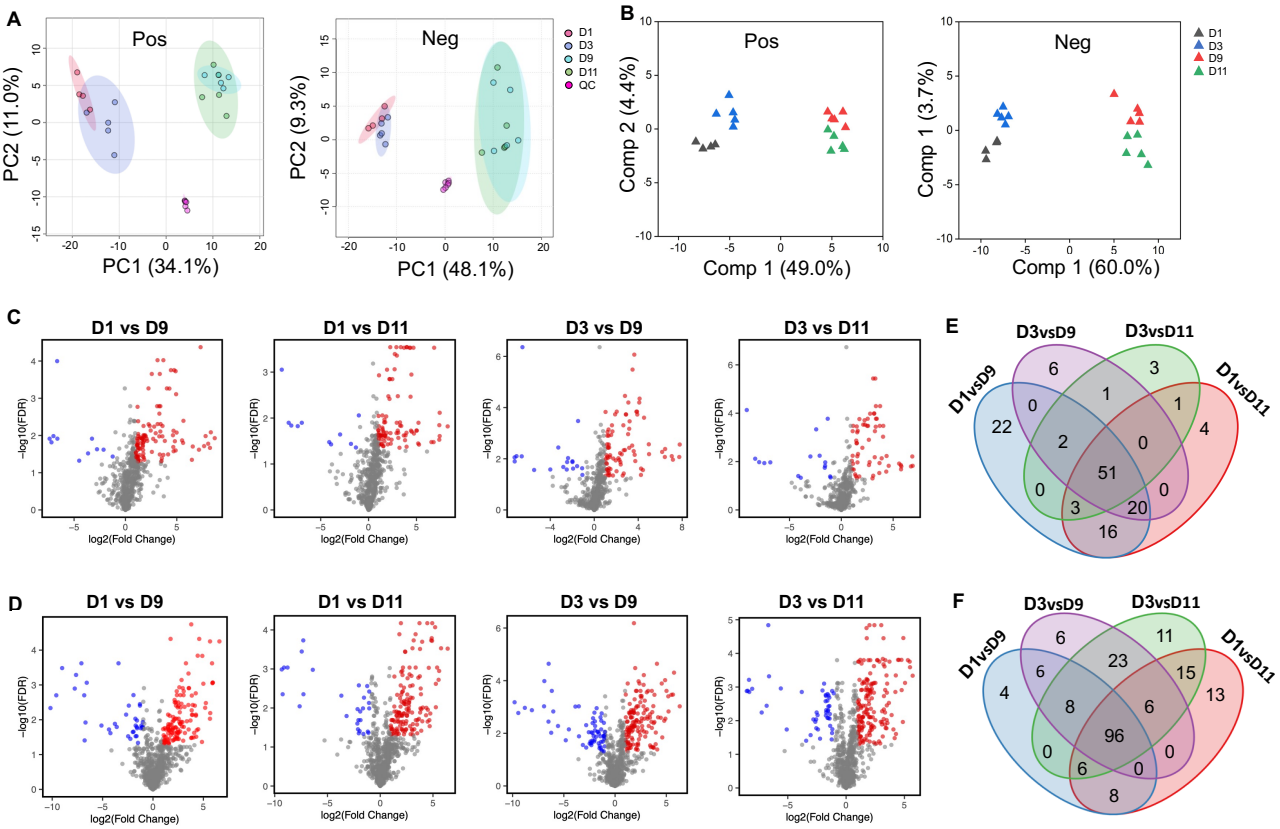

Figure 5.5 Untargeted metabolomic analysis of eggs at different embryonic days. (A) Score plots of principal component analysis (PCA) based on metabolite profiling in both positive and negative ion modes. (B) Partial least squares-discriminant analysis (PLS-DA) based on metabolite profiling in both positive and negative modes. (C-D) Volcano plots to select the differential metabolites between different egg groups in both positive (C) and negative (D) modes. Selection threshold was set as FC >2 or <0.5, and P <0.05 in the t-test. Each dot represents a specific metabolite, with color indicating a significantly higher (red) or lower (blue) abundance in the latter group. Gray dots indicate no significant difference. (E-F) Venn plot to show the overlap of significantly increased metabolites selected in each pair of the compared groups using volcano plots in both positive (E) and negative (F) modes.

We further used volcano plot analysis to identify the differential metabolites between different egg groups. As eggs at both D9 and D11 exhibited superior capability of facilitating VBNC resuscitation compared to those at D1 and D3, multiple comparisons were conducted between D1 and D9, D1 and D11, D3 and D9, as well as D3 and D11 (**Figure 5.5cd**). The criteria of p <0.05

in t-test, FC >2, and VIP score >1 were used to screen out the metabolites with significantly different abundance in each pair of the compared groups. The shared differential metabolites among all the comparison pairs were selected in the Venn diagrams, with 51 metabolites in positive mode (**Figure 5.5e**) and 96 metabolites in negative mode (**Figure 5.5f**). These metabolites showed significantly higher abundance in both egg groups with high resuscitation capability (i.e., D9 and D11) so that they hold high potential to contribute to the resuscitation of VBNC *C. jejuni*. Among these metabolites, a total of 122 were assigned to putative identities and the top 30 metabolites with the highest abundance are listed in **Table S5.1**, including amino acids, nucleotides, fatty acids and amino sugars.

Using KEGG analysis, major biochemical metabolic pathways associated with these differential metabolites were identified (**Figure S5.5**). Most of the pathways are related to the amino acids, such as valine, leucine and isoleucine biosynthesis; glycine, serine and threonine metabolism; and phenylalanine, tyrosine and tryptophan metabolism. Amino acids are recognized as the primary nutrients and energy sources for *C. jejuni*. Several major amino acids can be metabolized by *C. jejuni* to fuel the tricarboxylic acid (TCA) cycle and other anabolic pathways, including serine, glutamine, asparagine, glutamate, aspartate and proline (46). Noticeably, serine, pyroglutamic acid (a precursor for glutamate) and glutamine were all identified with significantly higher abundances in late-stage eggs (**Table S5.1**). These free amino acids might be taken up by VBNC bacterial cells and stimulate the resuscitation. According to Pinto and coauthors (12), resuscitation of VBNC *E. coli* was achieved by supplementing a mixture of amino acids (i.e., leucine, glutamine, methionine and threonine) into the media. The presence of glutamate could also enhance the stress response in bacterial cells (47). Therefore, the high abundance of these

essential amino acids in late-stage eggs may play a critical role in the resuscitation of VBNC *C. jejuni*. In addition, fumarate (a TCA intermediate) was also overexpressed in the eggs with high resuscitation capabilities (**Table S5.1**). Fumarate can be directly transported into *C. jejuni* via C_4-dicarboxylate transporters and utilized in TCA cycle for ATP production (48). As energy is crucial to all cellular activities, restoring the ATP generation might be a prerequisite for VBNC bacterial resuscitation. Yang and coauthors recently reported that resuscitation of VBNC *E. coli* was promoted by ATP-mediated NAD^+ synthesis (49). Thus, fumarate identified in eggs might be another potential stimulus to trigger the resuscitation of VBNC *C. jejuni.*

Lipids are essential components of chicken eggs and play critical roles in various biological processes, such as cell membrane synthesis, energy supply and signal transduction (42). Therefore, lipid profiles in eggs with different VBNC resuscitation potentials were also investigated. Diverse lipid species were identified in the eggs, including 1191 lipids under positive mode and 383 under negative mode. These lipid species belong to six major lipid categories, including fatty acyls (FA), glycerolipids (GL), glycerophospholipids (GP), sphingolipids (SP), prenol lipids (PR) and sterols (ST), and were further divided into subclasses based on their head groups and linkage types (**Figure S5.6**).

PCA and PLS-DA were performed with the total lipids detected from positive mode and negative mode, respectively. Similar to the metabolomic data, QC samples showed a tight clustering in PCA plot, and eggs at early stages (D1 and D3) and late stages (D9 and D11) were clearly distinguished in both PCA and PLSDA (**Figure 5.6**). These results revealed a notable variation in the lipid profiles among eggs at different embryonic stages, potentially influencing their

capabilities of resuscitating VBNC *C. jejuni*. The differently expressed lipid species were also selected using volcano plots and Venn analysis as aforementioned. A total of 47 lipids features were screened out and 27 had totative assignments (**Table S5.2**). Most differential lipids are fatty acids, such as FA 22:6, FA 20:4 and FA 18:2. The oxidative degradation of fatty acids produces acetyl-CoA, which can be involved in the energy metabolism of *C. jejuni* (46). The replacement of carbon sources with lipids to generate energy might be one of the strategies of VBNC bacteria to restore normal metabolic activity and culturability (50). Unsaturated fatty acids have shown the ability to reduce free radicals (51), offering protection to bacterial cells. The extensive metabolisms of fatty acids in late-stage egg might provide a suitable condition to support the regrowth of VBNC cells. Besides, phospholipids are essential components of bacterial cell membranes. Several lipids with significantly higher abundance in eggs of D9 and D11 belong to phospholipids, such as PC O-9:0_26:2, PE 18:0_18:0, PE O-20:3_22:5;O2, and PE O-8:0_4:0;O1 (**Table S5.2**). This high concentration of phospholipids in embryonated eggs may serve as the building blocks to support the reproduction of *C. jejuni* cells when they were resuscitated in eggs.

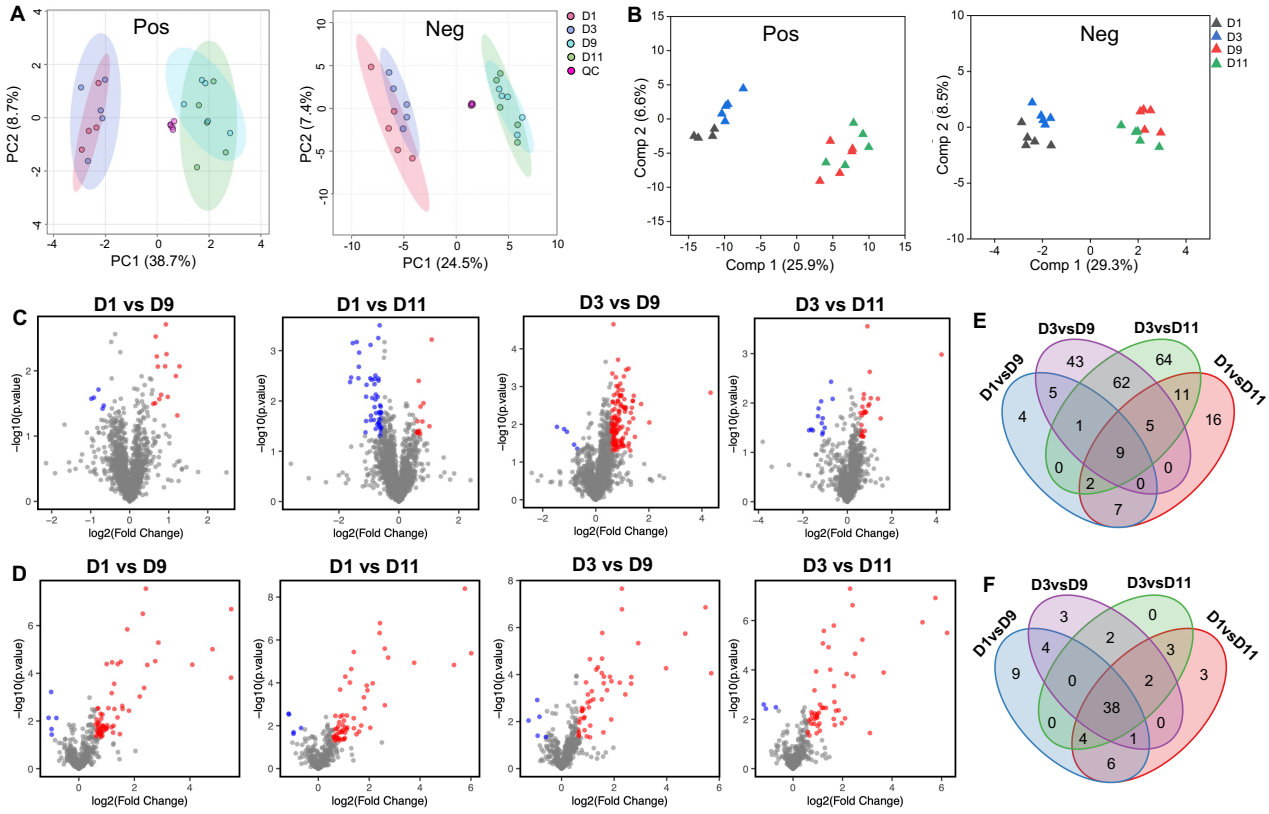

Figure 5.6 Untargeted lipidomic analysis of eggs at different embryonic days. (A) PCA based on lipid profiles in both positive and negative ion modes. (B) PLS-DA based on lipid profiles in both positive and negative modes. (C-D) Volcano plots to select the differential lipids between different egg groups in both positive (C) and negative (D) modes. Selection threshold was set as FC >2 or <0.5, and P <0.05 in the t-test. Each dot represents a specific lipid, with color indicating a significantly higher (red) or lower (blue) abundance in the latter group. Gray dots indicate no significant difference. (E-F) Venn plot to show the overlap of significantly increased lipids selected in each pair of the compared groups using volcano plots in both positive (E) and negative (F) modes.

5.5 Conclusion

Refrigeration temperature is commonly used in food processing, transportation, and storage, especially for poultry products. In this study, we confirmed the formation of VBNC *C. jejuni* at low temperature (4°C) and demonstrated their resuscitation capability in embryonated chicken eggs. This brings up a greater threat to food microbial safety and additional efforts are required

to combat the VBNC *C. jejuni*. As eggs at late embryonic stages (i.e., D9 and D11) indicated enhanced capability of supporting resuscitation than those at early stages (i.e., D1 and D3), we further evaluated the compositional variations among eggs at different embryonic stages using untargeted metabolomics and lipidomics. Potential resuscitation-stimulating compounds were identified, and they might play important roles in the energy production via citric acid cycle, leading to a better understanding of the resuscitation mechanisms of VBNC *C. jejuni*. Supplementing the resuscitation stimuli into conventional culture media has the potential to enable the resuscitation and detection of *C. jejuni* in the VBNC state. To validate this, future works need to be conducted to examine the impact of these potential compounds on the VBNC resuscitation, both individually and in combination. The knowledge gained from this study provides insights for developing novel cultivation media to monitor VBNC *C. jejuni*, thereby contributing to the mitigation of *Campylobacter* contamination in agri-food systems.

5.6 References

1. Kaakoush NO, Castaño-Rodríguez N, Mitchell HM, Man SM. 2015. Global epidemiology of *Campylobacter* infection. Clinical Microbiology Reviews 28:687-720.
2. Ruiz-Palacios GM. 2007. The health burden of *Campylobacter* infection and the impact of antimicrobial resistance: playing chicken, vol 44, p 701-703. The University of Chicago Press.
3. Silva J, Leite D, Fernandes M, Mena C, Gibbs PA, Teixeira P. 2011. *Campylobacter* spp. as a foodborne pathogen: a review. Frontiers in Microbiology 2:200.
4. Bronowski C, James CE, Winstanley C. 2014. Role of environmental survival in transmission of *Campylobacter jejuni*. FEMS Microbiology Letters 356:8-19.
5. Svensson SL, Frirdich E, Gaynor EC. 2008. Survival strategies of *Campylobacter jejuni*: stress responses, the viable but nonculturable state, and biofilms. Campylobacter:571-590.
6. Ramamurthy T, Ghosh A, Pazhani GP, Shinoda S. 2014. Current perspectives on viable but non-culturable (VBNC) pathogenic bacteria. Frontiers in Public Health 2:103.
7. Dong K, Pan H, Yang D, Rao L, Zhao L, Wang Y, Liao X. 2020. Induction, detection, formation, and resuscitation of viable but non-culturable state microorganisms. Comprehensive Reviews in Food Science and Food Safety 19:149-183.
8. Zhang X-H, Ahmad W, Zhu X-Y, Chen J, Austin B. 2021. Viable but nonculturable bacteria and their resuscitation: implications for cultivating uncultured marine microorganisms. Marine Life Science & Technology 3:189-203.

9. Mizunoe Y, Wai SN, Ishikawa T, Takade A, Yoshida S-i. 2000. Resuscitation of viable but nonculturable cells of *Vibrio parahaemolyticus* induced at low temperature under starvation. FEMS Microbiology Letters 186:115-120.

10. Fu Y, Jia Y, Fan J, Yu C, Yu C, Shen C. 2020. Induction of *Escherichia coli* O157: H7 into a viable but non-culturable state by high temperature and its resuscitation. Environmental Microbiology Reports 12:568-577.

11. Wei C, Zhao X. 2018. Induction of viable but nonculturable *Escherichia coli* O157: H7 by low temperature and its resuscitation. Frontiers in Microbiology 9:2728.

12. Pinto D, Almeida V, Almeida Santos M, Chambel L. 2011. Resuscitation of *Escherichia coli* VBNC cells depends on a variety of environmental or chemical stimuli. Journal of Applied Microbiology 110:1601-1611.

13. Zhao X, Zhong J, Wei C, Lin C-W, Ding T. 2017. Current perspectives on viable but non-culturable state in foodborne pathogens. Frontiers in Microbiology 8:580.

14. Senoh M, Ghosh-Banerjee J, Ramamurthy T, Hamabata T, Kurakawa T, Takeda M, Colwell RR, Nair GB, Takeda Y. 2010. Conversion of viable but nonculturable *Vibrio cholerae* to the culturable state by co-culture with eukaryotic cells. Microbiology and Immunology 54:502-507.

15. Baffone W, Casaroli A, Citterio B, Pierfelici L, Campana R, Vittoria E, Guaglianone E, Donelli G. 2006. *Campylobacter jejuni* loss of culturability in aqueous microcosms and ability to resuscitate in a mouse model. International Journal of Food Microbiology 107:83-91.

16. Stern N, Jones D, Wesley I, Rollins D. 1994. Colonization of chicks by non-culturable *Campylobacter* spp. Letters in Applied Microbiology 18:333-336.

17. Meng Y, Qiu N, Guyonnet V, Mine Y. 2021. Omics as a window to unravel the dynamic changes of egg components during chicken embryonic development. Journal of Agricultural and Food Chemistry 69:12947-12955.

18. Hincke MT, Da Silva M, Guyot N, Gautron J, McKee MD, Guabiraba-Brito R, Réhault-Godbert S. 2019. Dynamics of structural barriers and innate immune components during incubation of the avian egg: critical interplay between autonomous embryonic development and maternal anticipation. Journal of Innate Immunity 11:111-124.

19. Cappelier J, Besnard V, Roche S, Velge P, Federighi MM. 2007. Avirulent viable but non culturable cells of *Listeria monocytogenes* need the presence of an embryo to be recovered in egg yolk and regain virulence after recovery. Veterinary Research 38:573-583.

20. Panutdaporn N, Kawamoto K, Asakura H, Makino S-I. 2006. Resuscitation of the viable but non-culturable state of *Salmonella enterica* serovar Oranienburg by recombinant resuscitation-promoting factor derived from *Salmonella* Typhimurium strain LT2. International Journal of Food Microbiology 106:241-247.

21. Zeng B, Zhao G, Cao X, Yang Z, Wang C, Hou L. 2013. Formation and resuscitation of viable but nonculturable *Salmonella* typhi. BioMed Research International 2013.

22. Lv R, Wang K, Feng J, Heeney DD, Liu D, Lu X. 2020. Detection and quantification of viable but non-culturable *Campylobacter jejuni*. Frontiers in Microbiology 10:2920.

23. Bang DD, Wedderkopp A, Pedersen K, Madsen M. 2002. Rapid PCR using nested primers of the 16S rRNA and the hippuricase (hip O) genes to detect *Campylobacter jejuni* and *Campylobacter coli* in environmental samples. Molecular and Cellular Probes 16:359-369.

24. Lázaro B, Cárcamo J, Audícana A, Perales I, Fernández-Astorga A. 1999. Viability and DNA maintenance in nonculturable spiral *Campylobacter jejuni* cells after long-term exposure to low temperatures. Applied and Environmental Microbiology 65:4677-4681.

25. Yagi S, Okada A, Inoshima Y. 2022. Role of temperature, nutrition, oxygen, osmolality, and bacterial strain in inducing a viable but non-culturable state in *Campylobacter jejuni*. Journal of Microbiological Methods 195:106456.

26. Ermolenko D, Makhatadze G. 2002. Bacterial cold-shock proteins. Cellular and Molecular Life Sciences CMLS 59:1902-1913.

27. Hazeleger WC, Wouters JA, Rombouts FM, Abee T. 1998. Physiological activity of *Campylobacter jejuni* far below the minimal growth temperature. Applied and Environmental Microbiology 64:3917-3922.

28. Liu Y, Wang C, Tyrrell G, Hrudey SE, Li XF. 2009. Induction of *Escherichia coli* O157: H7 into the viable but non-culturable state by chloraminated water and river water, and subsequent resuscitation. Environmental Microbiology Reports 1:155-161.

29. Gupte A, De Rezende C, Joseph S. 2003. Induction and resuscitation of viable but nonculturable *Salmonella enterica* serovar Typhimurium DT104. Applied and Environmental Microbiology 69:6669-6675.

30. Ayrapetyan M, Williams TC, Oliver JD. 2014. Interspecific quorum sensing mediates the resuscitation of viable but nonculturable *Vibrios*. Applied and Environmental Microbiology 80:2478-2483.

31. Cappelier J, Magras C, Jouve J, Federighi M. 1999. Recovery of viable but non-culturable *Campylobacter jejuni* cells in two animal models. Food Microbiology 16:375-383.

32. Saha S, Saha S, Sanyal S. 1991. Recovery of injured *Campylobacter jejuni* cells after animal passage. Applied and Environmental Microbiology 57:3388-3389.

33. Van de Giessen A, Heuvelman C, Abee T, Hazeleger W. 1996. Experimental studies on the infectivity of non-culturable forms of *Campylobacter* spp. in chicks and mice. Epidemiology & Infection 117:463-470.

34. Hald B, Knudsen K, Lind P, Madsen M. 2001. Study of the infectivity of saline-stored *Campylobacter jejuni* for day-old chicks. Applied and Environmental Microbiology 67:2388-2392.

35. Mederma G, Schets F, Van de Giessen A, Havelaar A. 1992. Lack of colonization of 1 day old chicks by viable, non-culturable *Campylobacter jejuni*. Journal of Applied Microbiology 72:512-516.

36. Cellini L, Robuffo I, Dicampli E, Di Bartolomeo S, Taraborelli T, Dainelli B. 1998. Recovery of *Helicobacter pylori* ATCC43504 from a viable but not culturable state: regrowth or resuscitation? Apmis 106:571-579.

37. Cappelier J, Minet J, Magras C, Colwell R, Federighi M. 1999. Recovery in embryonated eggs of viable but nonculturable *Campylobacter jejuni* cells and maintenance of ability to adhere to HeLa cells after resuscitation. Applied and Environmental Microbiology 65:5154-5157.

38. Chaveerach P, Ter Huurne A, Lipman L, Van Knapen F. 2003. Survival and resuscitation of ten strains of *Campylobacter jejuni* and *Campylobacter coli* under acid conditions. Applied and Environmental Microbiology 69:711-714.

39. Talibart R, Denis M, Castillo A, Cappelier J, Ermel G. 2000. Survival and recovery of viable but noncultivable forms of *Campylobacter* in aqueous microcosm. International Journal of Food Microbiology 55:263-267.

40. Akil R, Zakaria A. 2015. Egg laying characteristics, egg weight, embryo development, hatching weight and post-hatch growth in relation to oviposition time of broiler breeders. Animal Reproduction Science 156:103-110.

41. Fang J, Ma MH, Qiu N, Jin YG. 2012. Analysis of the low-molecular weight protein profile of egg-white and its changes during early chicken embryological development. Zeitschrift für Naturforschung C 67:208-214.

42. Meng Y, Qiu N, Mine Y, Keast R. 2021. Comparative lipidomics of chick yolk sac during the embryogenesis provides insight into understanding the development-related lipid supply. Journal of Agricultural and Food Chemistry 69:7467-7477.

43. Rehault-Godbert S, Mann K, Bourin M, Brionne A, Nys Y. 2014. Effect of embryonic development on the chicken egg yolk plasma proteome after 12 days of incubation. Journal of Agricultural and Food Chemistry 62:2531-2540.

44. Yadgary L, Wong EA, Uni Z. 2014. Temporal transcriptome analysis of the chicken embryo yolk sac. BMC Genomics 15:1-15.

45. Liu H, Ding P, Tong Y, He X, Yin Y, Zhang H, Song Z. 2021. Metabolomic analysis of the egg yolk during the embryonic development of broilers. Poultry Science 100:101014.

46. Stahl M, Butcher J, Stintzi A. 2012. Nutrient acquisition and metabolism by Campylobacter jejuni. Frontiers in Cellular and Infection Microbiology 2:5.

47. Han M-L, Liu X, Velkov T, Lin Y-W, Zhu Y, Creek DJ, Barlow CK, Yu HH, Zhou Z, Zhang J. 2019. Comparative metabolomics reveals key pathways associated with the

synergistic killing of colistin and sulbactam combination against multidrug-resistant *Acinetobacter baumannii*. Frontiers in Pharmacology 10:754.

48. Guccione E, Del Rocio Leon-Kempis M, Pearson BM, Hitchin E, Mulholland F, Van Diemen PM, Stevens MP, Kelly DJ. 2008. Amino acid-dependent growth of *Campylobacter jejuni*: key roles for aspartase (AspA) under microaerobic and oxygen-limited conditions and identification of AspB (Cj0762), essential for growth on glutamate. Molecular Microbiology 69:77-93.

49. Yang D, Wang W, Zhao L, Rao L, Liao X. 2023. Resuscitation of viable but nonculturable bacteria promoted by ATP-mediated NAD^+ synthesis. Journal of Advanced Research.

50. Qi Z, Liu C. 2022. Metabolic characteristics and markers in viable but nonculturable state of *Pseudomonas aeruginosa* induced by chlorine stress. Environmental Research 214:114111.

51. Das U, Begin M, Ells G, Huang Y, Horrobin D. 1987. Polyunsaturated fatty acids augment free radical generation in tumor cells in vitro. Biochemical and Biophysical Research Communications 145:15-24.

5.7 Supplementary information

Materials and methods

Propidium monoazide (PMA) treatment and DNA extraction

Bacterial solution was mixed with PMA (15 μM) and PMA enhancer (1×, Biotium Inc., Hayward, CA, USA) with a total volume of 500 μL in a 1.7-mL micro-centrifuge tube (Froggabio, Concord, ON, Canada). The mixture was incubated in dark with a constant shaking at 150 rpm for 10 min, followed by exposing the tubes horizontally to a 600-W halogen lamp (Smith Victor, Bartlett, IL, USA) for 10 min to initiate DNA crosslinking. The samples were kept on ice and maintained a distance of 20 cm to the lamp during light exposure to avoid overheating. The mixture was then centrifuged at 15,000 ×*g* for 5 min and washed one time with phosphate buffer saline (PBS) to remove the residual PMA. The cell pellet was resuspended in sterile distilled deionized water (ddH_2O) and the genomic DNA was extracted by boiling at 100°C for 10 min. DNA was stored at -20°C until qPCR analysis.

Conduction of qPCR assay

The primers (*rpoB* 1: 5′-GAGTAAGCTTGCTAAGATTAAAG-3′ and *rpoB* 2: 5′-AAGAAGTTTTAGAGTTTCTCC-3′) targeting on a RNA polymerase *rpoB* of *C. jejuni* was used in the qPCR assay. The total volume for each qPCR reaction was 20 μL, containing 1× SensiFAST SYBR Mix (Bioline, Taunton, USA), 100 nM of each primer, 2 μL of DNA temple and sterile ddH_2O. The qPCR was conducted in an Mx3005P real-time PCR system (Agilent, Santa Clara, CA, USA) with an initial denaturation step at 50°C for 2 min and 95°C for 10 min, and then 40 cycles of 95°C for 15 s and 60°C for 1 min. Sterile DNase-free ddH_2O was included in each run of qPCR as negative control and each sample was tested at least in triplicate.

Results

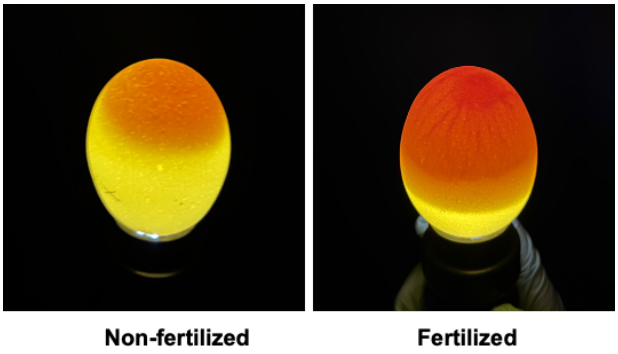

Figure S5.1 Images of non-fertilized and fertilized chicken eggs upon candling. A network of blood vessel could be observed in the fertilized eggs starting from ~D5. Unfertilized eggs would be excluded from the following experiments.

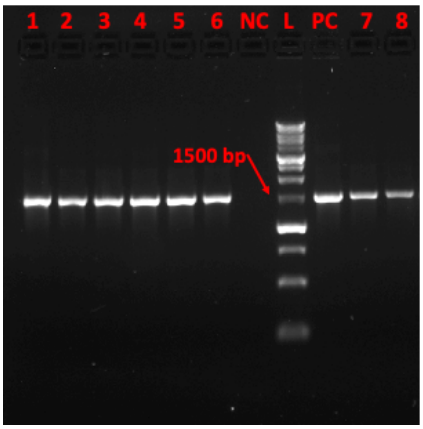

Figure S5.2 Representative PCR products of the resuscitated bacterial cells using *C. jejuni*-specific primers targeting on the 16S rRNA gene. Lanes 1-8: resuscitated bacterial cells collected from different samples; Lane L: DNA ladder; Positive control (PC): *C. jejuni* ATCC33560; Negative control (NC): H_2O. All the amplicons from the resuscitated cells indicated an expected size of 1495 bp. The subsequent 16S rRNA sequencing of the amplicons confirmed their identify to the inoculated *C. jejuni* strains.

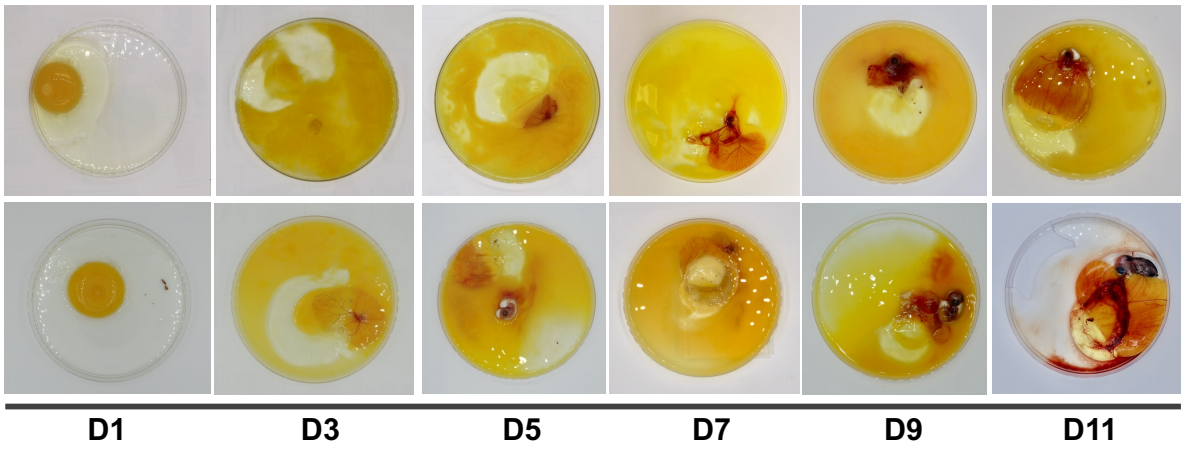

Figure S5.3 Representative images of embryonated chicken eggs at different embryonic days ranging from D1 to D11. Eggs exhibited an enhanced capability of promoting the resuscitation of VBNC *C. jejuni* along with the embryo development.

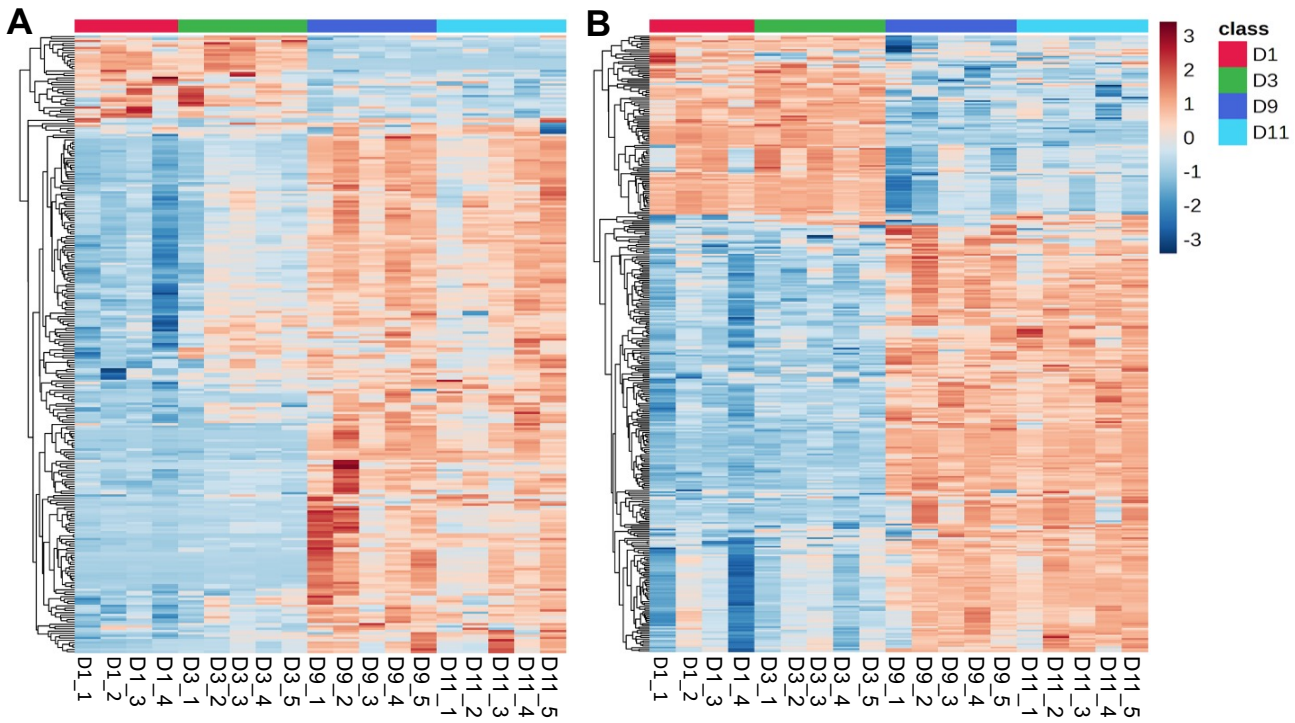

Figure S5.4 Heatmap visualization of the relative abundances of metabolites in eggs at different embryonic days. Rows: metabolites; Columns: samples; Color indicates the relative abundance of the metabolite, where blue is the lowest and red is the highest.

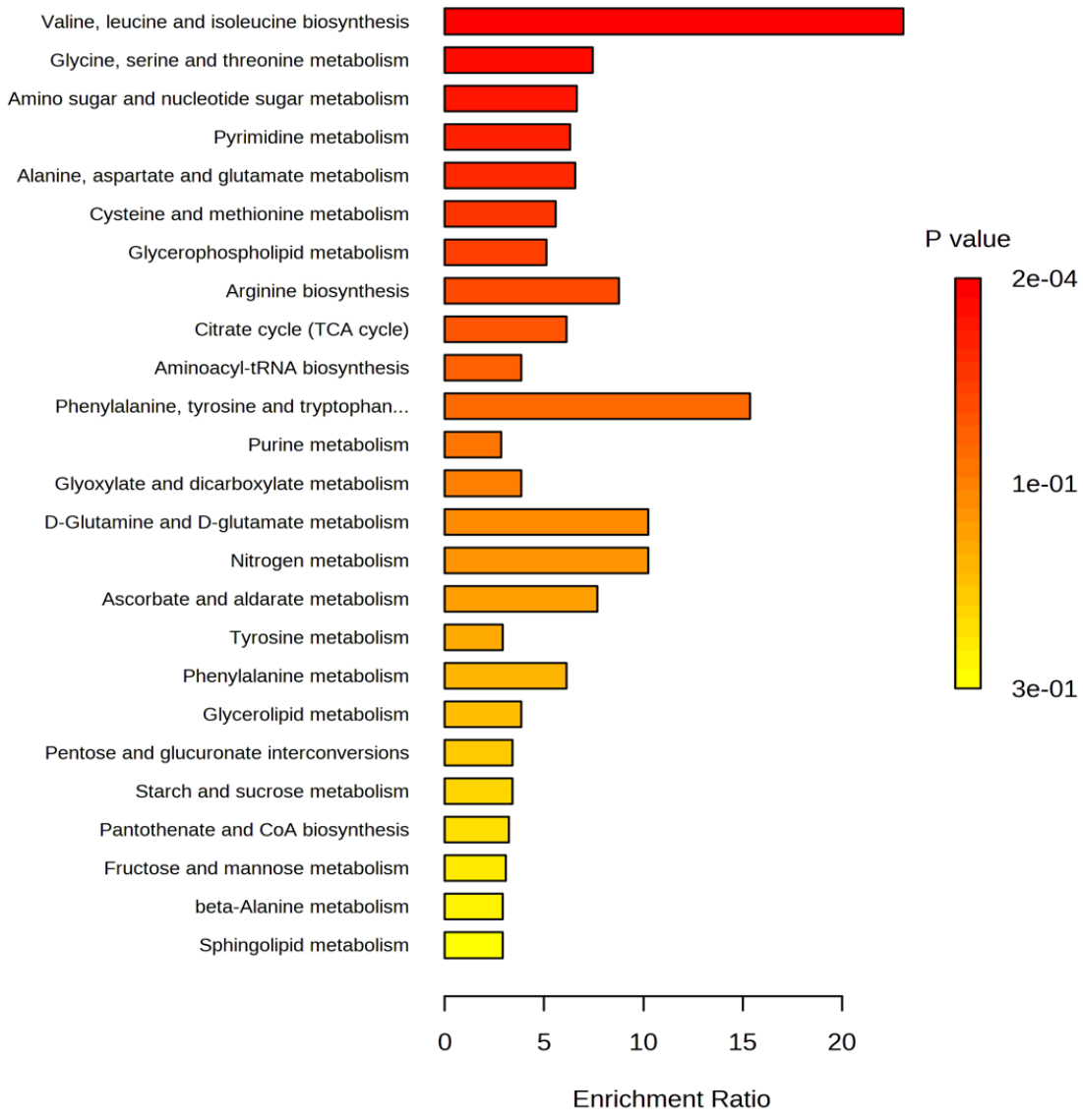

Figure S5.5 Pathway enrichment analysis of the selected significantly differential metabolites between eggs at different embryonic stages.

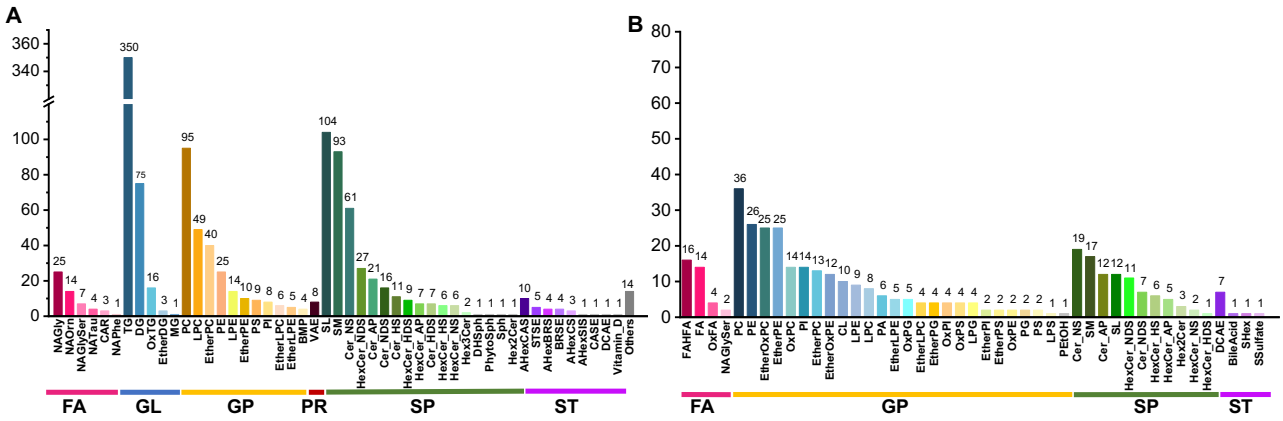

Figure S5.6 Number of lipid species detected in the embryonated chicken eggs using UHPLC-Q/TOF in both positive (A) and negative (B) modes. FA: fatty acids; GL: glycerolipids; GP: glycerophospholipids; SP: sphingolipids; PR: prenol lipids; ST: sterols.

Table S5.1 Putative identities of significantly differential lipids among different egg groups

Average RT (min)	Average Mass	Lipid species	Adduct	Formula	Lipid Class
3.6	436.28296	LPE O-16:1	[M-H]-	C21H44NO6P	EtherLPE
3.795	463.20822	LPG 15:3	[M+Na-2H]-	C21H37O9P	LPG
3.796	677.45496	SM 28:2;O3	[M+Na-2H]-	C33H65N2O7P	SM
3.797	327.23346	FA 22:6	[M-H]-	C22H32O2	FA
3.806	412.21707	PE O-8:0_4:0;O1	[M-H]-	C17H36NO8P	EtherOxPE
4.156	303.23331	FA 20:4	[M-H]-	C20H32O2	FA
4.156	607.47241	FAHFA 20:4_20:3	[M-H]-	C40H68O4	FAHFA
4.157	955.67603	PI O-16:0_28:4	[M-H_2O-H]-	C53H97O12P	EtherPI
4.158	629.45422	PA 16:0_16:0	[M+Na-2H]-	C35H69O8P	Unknown

4.161	697.44238	PG O-8:0_24:5	[M-H]-	C38H67O9P	EtherPG
4.163	765.42847	PG 9:0_22:3;O4	[M-H]-	C37H67O14P	OxPG
4.308	329.24802	FA 22:5	[M-H]-	C22H34O2	FA
4.316	480.30893	LPE 18:0	[M-H]-	C23H48NO7P	LPE
4.426	279.23318	FA 18:2	[M-H]-	C18H32O2	FA
4.427	559.47272	FAHFA 18:2_18:1	[M-H]-	C36H64O4	FAHFA
4.43	581.45514	FAHFA 18:2_20:4	[M+Na-2H]-	C38H62O4	FAHFA
4.437	802.59613	PC O-9:0_26:2	[M-H]-	C43H84NO7P	EtherPC
4.647	832.54547	PE O-20:3_22:5;O2	[M-H]-	C47H80NO9P	EtherOxPE
4.858	305.24817	FA 20:3	[M-H]-	C20H34O2	FA
7.472	746.56769	PE 18:0_18:0	[M-H]-	C41H82NO8P	PE
10.36	892.74121	SL 18:1;O/36:3;O	$[M+NH^4]+$	C54H101NO6S	SL
11.065	952.83661	Cer 25:3;O2/38:5	[M+H]+	C63H111NO3	Cer_NS
11.066	868.742	SL 16:1;O/36:1;O	$[M+NH^4]+$	C52H101NO6S	SL
11.147	894.758	Cer 21:3;O2/38:6	$[M+NH^4]+$	C59H101NO3	Cer_NS
11.148	964.83698	TG 8:0_13:0_38:7	$[M+NH^4]+$	C62H106O6	TG
11.149	978.85217	TG 8:0_14:0_38:7	[M+Na]+	C63H108O6	TG
11.574	882.75745	TG 17:2_18:2_18:2	$[M+NH^4]+$	C56H96O6	TG

RT: retention time; Lipid class were verified from the LIPID MAPS Database.

Chapter 6: General Conclusion

6.1 Conclusions and contributions to original knowledge

The rationale behind this Ph.D. thesis project is that VBNC state is a critical strategy for *C. jejuni* to survive in the environment and agri-food systems (Chapter 2). VBNC cells can evade conventional culture-based detection and their capability of resuscitating under favorable conditions poses a significant risk to the food industry and public health. Therefore, a culture-independent and reliable approach is highly demanded to accurately identify *C. jejuni* at the VBNC state, and it is necessary to better understand the resuscitation of VBNC *C. jejuni*. In this thesis, we identified and characterized VBNC *C. jejuni* at the single-cell level using the developed Raman tweezers system, as well as investigated the resuscitation of VBNC *C. jejuni* in embryonated chicken eggs. The underlying mechanisms of VBNC formation and resuscitation were also explored.

In Chapter 3, we proposed a novel Raman tweezers system combined with a microfluidic device and machine learning algorithms for single-cell identification and sorting in a label-free and noninvasive manner. Specifically, an individual bacterial cell in the microfluidic channel was captured by the optical tweezers, identified based on the Raman spectral patterns and then selectively isolated to a collection container. Automatic operations were realized by using an in-house LabVIEW program with minimized human supervision. We also developed a novel SRGAN that could increase the SNR of single-cell Raman spectra, thereby significantly accelerating the data collection by a factor of 10. We verified the performance of the proposed optofluidic platform for single-cell identification of 5 leading foodborne bacteria, including *C. jejuni*, and an overall accuracy of 94.9% was achieved by using CNN. This approach enables

rapid identification and non-destructive sorting of single living cells, presenting the potential to reveal the cellular heterogeneity within complex microbial communities.

We further applied the proposed Raman tweezers system to identify VBNC *C. jejuni* at single-cell level in Chapter 4. *C. jejuni* strains were induced into the VBNC state under osmotic pressure and aerobic stress, respectively. Morphological alterations of VBNC cells were revealed in the images of phase-contrast microscopy and transmission electron microscopy. Based on the single-cell Raman spectra and CNN, VBNC *C. jejuni* cells could be successfully distinguished from their culturable counterparts with high accuracies of over 90%. Furthermore, we visualized the contribution of Raman spectral features to the identification of VBNC *C. jejuni* using a gradient-weighted class activation mapping technique. Molecular changes in proteins, nucleic acids, lipids and peptidoglycans are most potentially responsible for the differentiation of VBNC cells from the culturable counterparts. This approach represents a promising tool for identifying VBNC bacteria at the single-cell resolution in heterogeneous real-world samples. The knowledge from this study provided valuable insights to the molecular mechanisms of VBNC formation.

In Chapter 5, resuscitation of VBNC *C. jejuni* was achieved in embryonated chicken eggs and the potential resuscitation stimuli in eggs were investigated. VBNC *C. jejuni* cells induced at low temperature (4°C) retrieved culturability following passage through the embryonated chicken eggs. Eggs at late embryonic stages (i.e., D9 and D11) demonstrated enhanced capabilities of resuscitating VBNC *C. jejuni* compared to the early-stage eggs (i.e., D1 and D3). Using untargeted metabolomics and lipidomics, compounds with significantly higher abundance in late-stage eggs were identified and some of them potentially contributed to the resuscitation of

VBNC *C. jejuni* based on the biological relevance. This study validated the capability of embryonated eggs in facilitating the recovery of VBNC *C. jejuni*, shedding lights on the resuscitation mechanisms of VBNC pathogens.

In conclusion, the research outcome from this thesis project advanced our knowledge in the identification, characterization, and resuscitation of VBNC *C. jejuni* in the environment and within agri-food systems. A better understanding of the survival of *C. jejuni* under stresses could contribute to the development of more effective mitigation strategies, ultimately reducing the prevalence of *Campylobacter* contamination in the agroecosystem.

6.2 Future work

The knowledge gained from this thesis opens new windows for further exploration. Following recommendations are proposed for future research works.

1) The identified VBNC *C. jejuni* cells can be selectively sorted from the bacterial population using the Raman optical tweezers system and subjected to other molecular analysis (e.g., single-cell RNA sequencing) for downstream characterization. These multi-perspective analyses on individual VBNC cells will aid in a better understanding of the mechanism of VBNC formation.

2) Based on the rapid and non-destructive characteristics, Raman tweezers system can be further applied to monitor the molecular dynamics of individual *C. jejuni* cells during the transition from normal state to VBNC state. This real-time monitoring holds the potential to

unravel the molecular mechanisms underlying the formation of bacterial dormancy, shedding light on the microbial ecology of *C. jejuni* under environmental stresses.

3) For the identified potential resuscitation stimuli in the embryonated eggs, we can test their effect on resuscitating VBNC *C. jejuni* cells individually or in combination. The knowledge from this study will aid in elucidating the mechanisms of VBNC *C. jejuni* resuscitation and provide insights on developing new cultivation media for testing VBNC bacteria.

Bibliography

Abdallah, F. B., Lagha, R., & Bakhrouf, A. (2008). Resuscitation and morphological alterations of *Salmonella bovismorbificans* cells under starvation in soil. *World Journal of Microbiology and Biotechnology*, *24*, 1507-1512.

Amel, B. K.-N., Amine, B., & Amina, B. (2008). Survival of *Vibrio fluvialis* in seawater under starvation conditions. *Microbiological Research*, *163*(3), 323-328.

Asakura, H., Makino, S.-i., Takagi, T., Kuri, A., Kurazono, T., Watarai, M., & Shirahata, T. (2002). Passage in mice causes a change in the ability of *Salmonella enterica* serovar Oranienburg to survive NaCl osmotic stress: resuscitation from the viable but non-culturable state. *FEMS Microbiology Letters*, *212*(1), 87-93.

Asakura, H., Yamasaki, M., Yamamoto, S., & Igimi, S. (2007). Deletion of peb4 gene impairs cell adhesion and biofilm formation in *Campylobacter jejuni*. *FEMS Microbiology Letters*, *275*(2), 278-285.

Ashfaq, M. Y., Da'na, D. A., & Al-Ghouti, M. A. (2022). Application of MALDI-TOF MS for identification of environmental bacteria: A review. *Journal of Environmental Management*, *305*, 114359.

Aurass, P., Prager, R., & Flieger, A. (2011). EHEC/EAEC O104: H4 strain linked with the 2011 German outbreak of haemolytic uremic syndrome enters into the viable but non-culturable state in response to various stresses and resuscitates upon stress relief. *Environmental Microbiology*, *13*(12), 3139-3148.

Avila-Ramirez, C., Tinajero-Trejo, M., Davidge, K. S., Monk, C. E., Kelly, D. J., & Poole, R. K. (2013). Do globins in microaerophilic *Campylobacter jejuni* confer nitrosative stress

tolerance under oxygen limitation? In: Mary Ann Liebert, Inc. 140 Huguenot Street, 3rd Floor New Rochelle, NY 10801 USA.

Ayrapetyan, M., Williams, T. C., & Oliver, J. D. (2014). Interspecific quorum sensing mediates the resuscitation of viable but nonculturable *Vibrios*. *Applied and Environmental Microbiology*, *80*(8), 2478-2483.

Baffone, W., Casaroli, A., Citterio, B., Pierfelici, L., Campana, R., Vittoria, E., Guaglianone, E., & Donelli, G. (2006). *Campylobacter jejuni* loss of culturability in aqueous microcosms and ability to resuscitate in a mouse model. *International Journal of Food Microbiology*, *107*(1), 83-91.

Bari, S. N., Roky, M. K., Mohiuddin, M., Kamruzzaman, M., Mekalanos, J. J., & Faruque, S. M. (2013). Quorum-sensing autoinducers resuscitate dormant *Vibrio cholerae* in environmental water samples. *Proceedings of the National Academy of Sciences*, *110*(24), 9926-9931.

Barron, J. C., & Forsythe, S. J. (2007). Dry stress and survival time of *Enterobacter sakazakii* and other *Enterobacteriaceae* in dehydrated powdered infant formula. *Journal of Food Protection*, *70*(9), 2111-2117.

Begley, M., & Hill, C. (2015). Stress adaptation in foodborne pathogens. *Annual Review of Food Science and Technology*, *6*, 191-210.

Blaser, M. J., LaForce, F. M., Wilson, N. A., & Wang, W. L. L. (1980). Reservoirs for human campylobacteriosis. *Journal of Infectious Diseases*, *141*(5), 665-669.

Bolton, D. J. (2015). *Campylobacter* virulence and survival factors. *Food Microbiology*, *48*, 99-108.

Bronowski, C., James, C. E., & Winstanley, C. (2014). Role of environmental survival in transmission of *Campylobacter jejuni*. *FEMS Microbiology Letters*, *356*(1), 8-19.

Burnham, P. M., & Hendrixson, D. R. (2018). *Campylobacter jejuni*: collective components promoting a successful enteric lifestyle. *Nature Reviews Microbiology*, *16*(9), 551-565.

Butler, H. J., Ashton, L., Bird, B., Cinque, G., Curtis, K., Dorney, J., Esmonde-White, K., Fullwood, N. J., Gardner, B., & Martin-Hirsch, P. L. (2016). Using Raman spectroscopy to characterize biological materials. *Nature Protocols*, *11*(4), 664-687.

Cao, X., Zhao, L., Zhang, J., Chen, X., Shi, L., Fang, X., Xie, H., Chang, Y., & Wang, L. (2019). Detection of viable but nonculturable *Vibrio parahaemolyticus* in shrimp samples using improved real-time PCR and real-time LAMP methods. *Food Control*, *103*, 145-152.

Cappelier, J., Besnard, V., Roche, S., Garrec, N., Zundel, E., Velge, P., & Federighi, M. M. (2005). Avirulence of viable but non-culturable *Listeria monocytogenes* cells demonstrated by in vitro and in vivo models. *Veterinary Research*, *36*(4), 589-599.

Cappelier, J., Besnard, V., Roche, S., Velge, P., & Federighi, M. M. (2007). Avirulent viable but non culturable cells of *Listeria monocytogenes* need the presence of an embryo to be recovered in egg yolk and regain virulence after recovery. *Veterinary Research*, *38*(4), 573-583.

Cappelier, J., Minet, J., Magras, C., Colwell, R., & Federighi, M. (1999). Recovery in embryonated eggs of viable but nonculturable *Campylobacter jejuni* cells and maintenance of ability to adhere to HeLa cells after resuscitation. *Applied and Environmental Microbiology*, *65*(11), 5154-5157.

Centers for Disease Control and Prevention. (2018). National Outbreak Reporting System. Retrieved from https://wwwn.cdc.gov/norsdashboard/

Chaisowwong, W., Kusumoto, A., Hashimoto, M., Harada, T., Maklon, K., & Kawamoto, K. (2011). Phsysiological characterization of *Campylobacter jejuni* under cold stresses conditions: its potential for public threat. *Journal of Veterinary Medical Science*, 1108250619-1108250619.

Chaisowwong, W., Kusumoto, A., Hashimoto, M., Harada, T., Maklon, K., & Kawamoto, K. (2012). Physiological characterization of *Campylobacter jejuni* under cold stresses conditions: its potential for public threat. *Journal of Veterinary Medical Science*, *74*(1), 43-50.

Chang, C. W., & Lin, M. H. (2018). Optimization of PMA-qPCR for *Staphylococcus aureus* and determination of viable bacteria in indoor air. *Indoor Air*, *28*(1), 64-72.

Chaveerach, P., Ter Huurne, A., Lipman, L., & Van Knapen, F. (2003). Survival and resuscitation of ten strains of *Campylobacter jejuni* and *Campylobacter coli* under acid conditions. *Applied and Environmental Microbiology*, *69*(1), 711-714.

Chen, H., Zhao, Y. Y., Shu, M., Zhang, T. T., Bi, Y., Gao, Y. Y., & Wu, G. P. (2019). Detection and evaluation of viable but non-culturable *Escherichia coli* O157: H7 induced by low temperature with a BCAC-EMA-Rti-LAMP assay in chicken without enrichment. *Food Analytical Methods*, *12*, 458-468.

Chrimes, A. F., Khoshmanesh, K., Stoddart, P. R., Mitchell, A., & Kalantar-zadeh, K. (2013). Microfluidics and Raman microscopy: current applications and future challenges. *Chemical Society Reviews*, *42*(13), 5880-5906.

Cohn, M. T., Ingmer, H., Mulholland, F., Jørgensen, K., Wells, J. M., & Brøndsted, L. (2007). Contribution of conserved ATP-dependent proteases of *Campylobacter jejuni* to stress tolerance and virulence. *Applied and Environmental Microbiology*, *73*(24), 7803-7813.

Combarros, R., Collado, S., & Díaz, M. (2016). Toxicity of titanium dioxide nanoparticles on *Pseudomonas putida*. *Water Research*, *90*, 378-386.

Costerton, J. W., Lewandowski, Z., Caldwell, D. E., Korber, D. R., & Lappin-Scott, H. M. (1995). Microbial biofilms. *Annual Review of Microbiology*, *49*(1), 711-745.

Coutard, F., Lozach, S., Pommepuy, M., & Hervio-Heath, D. (2007). Real-time reverse transcription-PCR for transcriptional expression analysis of virulence and housekeeping genes in viable but nonculturable *Vibrio parahaemolyticus* after recovery of culturability. *Applied and Environmental Microbiology*, *73*(16), 5183-5189.

Crim, S. M., Iwamoto, M., Huang, J. Y., Griffin, P. M., Gilliss, D., Cronquist, A. B., Cartter, M., Tobin-D'Angelo, M., Blythe, D., & Smith, K. (2014). Incidence and trends of infection with pathogens transmitted commonly through food-Foodborne Diseases Active Surveillance Network, 10 US sites, 2006-2013. *Morbidity and Mortality Weekly Report*, *63*(15), 328.

Cunningham, E., O'Byrne, C., & Oliver, J. D. (2009). Effect of weak acids on *Listeria monocytogenes* survival: evidence for a viable but nonculturable state in response to low pH. *Food Control*, *20*(12), 1141-1144.

Debruyne, L., Gevers, D., & Vandamme, P. (2008). Taxonomy of the family Campylobacteraceae. *Campylobacter*, 1-25.

Del Rocio Leon-Kempis, M., Guccione, E., Mulholland, F., Williamson, M. P., & Kelly, D. J. (2006). The *Campylobacter jejuni* PEB1a adhesin is an aspartate/glutamate-binding protein of an ABC transporter essential for microaerobic growth on dicarboxylic amino acids. *Molecular Microbiology*, *60*(5), 1262-1275.

Devleesschauwer, B., Bouwknegt, M., Mangen, M.-J. J., & Havelaar, A. H. (2017). Health and economic burden of *Campylobacter*. In *Campylobacter* (pp. 27-40). Elsevier.

Dinu, L.-D., & Bach, S. (2011). Induction of viable but nonculturable *Escherichia coli* O157: H7 in the phyllosphere of lettuce: a food safety risk factor. *Applied and Environmental Microbiology*, *77*(23), 8295-8302.

Dinu, L.-D., & Bach, S. (2013). Detection of viable but non-culturable *Escherichia coli* O157: H7 from vegetable samples using quantitative PCR with propidium monoazide and immunological assays. *Food Control*, *31*(2), 268-273.

Dong, K., Pan, H., Yang, D., Rao, L., Zhao, L., Wang, Y., & Liao, X. (2020). Induction, detection, formation, and resuscitation of viable but non-culturable state microorganisms. *Comprehensive Reviews in Food Science and Food Safety*, *19*(1), 149-183.

Einsle, O. (2011). Structure and function of formate-dependent cytochrome c nitrite reductase, NrfA. In *Methods in Enzymology* (Vol. 496, pp. 399-422). Elsevier.

Elvers, K. T., Wu, G., Gilberthorpe, N. J., Poole, R. K., & Park, S. F. (2004). Role of an inducible single-domain hemoglobin in mediating resistance to nitric oxide and nitrosative stress in *Campylobacter jejuni* and *Campylobacter coli*. *Journal of Bacteriology*, *186*(16), 5332-5341.

Fang, T., Shang, W., Liu, C., Xu, J., Zhao, D., Liu, Y., & Ye, A. (2019). Nondestructive identification and accurate isolation of single cells through a chip with Raman optical tweezers. *Analytical Chemistry*, *91*(15), 9932-9939.

Fey, A., Eichler, S., Flavier, S., Christen, R., Höfle, M. G., & Guzmán, C. A. (2004). Establishment of a real-time PCR-based approach for accurate quantification of bacterial

RNA targets in water, using *Salmonella* as a model organism. *Applied and Environmental Microbiology*, *70*(6), 3618-3623.

Fisher, R. A., Gollan, B., & Helaine, S. (2017). Persistent bacterial infections and persister cells. *Nature Reviews Microbiology*, *15*(8), 453-464.

Fux, C. A., Costerton, J. W., Stewart, P. S., & Stoodley, P. (2005). Survival strategies of infectious biofilms. *Trends in Microbiology*, *13*(1), 34-40.

Gangaiah, D., Liu, Z., Arcos, J., Kassem, I. I., Sanad, Y., Torrelles, J. B., & Rajashekara, G. (2010). Polyphosphate kinase 2: a novel determinant of stress responses and pathogenesis in *Campylobacter jejuni*. *PLoS One*, *5*(8), e12142.

Gao, B., Vorwerk, H., Huber, C., Lara-Tejero, M., Mohr, J., Goodman, A. L., Eisenreich, W., Galán, J. E., & Hofreuter, D. (2017). Metabolic and fitness determinants for in vitro growth and intestinal colonization of the bacterial pathogen *Campylobacter jejuni*. *PLoS biology*, *15*(5), e2001390.

Gao, R., Liao, X., Zhao, X., Liu, D., & Ding, T. (2021). The diagnostic tools for viable but nonculturable pathogens in the food industry: Current status and future prospects. *Comprehensive Reviews in Food Science and Food Safety*, *20*(2), 2146-2175.

Guccione, E., Del Rocio Leon-Kempis, M., Pearson, B. M., Hitchin, E., Mulholland, F., Van Diemen, P. M., Stevens, M. P., & Kelly, D. J. (2008). Amino acid-dependent growth of *Campylobacter jejuni*: key roles for aspartase (AspA) under microaerobic and oxygen-limited conditions and identification of AspB (Cj0762), essential for growth on glutamate. *Molecular Microbiology*, *69*(1), 77-93.

Gunasekera, T. S., Sørensen, A., Attfield, P. V., Sørensen, S. J., & Veal, D. A. (2002). Inducible gene expression by nonculturable bacteria in milk after pasteurization. *Applied and Environmental Microbiology*, *68*(4), 1988-1993.

Guo, L., Ye, C., Cui, L., Wan, K., Chen, S., Zhang, S., & Yu, X. (2019). Population and single cell metabolic activity of UV-induced VBNC bacteria determined by CTC-FCM and D_2O-labeled Raman spectroscopy. *Environment International*, *130*, 104883.

Gupta, R. K., & Srivastava, R. (2012). Resuscitation promoting factors: a family of microbial proteins in survival and resuscitation of dormant mycobacteria. *Indian Journal of Microbiology*, *52*, 114-121.

Han, L., Wang, K., Ma, L., Delaquis, P., Bach, S., Feng, J., & Lu, X. (2020). Viable but nonculturable *Escherichia coli* O157: H7 and *Salmonella enterica* in fresh produce: Rapid determination by loop-mediated isothermal amplification coupled with a propidium monoazide treatment. *Applied and Environmental Microbiology*, *86*(7), e02566-02519.

Havelaar, A., Ivarsson, S., Löfdahl, M., & Nauta, M. (2013). Estimating the true incidence of campylobacteriosis and salmonellosis in the European Union, 2009. *Epidemiology & Infection*, *141*(2), 293-302.

Hazards, E. P. o. B. (2011). Scientific Opinion on *Campylobacter* in broiler meat production: control options and performance objectives and/or targets at different stages of the food chain. *EFSA Journal*, *9*(4), 2105.

Hofreuter, D. (2014). Defining the metabolic requirements for the growth and colonization capacity of *Campylobacter jejuni*. *Frontiers in Cellular and Infection Microbiology*, *4*, 137.

Huang, W. E., Ward, A. D., & Whiteley, A. S. (2009). Raman tweezers sorting of single microbial cells. *Environmental Microbiology Reports*, *1*(1), 44-49.

Imamura, D., Mizuno, T., Miyoshi, S. i., & Shinoda, S. (2015). Stepwise changes in viable but nonculturable *Vibrio cholerae* cells. *Microbiology and Immunology*, *59*(5), 305-310.

Joshua, G. P., Guthrie-Irons, C., Karlyshev, A., & Wren, B. W. (2006). Biofilm formation in *Campylobacter jejuni*. *Microbiology*, *152*(2), 387-396.

Kaakoush, N. O., Castaño-Rodríguez, N., Mitchell, H. M., & Man, S. M. (2015). Global epidemiology of *Campylobacter* infection. *Clinical Microbiology Reviews*, *28*(3), 687-720.

Kaprelyants, A. S., Mukamolova, G. V., & Kell, D. B. (1994). Estimation of dormant *Micrococcus luteus* cells by penicillin lysis and by resuscitation in cell-free spent culture medium at high dilution. *FEMS Microbiology Letters*, *115*(2-3), 347-352.

Keep, N., Ward, J., Robertson, G., Cohen-Gonsaud, M., & Henderson, B. (2006). Bacterial resuscitation factors: revival of viable but non-culturable bacteria. *Cellular and Molecular Life Sciences*, *63*(22), 2555.

Kibbee, R. J., & Örmeci, B. (2017). Development of a sensitive and false-positive free PMA-qPCR viability assay to quantify VBNC *Escherichia coli* and evaluate disinfection performance in wastewater effluent. *Journal of Microbiological Methods*, *132*, 139-147.

Kim, S. H., Chelliah, R., Ramakrishnan, S. R., Perumal, A. S., Bang, W.-S., Rubab, M., Daliri, E. B.-M., Barathikannan, K., Elahi, F., & Park, E. (2021). Review on stress tolerance in *Campylobacter jejuni*. *Frontiers in Cellular and Infection Microbiology*, *10*, 596570.

Kogure, K., Simidu, U., & Taga, N. (1979). A tentative direct microscopic method for counting living marine bacteria. *Canadian Journal of Microbiology*, *25*(3), 415-420.

Kuehl, B., Marten, S.-M., Bischoff, Y., Brenner-Weiß, G., & Obst, U. (2011). MALDI-TOF mass spectrometry-multivariate data analysis as a tool for classification of reactivation and non-culturable states of bacteria. *Analytical and Bioanalytical Chemistry*, *401*, 1593-1600.

Landenberger, B., Höfemann, H., Wadle, S., & Rohrbach, A. (2012). Microfluidic sorting of arbitrary cells with dynamic optical tweezers. *Lab on a Chip*, *12*(17), 3177-3183.

Laranjo, M., & Oliveira, S. (2011). Tolerance of Mesorhizobium type strains to different environmental stresses. *Antonie Van Leeuwenhoek*, *99*, 651-662.

Liao, H., Jiang, L., & Zhang, R. (2018). Induction of a viable but non-culturable state in *Salmonella* Typhimurium by thermosonication and factors affecting resuscitation. *FEMS Microbiology Letters*, *365*(2), fnx249.

Lin, A. E., Krastel, K., Hobb, R. I., Thompson, S. A., Cvitkovitch, D. G., & Gaynor, E. C. (2009). Atypical roles for *Campylobacter jejuni* amino acid ATP binding cassette transporter components PaqP and PaqQ in bacterial stress tolerance and pathogen-host cell dynamics. *Infection and Immunity*, *77*(11), 4912-4924.

Lin, A. E. J. (2008). *Atypical roles for Campylobacter jejuni AA-ABC transporter components PaqP and PaqQ in bacterial stress tolerance and pathogen-host cell dynamics* (Doctoral dissertation, University of British Columbia).

Liu, J., Zhou, R., Li, L., Peters, B. M., Li, B., Lin, C.-w., Chuang, T.-L., Chen, D., Zhao, X., & Xiong, Z. (2017). Viable but non-culturable state and toxin gene expression of enterohemorrhagic *Escherichia coli* O157 under cryopreservation. *Research in Microbiology*, *168*(3), 188-193.

Lothigius, Å., Sjöling, Å., Svennerholm, A. M., & Bölin, I. (2010). Survival and gene expression of enterotoxigenic *Escherichia coli* during long-term incubation in sea water and freshwater. *Journal of Applied Microbiology*, *108*(4), 1441-1449.

Lussier, F., Thibault, V., Charron, B., Wallace, G. Q., & Masson, J.-F. (2020). Deep learning and artificial intelligence methods for Raman and surface-enhanced Raman scattering. *TrAC Trends in Analytical Chemistry*, *124*, 115796.

Makino, S.-I., Kii, T., Asakura, H., Shirahata, T., Ikeda, T., Takeshi, K., & Itoh, K. (2000). Does enterohemorrhagic *Escherichia coli* O157: H7 enter the viable but nonculturable state in salted salmon roe? *Applied and Environmental Microbiology*, *66*(12), 5536-5539.

Man, S. M. (2011). The clinical importance of emerging *Campylobacter* species. *Nature Reviews Gastroenterology & Hepatology*, *8*(12), 669-685.

Mariam, S. H., Zegeye, N., Aseffa, A., & Howe, R. (2017). Diffusible substances from lactic acid bacterial cultures exert strong inhibitory effects on *Listeria monocytogenes* and *Salmonella enterica* serovar enteritidis in a co-culture model. *BMC Microbiology*, *17*(1), 1-11.

Mendz, G. L., Ball, G. E., & Meek, D. J. (1997). Pyruvate metabolism in *Campylobacter* spp. *Biochimica et Biophysica Acta (BBA)-General Subjects*, *1334*(2-3), 291-302.

Morcrette, H., Kovacs-Simon, A., Tennant, R. K., Love, J., Wagley, S., Yang, Z. R., Studholme, D. J., Soyer, O. S., Champion, O. L., & Butler, C. S. (2020). *Campylobacter jejuni* 11168H exposed to penicillin forms persister cells and cells with altered redox protein activity. *Frontiers in Cellular and Infection Microbiology*, *10*, 565975.

Moreno, Y., Piqueres, P., Alonso, J. L., Jiménez, A., González, A., & Ferrús, M. A. (2007). Survival and viability of *Helicobacter pylori* after inoculation into chlorinated drinking water. *Water Research*, *41*(15), 3490-3496.

Morishige, Y., Fujimori, K., & Amano, F. (2013). Differential resuscitative effect of pyruvate and its analogues on viable but non-culturable *Salmonella*. *Microbes and Environments*, *28*(2), 180-186.

Mukamolova, G. V., Kaprelyants, A. S., Young, D. I., Young, M., & Kell, D. B. (1998). A bacterial cytokine. *Proceedings of the National Academy of Sciences*, *95*(15), 8916-8921.

Mukamolova, G. V., Murzin, A. G., Salina, E. G., Demina, G. R., Kell, D. B., Kaprelyants, A. S., & Young, M. (2006). Muralytic activity of *Micrococcus luteus* Rpf and its relationship to physiological activity in promoting bacterial growth and resuscitation. *Molecular Microbiology*, *59*(1), 84-98.

Murphy, C., Carroll, C., & Jordan, K. (2006). Environmental survival mechanisms of the foodborne pathogen *Campylobacter jejuni*. *Journal of Applied Microbiology*, *100*(4), 623-632.

Nicolo, M. S., Gioffre, A., Carnazza, S., Platania, G., Silvestro, I. D., & Guglielmino, S. P. P. (2011). Viable but nonculturable state of foodborne pathogens in grapefruit juice: a study of laboratory. *Foodborne Pathogens and Disease*, *8*(1), 11-17.

Nikitushkin, V. D., Demina, G. R., Shleeva, M. O., & Kaprelyants, A. S. (2013). Peptidoglycan fragments stimulate resuscitation of "non-culturable" mycobacteria. *Antonie Van Leeuwenhoek*, *103*, 37-46.

Oh, E., McMullen, L., & Jeon, B. (2015). Impact of oxidative stress defense on bacterial survival and morphological change in *Campylobacter jejuni* under aerobic conditions. *Frontiers in Microbiology*, *6*, 295.

Oliver, J. D. (2005). The viable but nonculturable state in bacteria. *Journal of Microbiology*, *43*(spc1), 93-100.

On, S. L. (2001). Taxonomy of *Campylobacter*, *Arcobacter*, *Helicobacter* and related bacteria: current status, future prospects and immediate concerns. *Journal of Applied Microbiology*, *90*(S6), 1S-15S.

Ovsepian, A., Larsen, M. H., Vegge, C. S., & Ingmer, H. (2020). Ciprofloxacin-induced persister-cells in *Campylobacter jejuni*. *Microbiology*, *166*(9), 849-853.

Panutdaporn, N., Kawamoto, K., Asakura, H., & Makino, S.-I. (2006). Resuscitation of the viable but non-culturable state of *Salmonella enterica* serovar Oranienburg by recombinant resuscitation-promoting factor derived from *Salmonella* Typhimurium strain LT2. *International Journal of Food Microbiology*, *106*(3), 241-247.

Park, S. F. (2002). The physiology of *Campylobacter* species and its relevance to their role as foodborne pathogens. *International Journal of Food Microbiology*, *74*(3), 177-188.

Parkhill, J., Wren, B., Mungall, K., Ketley, J., Churcher, C., Basham, D., Chillingworth, T., Davies, R., Feltwell, T., & Holroyd, S. (2000). The genome sequence of the food-borne pathogen *Campylobacter jejuni* reveals hypervariable sequences. *Nature*, *403*(6770), 665-668.

Parsons, C. M. (1984). Influence of caecectomy and source of dietary fibre or starch on excretion of endogenous amino acids by laying hens. *British Journal of Nutrition*, *51*(3), 541-548.

Pasquaroli, S., Zandri, G., Vignaroli, C., Vuotto, C., Donelli, G., & Biavasco, F. (2013). Antibiotic pressure can induce the viable but non-culturable state in *Staphylococcus aureus* growing in biofilms. *Journal of Antimicrobial Chemotherapy*, *68*(8), 1812-1817.

Pinto, D., Almeida, V., Almeida Santos, M., & Chambel, L. (2011). Resuscitation of *Escherichia coli* VBNC cells depends on a variety of environmental or chemical stimuli. *Journal of Applied Microbiology*, *110*(6), 1601-1611.

Pinto, D., Santos, M. A., & Chambel, L. (2015). Thirty years of viable but nonculturable state research: unsolved molecular mechanisms. *Critical Reviews in Microbiology*, *41*(1), 61-76.

Poli, V. F. S., Thorsen, L., Olesen, I., Wik, M. T., & Jespersen, L. (2012). Differentiation of the virulence potential of *Campylobacter jejuni* strains by use of gene transcription analysis and a Caco-2 assay. *International Journal of Food Microbiology*, *155*(1-2), 60-68.

Postnikova, O. A., Shao, J., Mock, N. M., Baker, C. J., & Nemchinov, L. G. (2015). Gene expression profiling in viable but nonculturable cells of *Pseudomonas syringae* pv. syringae. *Frontiers in Microbiology*, *6*, 1419.

Qi, Z., Huang, Z., & Liu, C. (2022). Metabolism differences of biofilm and planktonic *Pseudomonas aeruginosa* in viable but nonculturable state induced by chlorine stress. *Science of The Total Environment*, *821*, 153374.

Ramamurthy, T., Ghosh, A., Pazhani, G. P., & Shinoda, S. (2014). Current perspectives on viable but non-culturable pathogenic bacteria. *Frontiers in Public Health*, *2*, 103.

Redding, B., Schwab, M. J., & Pan, Y.-l. (2015). Raman spectroscopy of optically trapped single biological micro-particles. *Sensors*, *15*(8), 19021-19046.

Reuter, M., Mallett, A., Pearson, B. M., & van Vliet, A. H. (2010). Biofilm formation by *Campylobacter jejuni* is increased under aerobic conditions. *Applied and Environmental Microbiology*, *76*(7), 2122-2128.

Robinson, D. (1981). Infective dose of Campylobacter jejuni in milk. *British Medical Journal (Clinical research ed.)*, *282*(6276), 1584.

Rodriguez, G., Phipps, D., Ishiguro, K., & Ridgway, H. (1992). Use of a fluorescent redox probe for direct visualization of actively respiring bacteria. *Applied and Environmental Microbiology*, *58*(6), 1801-1808.

Rollins, D., & Colwell, R. (1986). Viable but nonculturable stage of *Campylobacter jejuni* and its role in survival in the natural aquatic environment. *Applied and Environmental Microbiology*, *52*(3), 531-538.

Santander, R. D., Figàs-Segura, À., & Biosca, E. G. (2018). Erwinia amylovora catalases KatA and KatG are virulence factors and delay the starvation-induced viable but non-culturable (VBNC) response. *Molecular Plant Pathology*, *19*(4), 922-934.

Sarabhai, S., Harjai, K., Sharma, P., & Capalash, N. (2015). Ellagic acid derivatives from *Terminalia chebula* Retz. increase the susceptibility of *Pseudomonas aeruginosa* to stress by inhibiting polyphosphate kinase. *Journal of Applied Microbiology*, *118*(4), 817-825.

Sellars, M. J., Hall, S. J., & Kelly, D. J. (2002). Growth of *Campylobacter jejuni* supported by respiration of fumarate, nitrate, nitrite, trimethylamine-N-oxide, or dimethyl sulfoxide requires oxygen. *Journal of Bacteriology*, *184*(15), 4187-4196.

Sheridan, G., Masters, C., Shallcross, J., & Mackey, B. (1998). Detection of mRNA by reverse transcription-PCR as an indicator of viability in *Escherichia coli* cells. *Applied and Environmental Microbiology*, *64*(4), 1313-1318.

Silva, J., Leite, D., Fernandes, M., Mena, C., Gibbs, P. A., & Teixeira, P. (2011). *Campylobacter* spp. as a foodborne pathogen: a review. *Frontiers in microbiology*, *2*, 200.

Stahl, M., Butcher, J., & Stintzi, A. (2012). Nutrient acquisition and metabolism by *Campylobacter jejuni*. *Frontiers in Cellular and Infection Microbiology*, *2*, 5.

Stahl, M., Friis, L. M., Nothaft, H., Liu, X., Li, J., Szymanski, C. M., & Stintzi, A. (2011). L-fucose utilization provides *Campylobacter jejuni* with a competitive advantage. *Proceedings of the National Academy of Sciences*, *108*(17), 7194-7199.

Stern, N., Jones, D., Wesley, I., & Rollins, D. (1994). Colonization of chicks by non-culturable *Campylobacter* spp. *Letters in Applied Microbiology*, *18*(6), 333-336.

Stöckel, S., Kirchhoff, J., Neugebauer, U., Rösch, P., & Popp, J. (2016). The application of Raman spectroscopy for the detection and identification of microorganisms. *Journal of Raman Spectroscopy*, *47*(1), 89-109.

Sun, F., Chen, J., Zhong, L., Zhang, X.-h., Wang, R., Guo, Q., & Dong, Y. (2008). Characterization and virulence retention of viable but nonculturable *Vibrio harveyi*. *FEMS Microbiology Ecology*, *64*(1), 37-44.

Svensson, S. L., Frirdich, E., & Gaynor, E. C. (2008). Survival strategies of *Campylobacter jejuni*: stress responses, the viable but nonculturable state, and biofilms. *Campylobacter*, 571-590.

Thomas, M. K., Murray, R., Flockhart, L., Pintar, K., Fazil, A., Nesbitt, A., Marshall, B., Tataryn, J., & Pollari, F. (2015). Estimates of foodborne illness-related hospitalizations and deaths in Canada for 30 specified pathogens and unspecified agents. *Foodborne Pathogens and Disease*, *12*(10), 820-827.

Thomas, M. T., Shepherd, M., Poole, R. K., van Vliet, A. H., Kelly, D. J., & Pearson, B. M. (2011). Two respiratory enzyme systems in *Campylobacter jejuni* NCTC 11168 contribute to growth on L-lactate. *Environmental Microbiology*, *13*(1), 48-61.

Vegge, C. S., Brøndsted, L., Li, Y.-P., Bang, D. D., & Ingmer, H. (2009). Energy taxis drives *Campylobacter jejuni* toward the most favorable conditions for growth. *Applied and Environmental Microbiology*, *75*(16), 5308-5314.

Velayudhan, J., Jones, M. A., Barrow, P. A., & Kelly, D. J. (2004). L-serine catabolism via an oxygen-labile L-serine dehydratase is essential for colonization of the avian gut by *Campylobacter jejuni*. *Infection and Immunity*, *72*(1), 260-268.

Velayudhan, J., & Kelly, D. J. (2002). Analysis of gluconeogenic and anaplerotic enzymes in *Campylobacter jejuni*: an essential role for phosphoenolpyruvate carboxykinase. *Microbiology*, *148*(3), 685-694.

Weingarten, R. A., Taveirne, M. E., & Olson, J. W. (2009). The dual-functioning fumarate reductase is the sole succinate: quinone reductase in *Campylobacter jejuni* and is required for full host colonization. *Journal of Bacteriology*, *191*(16), 5293-5300.

Whitesides, M. D., & Oliver, J. D. (1997). Resuscitation of *Vibrio vulnificus* from the viable but nonculturable state. *Applied and Environmental Microbiology*, *63*(3), 1002-1005.

Wood, T. K., Knabel, S. J., & Kwan, B. W. (2013). Bacterial persister cell formation and dormancy. *Applied and Environmental Microbiology*, *79*(23), 7116-7121.

Wright, J. A., Grant, A. J., Hurd, D., Harrison, M., Guccione, E. J., Kelly, D. J., & Maskell, D. J. (2009). Metabolite and transcriptome analysis of *Campylobacter jejuni* in vitro growth reveals a stationary-phase physiological switch. *Microbiology*, *155*(1), 80-94.

Xu, G., Li, C., & Yao, Y. (2009). Proteomics analysis of drought stress-responsive proteins in Hippophae rhamnoides L. *Plant Molecular Biology Reporter*, *27*, 153-161.

Xu, H.-S., Roberts, N., Singleton, F., Attwell, R., Grimes, D. J., & Colwell, R. (1982). Survival and viability of nonculturable *Escherichia coli* and *Vibrio cholerae* in the estuarine and marine environment. *Microbial Ecology*, *8*, 313-323.

Zhang, S., Ye, C., Lin, H., Lv, L., & Yu, X. (2015). UV disinfection induces a VBNC state in *Escherichia coli* and *Pseudomonas aeruginosa*. *Environmental Science & Technology*, *49*(3), 1721-1728.

Zhang, X.-H., Ahmad, W., Zhu, X.-Y., Chen, J., & Austin, B. (2021). Viable but nonculturable bacteria and their resuscitation: implications for cultivating uncultured marine microorganisms. *Marine Life Science & Technology*, *3*, 189-203.

Zhao, X., Zhong, J., Wei, C., Lin, C.-W., & Ding, T. (2017). Current perspectives on viable but non-culturable state in foodborne pathogens. *Frontiers in Microbiology*, *8*, 580.

Zhong, L., Chen, J., Zhang, X. h., & Jiang, Y. a. (2009). Entry of *Vibrio cincinnatiensis* into viable but nonculturable state and its resuscitation. *Letters in Applied Microbiology*, *48*(2), 247-252.

Zhong, Q., Tian, J., Wang, B., & Wang, L. (2016). PMA based real-time fluorescent LAMP for detection of *Vibrio parahaemolyticus* in viable but nonculturable state. *Food Control*, *63*, 230-238.

Zhu, W., Plikaytis, B. B., & Shinnick, T. M. (2003). Resuscitation factors from mycobacteria: homologs of *Micrococcus luteus* proteins. *Tuberculosis*, *83*(4), 261-269.